AQRP Final Report

Novel Observations and Quantified Source Apportionment of Ozone, Particulate Matter and Contributing Precursors in the El Paso Area

AQRP Project 24-024

Submitted by

Pawel K. Misztal, Lea Hildebrandt Ruiz, and David Sullivan
Center for Energy and Environmental Resources (CEER)
The University of Texas at Austin

Yosuke Kimura and Elena McDonald-Buller
Center for Energy and Environmental Systems Analysis (CEESA)
The University of Texas at Austin

Ling Huang and Chris Emery
Ramboll

Contributing UT Austin students and postdocs: Daniel Sung, Shihao Zhai, Evelyn Deveraux, Chun-Ying Chao, Kacper Przykaza, Kyle Druckman

August 31, 2025

This research was supported by funding from the Texas Commission on Environmental Quality. The findings, opinions, or conclusions do not necessarily represent those of the TCEQ.

QA Requirements: Audits of Data Quality – 10% minimum required; Report of findings in this report.

Executive Summary

The city of El Paso, Texas, faces unique air quality challenges as both a major urban area in West Texas and a border crossing site and international trade corridor with Juárez, Mexico. The objective of this study sponsored by the Texas Air Quality Research Program (AQRP; Project No. 24-024) was to improve the understanding of emission sources and formation processes that contribute to ozone (O_3) and fine particulate matter with a diameter of 2.5 micrometers or smaller ($PM_{2.5}$) in El Paso. The multidisciplinary approach in this project combined novel field observations and air quality modeling. An electric mobile laboratory equipped with state-of-the-science instruments was deployed in two intensive campaigns during winter and late spring 2025 to measure a broad suite of volatile organic compounds (VOCs) and to characterize size-resolved aerosol composition across the El Paso-Juárez airshed. These observations were analyzed in conjunction with simulations with a Comprehensive Air Quality Model with Extensions (CAMx) platform developed for El Paso-Juárez in this project as well as with data from existing continuous air monitoring stations in both cities.

Key findings from the project indicated that particulate matter in El Paso was dominated by crustal dust and vehicular emissions with significant influences from intermittent biomass burning and secondary aerosols. Windblown dust is not included for El Paso and Juárez and sources of area fugitive dust in Juárez appeared to be missing or underrepresented in a 2022 U.S. national emissions modeling platform assessed in this study. Measurements and air quality modeling of VOCs indicated enhanced concentrations of aromatics such as toluene and C_8 aromatics along the U.S.-Mexico border associated with cross-border industrial and traffic sources in addition to local emission sources in El Paso. In contrast, reduced sulfur compounds (e.g. ethanethiol and dimethyl sulfide) were elevated near specific local sources such as wastewater treatment facilities and agricultural areas in El Paso. Diurnal analyses at a fixed monitoring site showed that aromatic VOC enhancements often occurred during nighttime/early morning, whereas higher ratios of C aromatics to toluene during the late afternoon rush hour suggested local tailpipe emissions. Ozone formation in the El Paso area appeared to be largely VOC-limited, with both local and transboundary VOC sources having critical roles in episodic pollution. Collectively, these results have implications for attainment of U.S. and Mexico's federal air quality standards.

The findings of the study suggest that binational strategies are needed to achieve improvements in air quality within the El Paso-Juárez airshed. Future work is recommended to improve estimates of windblown and area fugitive dust across the airshed, pursue cooperative efforts to add speciated VOC measurements at monitoring sites in Mexico, refine the spatial resolution of the meteorological modeling for use with air quality modeling assessments, and develop and evaluate potential emissions reductions strategies from sources such as dust, motor vehicles, and industrial activity on air quality in both El Paso and Juárez.

Table of Contents

1. Introduction

1.1. Background

The El Paso metropolitan area experiences unique air quality challenges as a major urban area in West Texas and border crossing site and international trade corridor with Ciudad Juárez, Mexico, with diverse emission sources and complex terrain. Several ambient monitoring sites in El Paso have daily maximum eight-hour average (MDA8) ozone design values for 2024 (EPA, 2025) that exceed the level of the National Ambient Air Quality Standard (NAAQS). The EPA (2024) lowered the annual NAAQS for fine particulate matter ($PM_{2.5}$) from 12 to 9 $\mu g/m^3$ in 2024 which has placed El Paso closer to nonattainment. Previous analyses have indicated that transboundary pollutant transport from Juárez as well as domestic urban, industrial, and natural sources can significantly impact El Paso's air quality (Park et al., 2020; Ramboll, 2022; Lara et al., 2022). Air quality challenges in El Paso are shared by Juárez as measurements at ambient monitors across the border have exceeded Mexico's federal standards for ozone and $PM_{2.5}$ (INECC, 2022). Addressing these issues requires apportionment of emission sources, separating local, regional, and international contributions, as well as identifying chemical precursors that drive secondary formation of pollutants such as ozone and secondary organic aerosol (SOA) in the El Paso-Juárez airshed. This study sponsored by the Texas Air Quality Research Program (AQRP) addresses these challenges by applying new observational capabilities and air quality modeling to support air quality planning for El Paso.

1.2. Objectives

The overarching goal of this project is to improve understanding of the sources of $PM_{2.5}$ and its gas-phase precursors in the El Paso region. In service of this goal, the study had several specific objectives:

1) Quantify contributions of different sources to secondary $PM_{2.5}$ and ozone formation. This involves determining how much various source categories (e.g. vehicle exhaust, industrial emissions, dust, biomass burning, cross-border transport) contribute to observed particulate and ozone levels.
2) Provide novel spatiotemporal observations of ambient pollutants using advanced measurement techniques. The project aimed to collect data on a broad range of VOCs, trace gases, and particulate components with high time resolution and spatial coverage, to capture pollution patterns across the urban area and at the border.
3) Address key research questions (R1–R4) formulated for the El Paso-Juárez air shed. These guiding questions were:

   R1: Why does El Paso experience high concentration enhancements for toluene and other VOCs, and how do these enhancements influence the formation of O_3 and $PM_{2.5}$?

   R2: What is the quantified source apportionment of ozone and $PM_{2.5}$ (and their precursors) based on time-resolved measurements of a broad range of VOC markers, along with ozone and speciated PM measurements?

   R3: What is the transport contribution of gaseous and particulate pollutants from Mexico to air quality in El Paso?

   R4: What emission reduction scenarios are viable for meeting the new O_3 and $PM_{2.5}$ standards, based on sensitivity analyses of sources in the El Paso region?

4) Inform air quality management. A core objective was to translate the scientific findings into information that can directly benefit TCEQ in guiding how to manage El Paso's air quality under the new standards. This includes identifying which emission sources (or combinations of sources) are most responsible for observed pollution episodes, thereby pointing to effective targets for mitigation.

By pursuing these objectives, the project contributes to the AQRP priority research area of performing field campaigns and analyses to elucidate the chemical and physical processes leading to O_3 and fine PM formation and accumulation. The next sections describe the methods used to achieve these objectives and the results obtained.

2. Methods

2.1 Study Design and Overview

To address the objectives, the project employed an integrated approach consisting of pre-campaign data analysis and modeling, intensive field measurements, and post-campaign data analysis. Figure 2.1 summarizes the overall study design (attached photo figures in the Appendix C). First, the team analyzed existing air quality data and performed preliminary modeling to inform the field deployment. Then, two field measurement campaigns were conducted in different seasons to capture a range of conditions. Finally, the collected data were analyzed using advanced statistical and modeling techniques to apportion sources and interpret processes.

2.1.1 Pre-campaign analysis and modeling (Task 2a & 2b):

Before the field campaigns, researchers examined historical monitoring data and performed initial modeling simulations. For example, wind direction and pollutant concentration patterns from TCEQ monitoring sites were analyzed to identify likely source influence regions. It was observed that near-border sites (e.g. Chamizal in downtown El Paso) showed distinct enhancements of VOCs like toluene when winds blew from the direction of Juárez, whereas stations farther north showed no strong directional bias. These analyses helped pinpoint areas and conditions of interest. In parallel, a Comprehensive Air Quality Model with Extensions (CAMx) platform, described in Section 5, was developed for El Paso-Juárez for the 2022 base year and simulations conducted at the Texas Advanced Computing Center (TACC). The CAMx domain included emission sources from the EPA 2022v1 emissions modeling platform in the Paso del Norte region with increased spatial resolution over the El Paso-Juárez urban and international border areas. The Reactive Tracer (RTRAC) algorithm in CAMx was used to track emission contributions from source categories and regions for species of interest, including toluene. Preliminary model results, along with analyses of pollutant roses (concentration by wind direction), informed the design of mobile monitoring routes, and the selection of a site for intensive stationary monitoring.

2.1.2 Intensive field measurement campaigns (Task 3 & 4)

The experimental core of the project was two intensive field campaigns conducted in Winter 2024/2025 and late Spring/early Summer 2025. Each campaign spanned approximately two weeks. A fully electric Ford E-Transit mobile laboratory van was utilized, outfitted with a comprehensive suite of research-grade instrumentation. Key instruments included: a Vocus Proton-Transfer-Reaction Time-of-Flight Mass Spectrometer (Vocus PTR-TOFMS or Vocus) for real-time VOC measurements, a High-Resolution Time-of-Flight Aerosol Mass Spectrometer (HR-ToF-AMS or HR-AMS) for speciated fine particulate matter with a diameter of 1.0 micrometers or smaller (PM_1) composition, and analyzers for ozone, black carbon (aethalometer), carbon monoxide/CO_2, nitrogen oxides, and meteorological parameters. The van's battery system allowed ~6 hours of continuous mobile operation per charge. During each campaign, the team executed planned driving routes covering urban, industrial, and peripheral areas within roughly a 50-mile radius of El Paso (see Figure 2.1 for completed tracks). Survey drives were conducted on multiple days (covering different times of day) to scout for pollution "hotspots" – areas with elevated O_3, PM, or VOC levels. In the Winter campaign (late December 2024 into January 2025), conditions included cooler temperatures and occasional stagnant night times, whereas the Spring campaign (May – June 2025) captured warmer temperatures and different wind patterns. In addition to mobile sampling, the project included stationary measurements at a fixed site to obtain continuous multi-day data (Task 4). The mobile lab was parked for extended periods at a site on the University of Texas at El Paso (UTEP) campus that was equipped with a TCEQ AutoGC (automated gas chromatograph) trailer. This site, located near

downtown and not far from the border, provided an opportunity to collocate the project's advanced instruments with regulatory-grade monitors measuring VOCs and criteria pollutants. For example, during the Summer 2025 campaign, after completing daily mobile runs, the van was stationed at the UTEP site overnight and for several continuous days to collect baseline and diurnal data under more stable conditions. This approach provided complementary perspectives: the mobile surveys mapped spatial gradients, while the stationary deployment captured temporal patterns and allowed for cross-instrument comparisons (e.g., comparing our PTR-TOFMS VOC measurements with the AutoGC's speciated VOC data at the site). Throughout the campaigns, instrument calibrations and standard operating procedures were followed rigorously (as detailed in the QA/QC section). Field calibration checks included span checks for gas analyzers and dynamic dilution of standard gases for the PTR-TOFMS to ensure quantitative accuracy of key VOCs. The HR-AMS was calibrated for ionization efficiency and relative ionization efficiency with ammonium sulfate and ammonium nitrate aerosol before and after each deployment, and filters were regularly used to measure and then subtract gas-phase background concentrations.

2.1.3 Post-campaign data processing and analysis (Task 5 & 6):

After each field campaign, the collected data underwent thorough processing. Raw mass spectral data from the PTR-TOFMS followed a set of routines included in PTRwid (Holzinger, 2015) and Tofware (Stark et al., 2015). The integrated peaks from unified mass list for the entire VOC *m/z* spectrum were corrected for instrument background measured with the VocusAir catalyst and calibrated to concentration units using daily calibration runs with certified standard gases (Apel-Riemer, Inc.). Similarly, HR-AMS data were processed in Igor Pro 9.05 (Wavemetrics, Inc.) using the standard HR-AMS data analysis toolkit Squirrel version 1.26G to derive the aerosol mass spectrum at each time step and particle mass concentrations of sulfate, nitrate, ammonium, organics and chloride. Quality control steps included removal of data during periods of instrument malfunction or flow instability; for example, when TOF voltages are not at setpoint.

The observation team then performed advanced analyses to extract meaningful patterns from the large datasets. This included generating geospatial VOC maps and pollutant distributions along the mobile routes and computing diurnal profiles at the stationary site for various chemical species. To apportion sources of particulate matter, a statistical receptor modeling technique, Positive Matrix Factorization (PMF) was applied to speciate $PM_{2.5}$ data utilizing chemical speciation network data available for El Paso (e.g., from the Chamizal site). The PMF algorithm identified factors representing different source signatures (such as crustal dust, motor vehicle emissions, biomass burning, secondary sulfate, etc.) and quantified their contributions to the observed $PM_{2.5}$ mass. For PM_1 data collected using the HR-AMS as part of this project, we used the organic mass spectrum to approximate the concentrations of "hydrocarbon-like organic aerosol" (fresh, primary organic aerosol mostly due to emissions from traffic) and "oxygenated organic aerosol" (OOA, secondary organic aerosol) (Ng et al., 2011). More detailed PMF analysis on HR-AMS spectra should be conducted as part of future work and would likely identify additional factors.

All data from instruments were integrated and synthesized (Task 6) to produce the results presented in the next sections. The combination of observational data, as well as model simulations described in Section 6, provided a robust perspective of pollution sources and processes affecting the El Paso region.

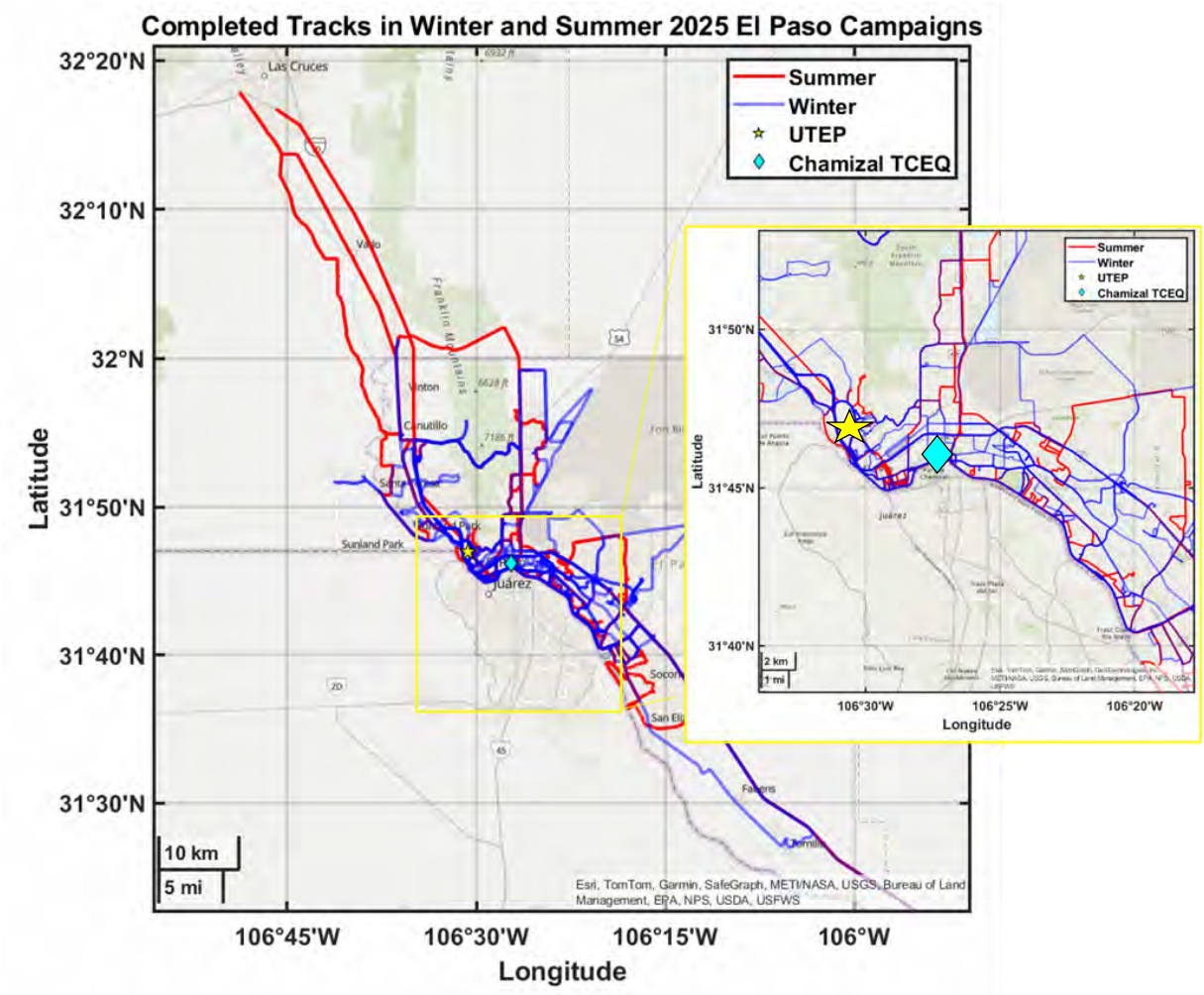

Figure 2.1. Completed mobile measurement tracks for the winter and summer campaigns. The star indicates the stationary UTEP site, and the diamond indicates the frequently collocated Chamizal station.

3. Quality Assurance and Quality Control (QA/QC)

3.1 Emission Inventory and Air Quality Modeling Assessments

Quality Assurance/Quality Control procedures were completed in accordance with the approved Quality Assurance Project Plan (QAPP). The QAPP was based on requirements for a Category III Project that included independent audits of at least 10% of the data.

The integrity of the dataset obtained from the EPA OAQPS 2022 modeling platform website was confirmed by rerunning CAMx at the Texas Advanced Computing Center (TACC) using all inputs files obtained from EPA and successfully reproducing the output file for January 1, 2022, which was shared by EPA staff. Emissions data obtained from the EPA 2022v1emissions modeling platform were processed by Drs. Kimura and Huang for the outer and inner flexi-nested grid domains used in the El Paso-Juárez CAMx platform. Summary tables of emissions of modeled pollutants by source category were independently produced for the 1-km and 4-km grids. Dr. McDonald-Buller reviewed and summarized the EPA technical support document (shown in Appendix A) that described the preparation of the 2022v1 inventory to ensure all source categories relevant to the El Paso-Juárez modeling domain were included. She also examined summaries of the 2018 National Inventory for Mexico, which was the base year for Chihuahua and other border states in the EPA 2022v1 inventory, from SEMARNAT for the Municipio de Juárez as an approximate benchmark. Dr. Kimura and Dr. McDonald-Buller independently ranked and compared all sources of $PM_{2.5}$ and toluene emissions in El Paso and Juárez. Contour maps showing the spatial distribution of criteria pollutants and precursor, toluene, and ethylene oxide emissions were evaluated for reasonableness and shared with the measurement teams and TCEQ during the initial phases of the project.

The CAMx run file developed by Dr. Kimura was independently checked by Dr. McDonald-Buller. CAMx predictions of ozone, $PM_{2.5}$, toluene, and NO_x concentrations were evaluated against observations at ambient monitoring sites in El Paso and Juárez during the 2022 base year using statistical metrics and box and whisker plots. Dr. Kimura overlayed the latitude/longitude coordinates of ambient monitoring sites given by the TCEQ with the 1-km modeling grid to confirm spatial matching of the data for the evaluation. Model performance metrics for ozone and fine particulate matter were compared with established benchmarks from Emery et al. (2016), which are typically used by the TCEQ and EPA for similar assessments. Dr. McDonald-Buller independently calculated metrics for > 10% of the data to confirm those determined by Dr. Kimura. She confirmed that maximum and 99th percentile metrics for MDA8 ozone and 24-hour average $PM_{2.5}$ concentrations, respectively, at Juárez monitoring sites matched those reported by INECC (2022) in reference to compliance with federal standards in Mexico. Dr. Kimura extracted CAMx predictions of ozone and fine particulate matter concentrations from the EPA OAQPS 2022 modeling platform for the continental United States and confirmed that trends with observed data were consistent with those found in this study. Contour plots of CAMx simulated percentile concentrations (50th, 75th, 90th, 95th, 98th, 99th, maximum) of pollutants were used to confirm that spatiotemporal patterns were reasonable for El-Paso-Juárez and were used to overlay with field measurements.

3.2 Instrument Calibration and Analysis

Below we summarize the key QA/QC activities and their outcomes: Instrument Calibration and Operation: All analytical instruments were calibrated and maintained following manufacturer recommendations and project-specific protocols. For the HR-ToF-AMS (aerosol mass spectrometer), an ionization efficiency calibration with ammonium sulfate aerosol was performed at the beginning of each campaign and approximately every two weeks during prolonged sampling. Flow rates through the AMS were also checked and calibrated on the same schedule. Daily mass calibration of the AMS was conducted to ensure accurate m/z alignment. The Vocus PTR-TOFMS underwent daily multi-point calibrations using certified gas standards prior to and during field deployments. In addition, each day

before sampling, a quick tuning check was done by examining the instrument's baseline ion signals (e.g., known reagent ion clusters in H_3O^+ mode) to verify proper operation. The mobile lab's meteorological sensors (wind, temperature, relative humidity) were factory-calibrated and checked against local reference measurements. Data Collection and Handling: During field measurements, data were collected with built-in redundancies and real-time monitoring. Team members kept an instrument log, noting any deviations or issues (such as power interruptions or sensor warnings). The mobile lab's GPS track logs ensured that all data points could be georeferenced accurately. At the stationary site, collocated measurements with the TCEQ AutoGC and reference $PM_{2.5}$ monitors provided a cross-check for our instruments' readings; for instance, our PTR-TOFMS toluene measurements were compared against the AutoGC toluene - showing good agreement within 5%, which increased confidence in both instruments' calibration.

3.3 Post-processing QA/QC

After data collection, a thorough screening was conducted to identify and remove invalid data. For the AMS, periods when the inlet clogged or flow dropped were flagged and those data were excluded from analysis. Similarly, Vocus PTR-TOFMS spectra were examined for anomalies. We followed the practice of removing data that did not meet quality criteria and reduced the dataset to the compounds above the limit of detection, so that the final dataset used for analysis was the highest quality. All data processing code (in Igor Pro for AMS and MATLAB for PTR-TOF, as well as Python/MATLAB for analysis) underwent peer review within the team to avoid transcription errors and ensure correct algorithm application. Audit of Data Quality: In accordance with AQRP requirements, an independent audit of at least 10% of the project's data was performed. Specifically, another investigator who was not involved in day-to-day data collection reviewed random samples of raw and processed data. This audit included checking 10% of the PTR-TOFMS data files and reprocessing them to see if the results matched the reported values; examining 10% of the AMS mass spectra for correct peak identification and integration.

Any discrepancies found during these audits were investigated and resolved. The audit confirmed that no systematic biases were present and that the data handling and reduction steps were performed correctly. Additionally, all custom code and calculation spreadsheets were cross-checked by a second team member as part of internal QA.

3.4 Reporting of QA Findings

We document here that all QA/QC procedures were followed, and any issues encountered were minor and corrected promptly. No significant deviations from the QAPP occurred. Calibration records, instrument logs, and audit records are on file and can be made available upon request. In summary, the project's data are considered valid and of high quality for use in addressing the research objectives. The successful implementation of the QA/QC plan gives confidence that the results and conclusions drawn in this report are based on sound and verified measurements and analyses. By adhering to these QA/QC protocols throughout the project, we ensured the integrity of the findings, thereby providing TCEQ and other stakeholders with dependable information to support air quality management decisions.

4. Observational Results

4.1 Observations of wind patterns and VOC directionality

The wind roses using data from 1/1/2014-12/31/2023 for El Paso monitoring stations (Figure 4.1) show how wind patterns differ over the area.

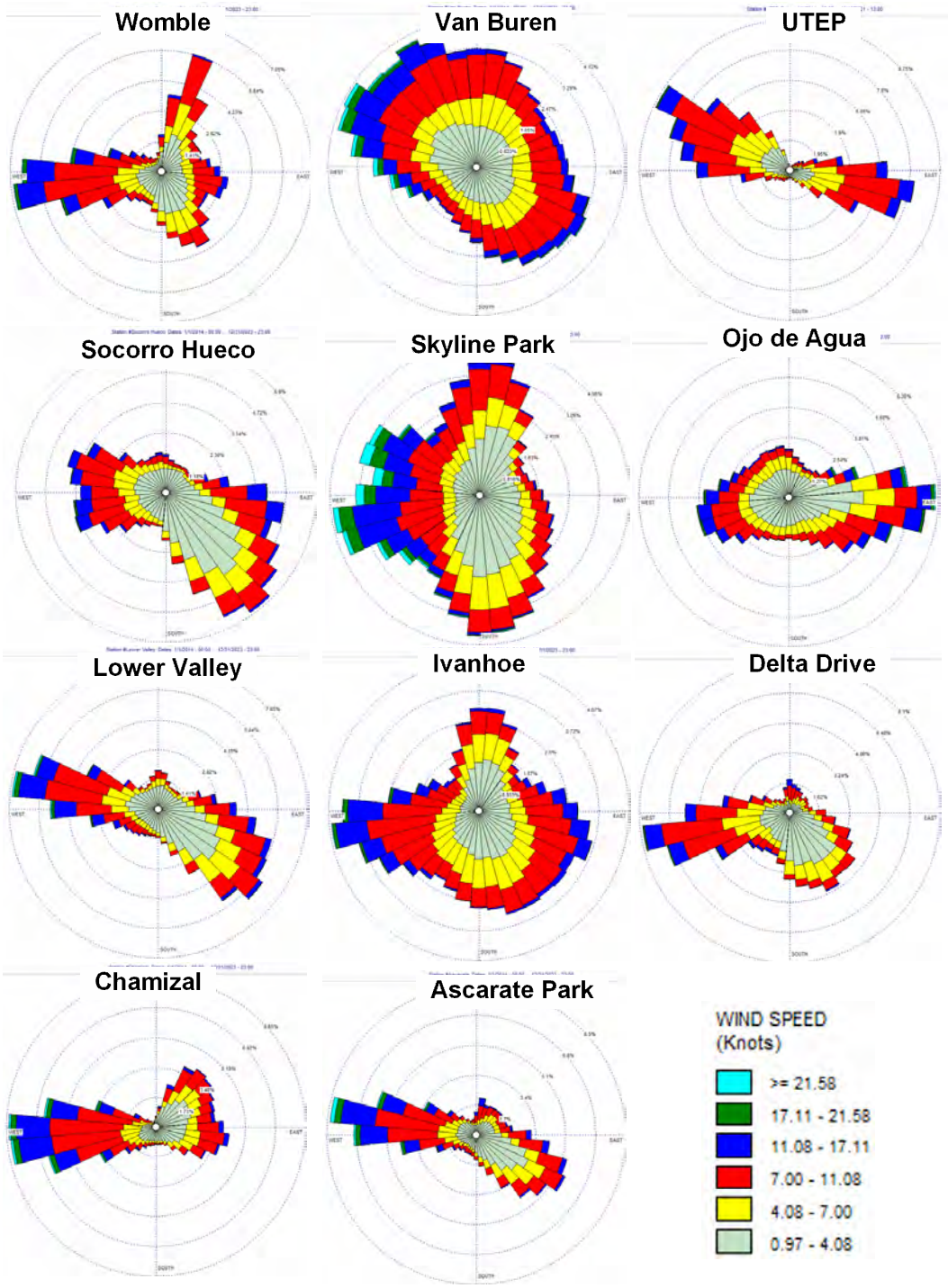

Figure 4.1. Windroses at 11 TCEQ and City of El Paso monitoring stations over ten years (2014-2024).

Wind direction and toluene patterns examined at different monitoring stations. While stations far from the border did not exhibit clear directionality of toluene concentrations, the analysis on the near-border Chamizal Station showed distinct increases in toluene during southerly winds, indicating a potential foreign origin (Figure 4.2)

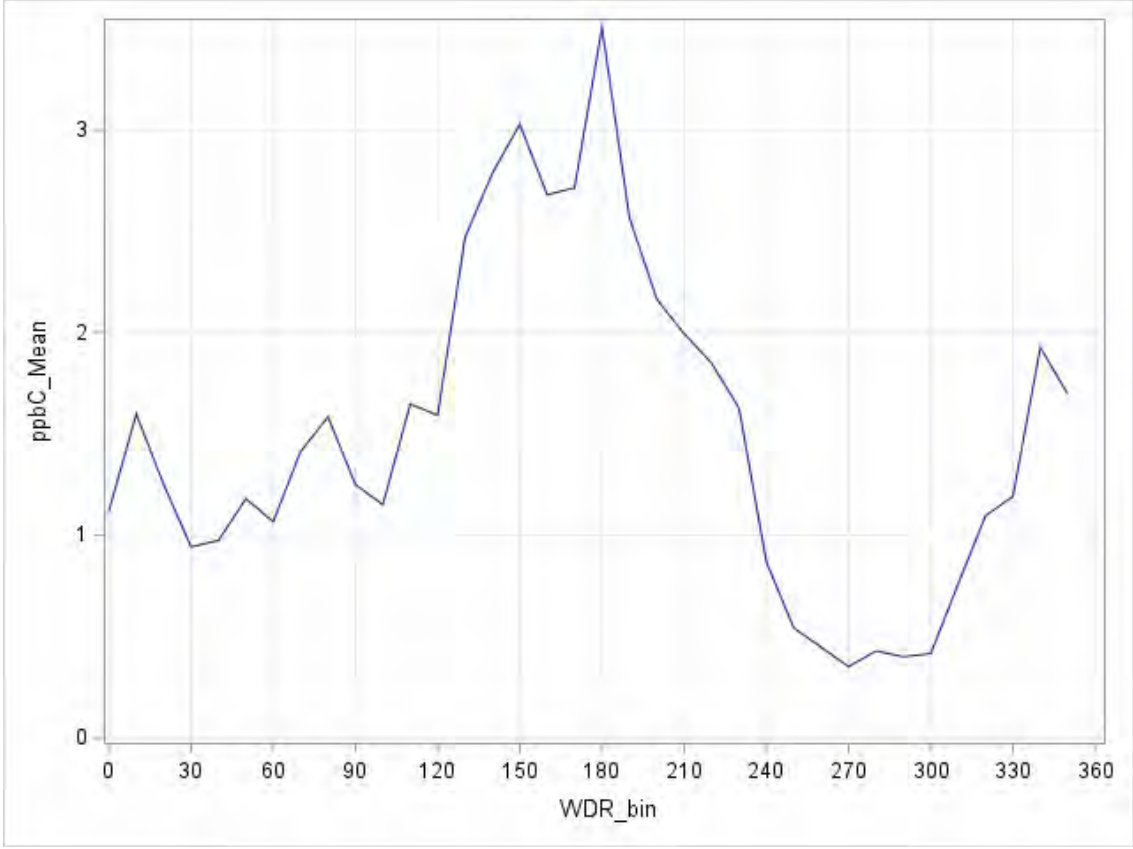

Figure 4.2. Wind directionality of the average toluene concentration at Chamizal monitoring station for Jan. 2022 to June 2024 at Chamizal Station.

4.2 VOC and PM/Ozone Precursor Observations

4.2.1 Spatial patterns of observed VOC concentrations

The mobile laboratory measurements revealed distinct spatial gradients in pollutant concentrations across the El Paso-Juárez area. Out of more than a thousand of VOC ions measured, the prominent compounds included aromatic volatile organic compounds such toluene and other $C_8 - C_{10}$ aromatics (which originate from sources such as fuel evaporation, industrial solvents, and vehicle exhaust). These compounds showed consistently elevated concentrations along the U.S.-Mexico border, especially downwind of the Ciudad Juárez urban/industrial areas during westerly wind conditions.

Figure 4.3 shows observed maps of toluene measured during the winter and summer 2025 campaigns, illustrating hotspots adjacent to the border crossings and industrial parks in south-central El Paso and Juárez.

Mobile measurements during the summer campaign were predominantly influenced by westerly winds, capturing emissions from Juárez along the US - Mexico border. As shown in Figure 4.3, toluene was elevated along the border, consistently in both seasons. In contrast, Figure 4.4a shows that ethanethiol plus dimethyl sulfide (DMS) exhibited different spatial patterns, with concentrations enhanced near wastewater treatment plants in Las Cruces and South El Paso, and in agricultural areas between Las Cruces and El Paso. Guaiacol (Figure 4.4b) also showed a distinct spatial pattern representing a wood smoke marker with particular enhancement near the burning house (Sect. 4.4.1) and agricultural areas in winter with less burning observed during summer except for in northern drives in New Mexico and in south El Paso.

By contrast, other trace gases exhibited hotspots in different locations and seasons. For example, reduced sulfur compounds (e.g., methanethiol) were found at higher concentrations near specific source locations away from the urban core. The mobile surveys detected spikes of these malodorous sulfur compounds in areas north of El Paso and near agricultural or waste management facilities (e.g., around the community of San Elizario southeast of El Paso) – locations where aromatics like benzene/toluene remained low.

This indicates that local sources such as wastewater treatment plants or possibly livestock operations (which emit sulfurous compounds) are contributing to the sulfur VOC plumes, whereas the aromatic VOC enhancements are more tied to urban/industrial emissions from the Juárez/El Paso binational metro area.

Special cases, source apportionment and plume analysis are shown in Sect. 4.4 whereas observed spatial patterns for the two seasons are compared with CAMx predictions in Sect. 6.4.

In addition, the maps for 40 prominent VOC ions in both seasons are shown in Appendix Figure E1 with a compound look-up Table E2. The observation summary statistics for 233 VOC ions are shown in Appendix Table F.1 summarizing encountered VOC mixing ratios in the winter and summer seasons.

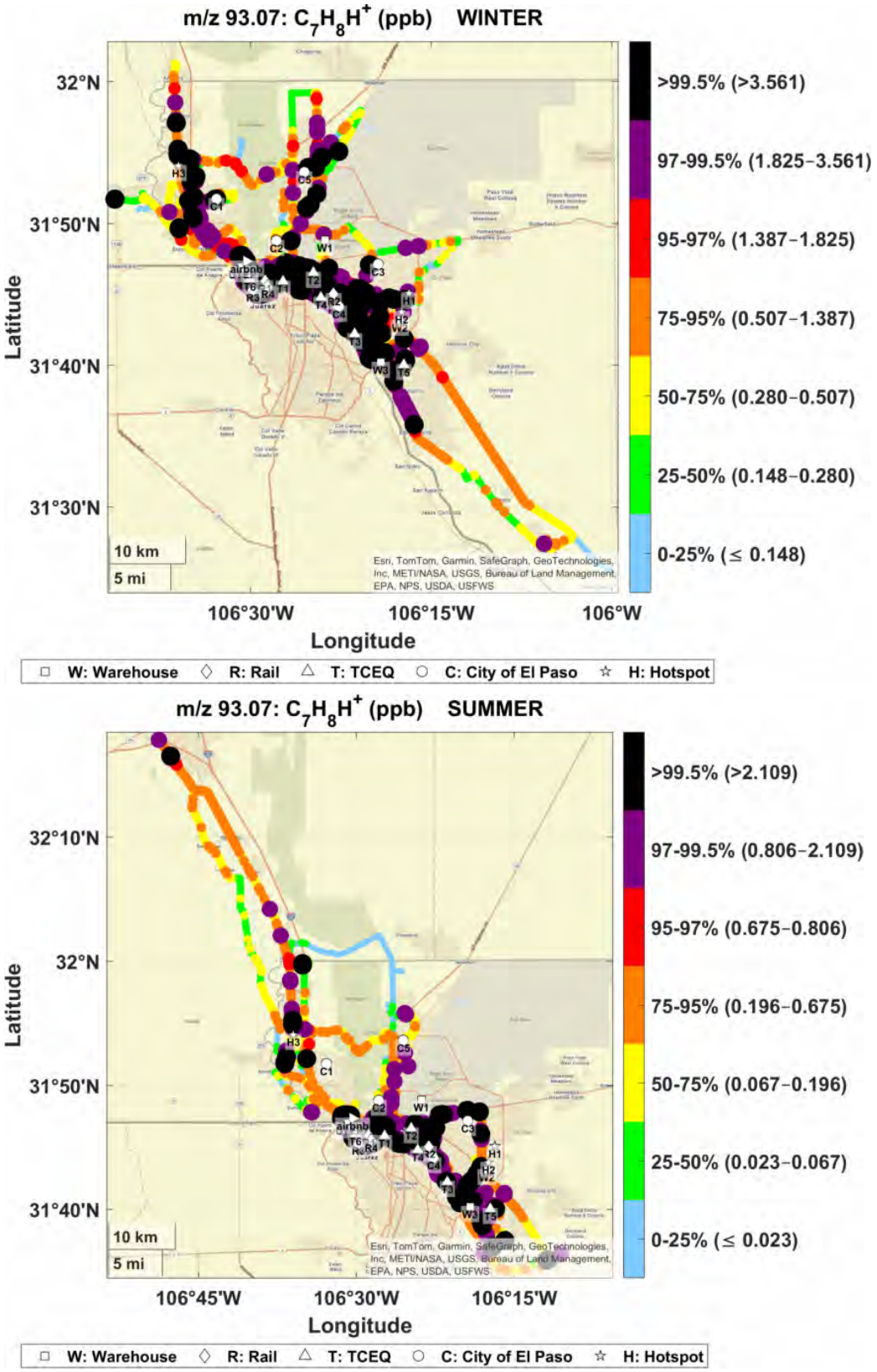

Figure 4.3. Spatial maps for toluene mobile observations in the winter and summer intensives.

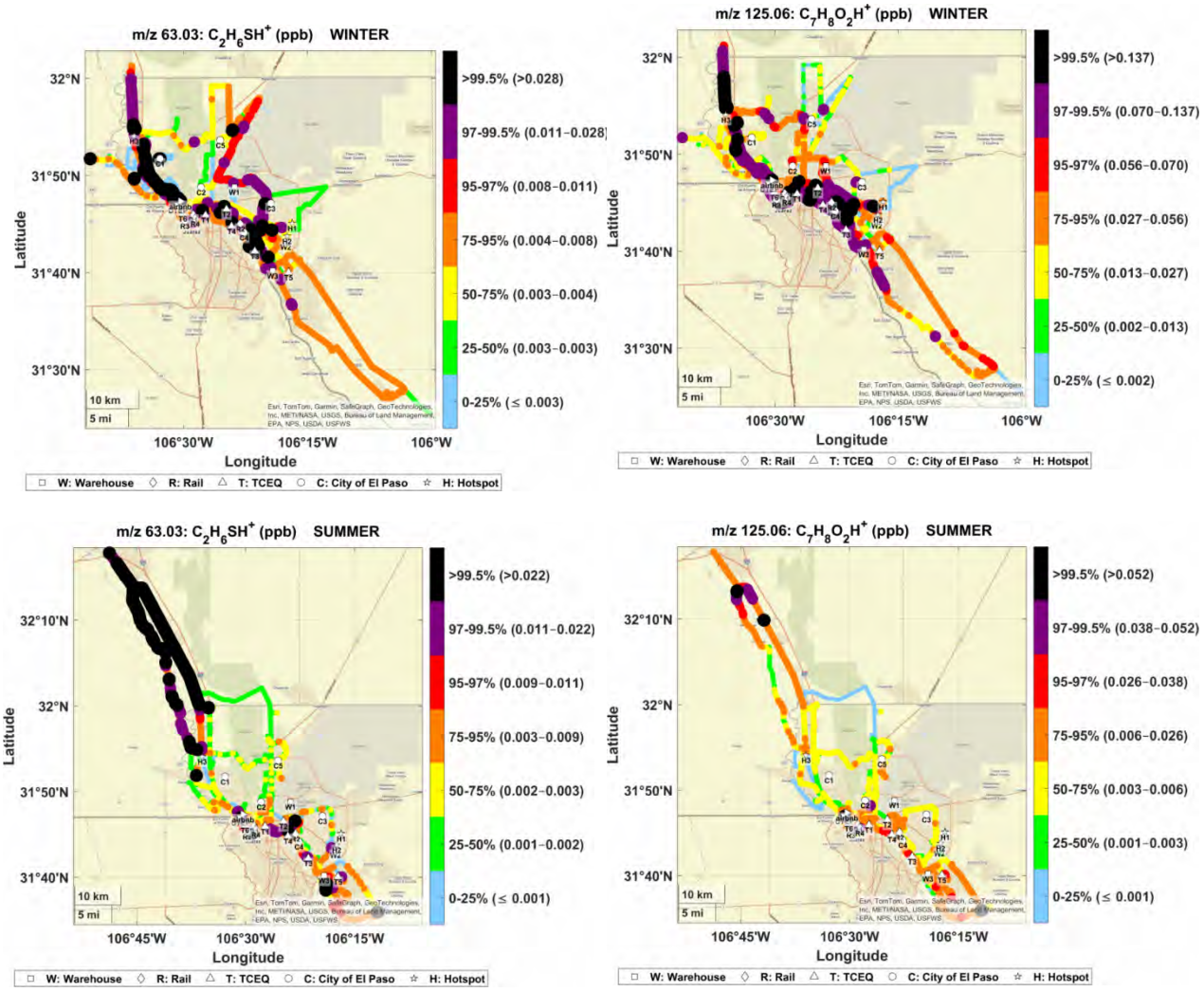

Figure 4.4. Maps of observed concentrations for $C_2H_6SH^+$ (DMS+Ethanethiol) and $C_7H_8O_2H^+$ (Guaiacol).

4.2.2 Stationary temporal patterns of VOC observations at UTEP and other colocation sites

Temporal patterns of continuous measurements at the UTEP stationary site provided insight into diurnal variability and source influences on different timescales. The UTEP site, being near downtown and close to major roadways and the border, captured pollution episodes under different wind regimes. During the summer campaign's 3+ days of continuous monitoring at UTEP, daytime periods (especially late afternoon rush hours) and nighttime periods showed contrasting signatures. Figure 4.5 presents time-series of select VOC tracer concentrations over several days (June 5–8, 2025).

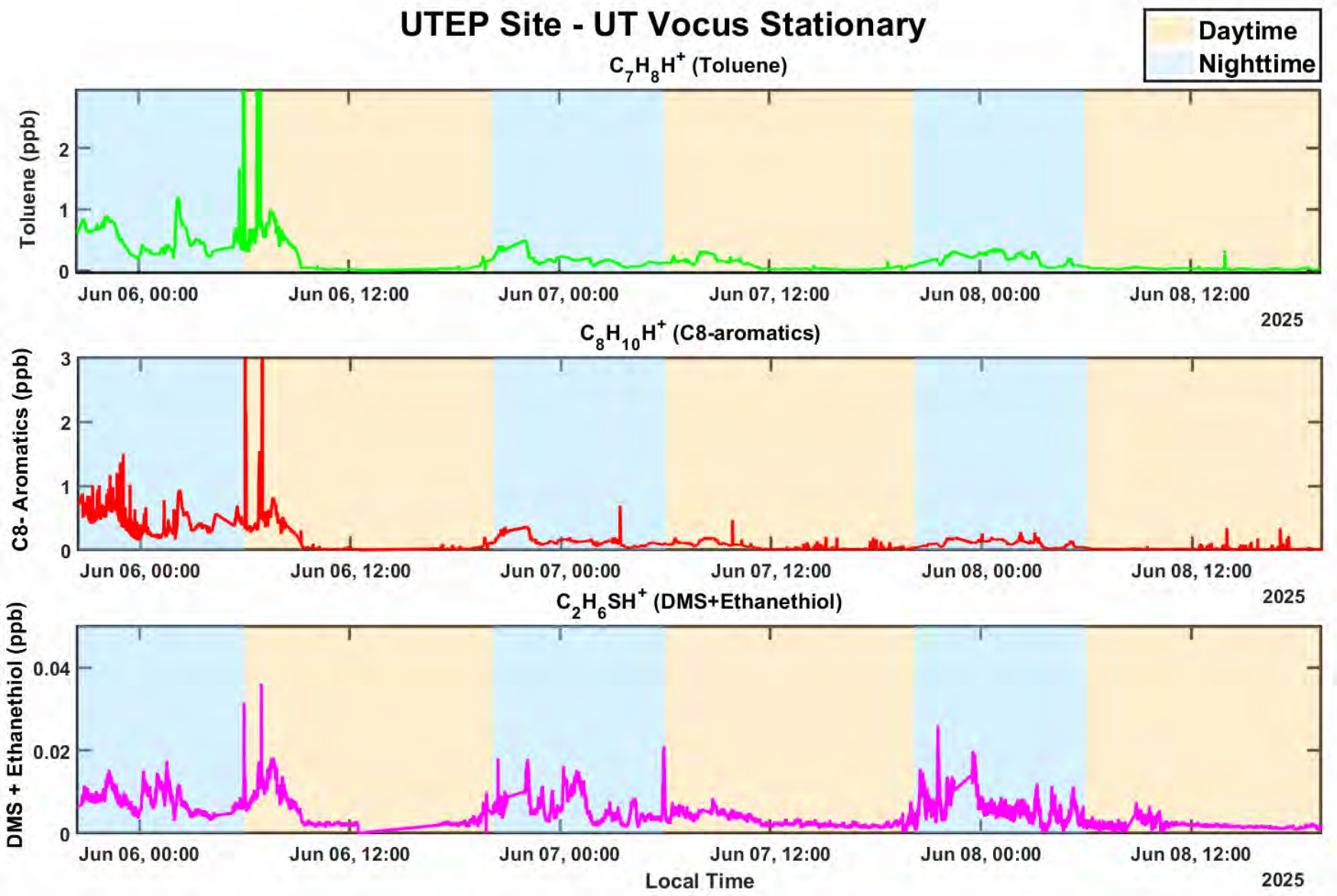

Figure 4.5. Preliminary time series of VOC abundance variability from stationary measurements at UTEP site Summer.

A few clear patterns emerged: (1) Nighttime and early-morning hours often showed sharp increases in aromatic VOCs and other pollutants when drainage flows brought air from Juárez into the El Paso valley. For instance, on the nights of June 6 and 7, elevated toluene and C_8-aromatic levels were observed between midnight and 6 AM, coinciding with gentle westerly drainage winds. These nighttime spikes were also accompanied by increases in carbon monoxide and particulate nitrate, suggesting a buildup of pollutants under stable overnight conditions. (2) During daytime, especially late afternoon, the overall pollutant levels were lower due to enhanced mixing, but a different pattern emerged: the ratio of C_8 aromatics to toluene tended to increase in the late afternoon relative to nighttime. This was noted by comparing species like ethylbenzene (an archetypal tailpipe emission marker) to toluene – higher ratios in afternoon imply a stronger influence of fresh vehicular emissions (rush-hour traffic) during those times, since vehicle exhaust tends to have proportionally more C_8 aromatics. Meanwhile, toluene (which has many solvent and industrial sources) was relatively more enhanced at night, pointing toward industrial or stationary source contributions after hours. (3) Ozone at the UTEP site peaked in the late afternoon (as expected with photochemical production), but interestingly the highest ozone did not always coincide with the highest VOC periods – rather, ozone peaked when the diluted urban plume had moved overhead, consistent with regional photochemical production downwind. In summary, the field observations indicate a strong transboundary influence on VOC levels, especially at night, and a significant local traffic influence during the day. These VOCs are important precursors to both ozone and secondary organic aerosol. The presence of elevated sulfur compounds in specific locales also highlights additional sources (agricultural/industrial) that are relevant for nuisance odors and aerosol formation (sulfur compounds can oxidize to sulfate aerosol). The spatial and temporal patterns observed provided a detailed empirical foundation for source attribution, which we quantify through the $PM_{2.5}$ composition analysis and modeling results below.

The auto-GC at UTEP provides continuous speciated VOC measurements on hourly basis sampling for each 40 minutes. The UT mobile lab parked at this site and was able to co-sample for the stationary period. Figure 4.6 shows an example of a co-located comparison for toluene which agreed within 5% and shows that both instruments are able to capture short-term variabilities and fascinating plumes arriving at the site as the wind direction changes from Juárez and accumulates in the shallow boundary layer.

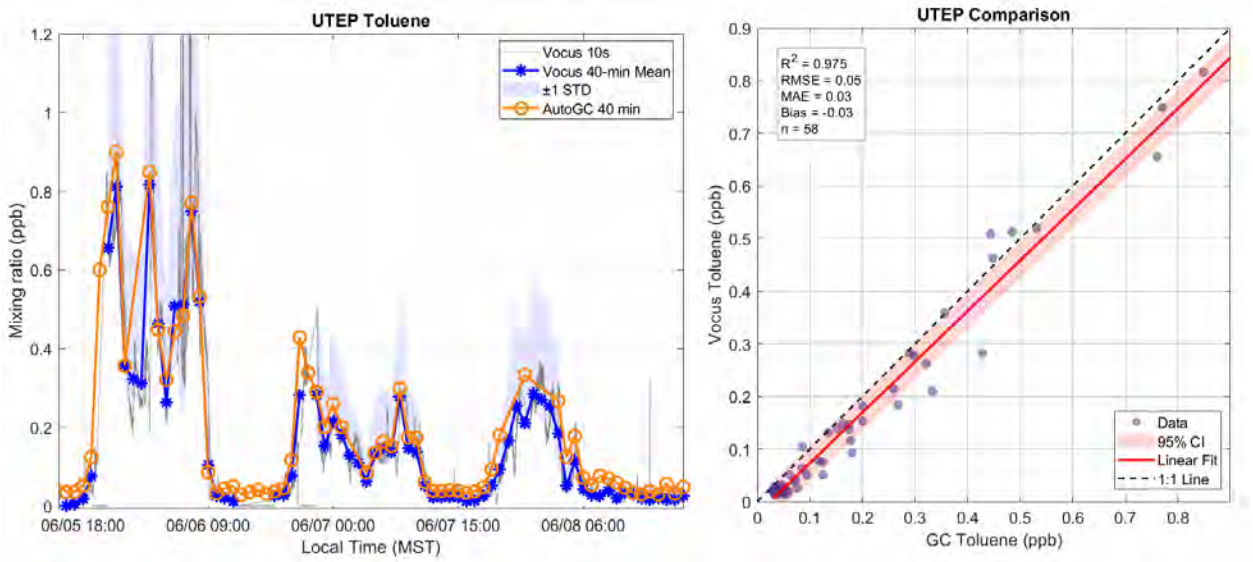

Figure 4.6. Continuous collocation at the UTEP site. Example of toluene is shown with excellent agreement between the Vocus and Auto-GC (R^2 =0.975) within 5%.

During the winter campaign the UTEP Rec Center site was not yet operational so the times when the van was not driving were used to measure continuously near an AirBnB house (a short term rental via https://www.airbnb.com/) at the UTEP campus (Figure 4.7)

a)

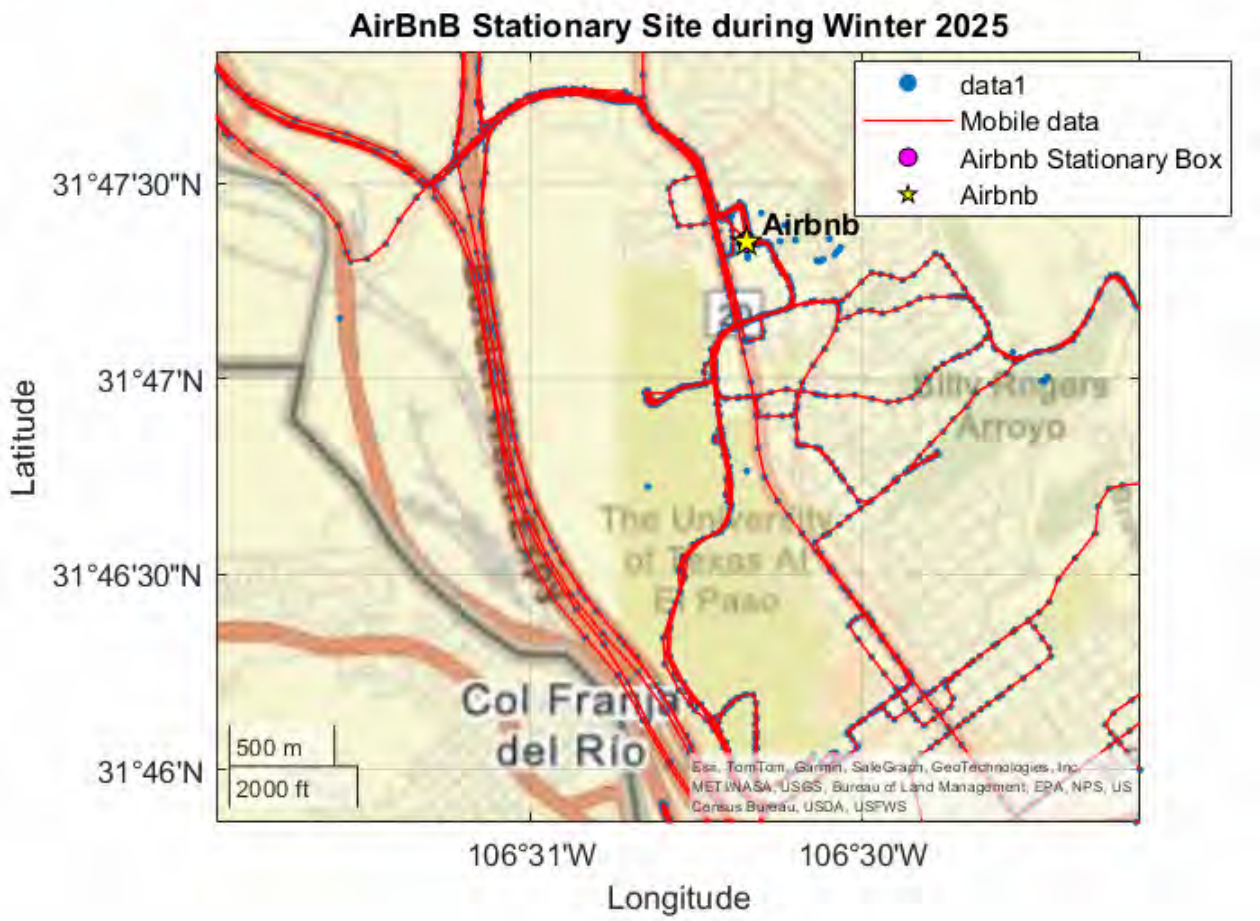

b)

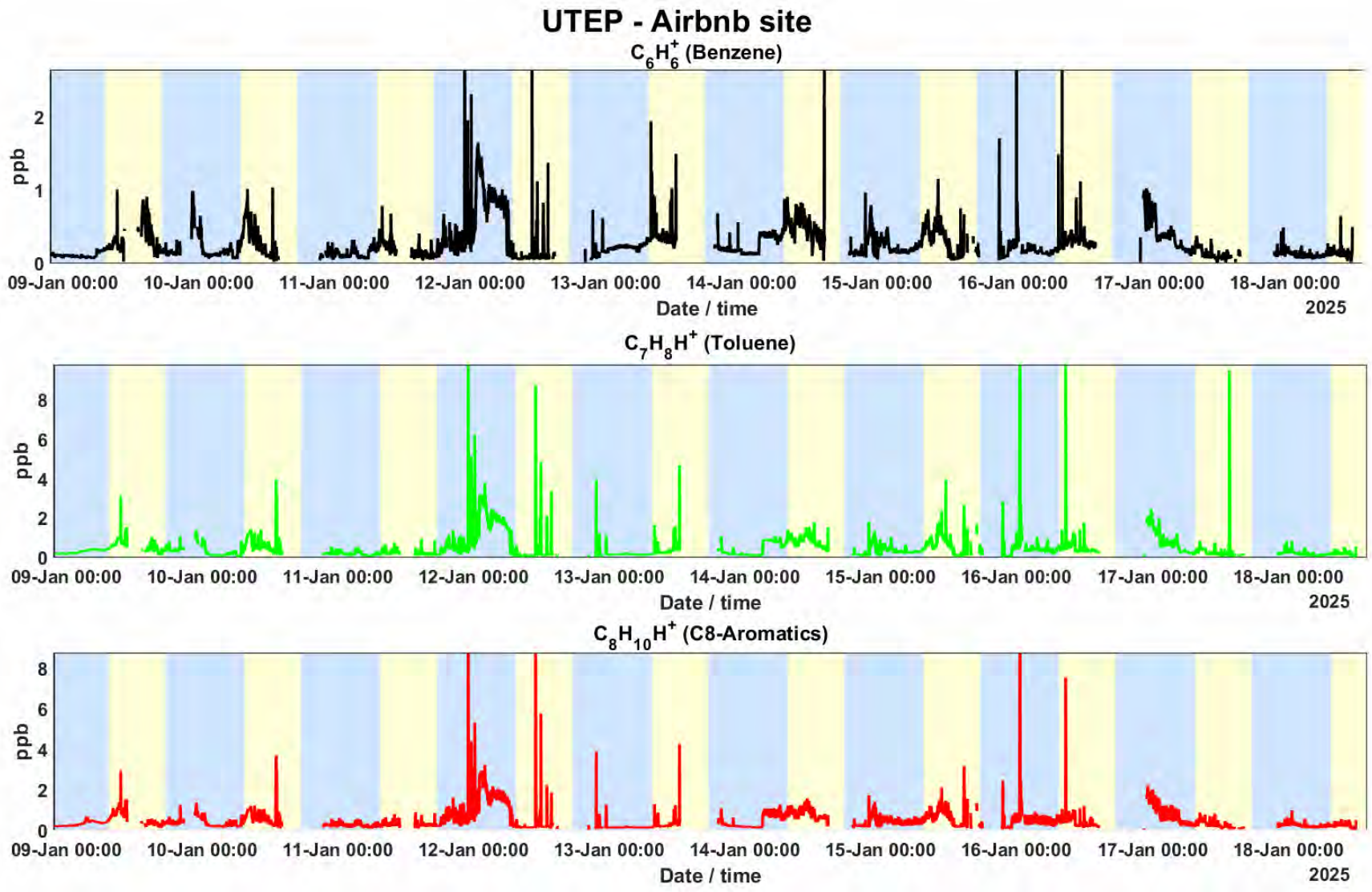

Figure 4.7. (a) Location of the AirBnB location at UTEP (b) Stationary measurements during the winter campaign.

As in winter VOC accumulation likely from the Juárez air shed commonly occurred overnight when the PBL was shallow.

4.2.3 Other Stationary VOC measurements at Monitoring Sites

The map below in Figure 4.8 shows the three locations for automated gas chromatograph (Auto-GC) instruments that have operated in El Paso in recent years. UT operated the Delta station for several years in the early 2020s and now operates the UTEP Rec Center station (which was also collocating with UT van for the summer campaign). TCEQ has operated the Chamizal station since 1988.

Figure 4.8. Three stations, Delta and UTEP operated by UT, and Chamizal, a TCEQ station.

A meteorological instrument was added to the UTEP station in late June 2025, and so collocated wind direction and hydrocarbon measurements exist for a little more than one month (878 hours of measurement data). Figure 4.9 shows a histogram graph of the winds over this one month. It appears the winds are somewhat channelized at the UTEP station, as over the same time period, all of the other El Paso CAMS sites have a wider, more spread-out distribution of surface winds, with south and southeast the most popular directions.

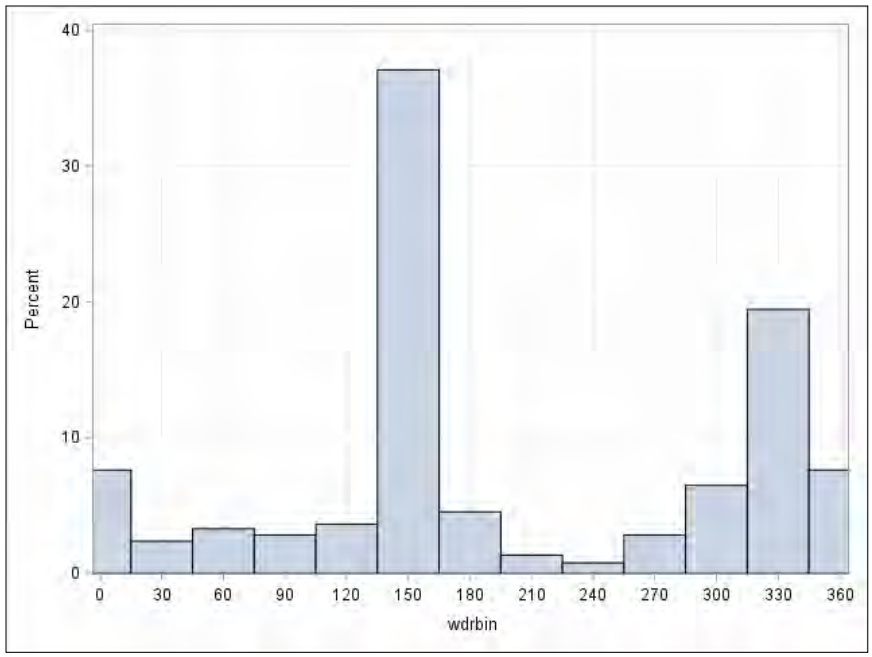

Figure 4.9. Distribution of wind directions at the UTEP station June 24 – July 29, 2025

Toluene concentrations at the UTEP station were averaged by 30-degree wind bins, and the result appears in Figure 4.10. As a second approach, the toluene concentrations were adjusted by wind speed by multiplying by coincident wind speed and dividing by the overall average wind speed. This approach led to the image in Figure 4.11, which points more to 150 degrees than the preceding graph.

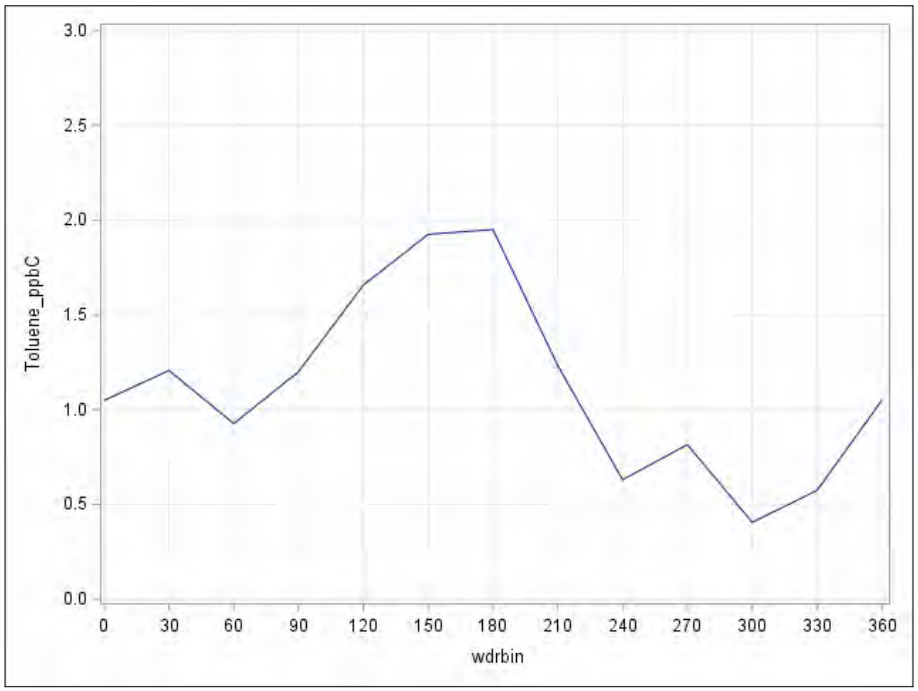

Figure 4.10. Mean toluene from June 24 – July 29, 2025 at the UTEP station

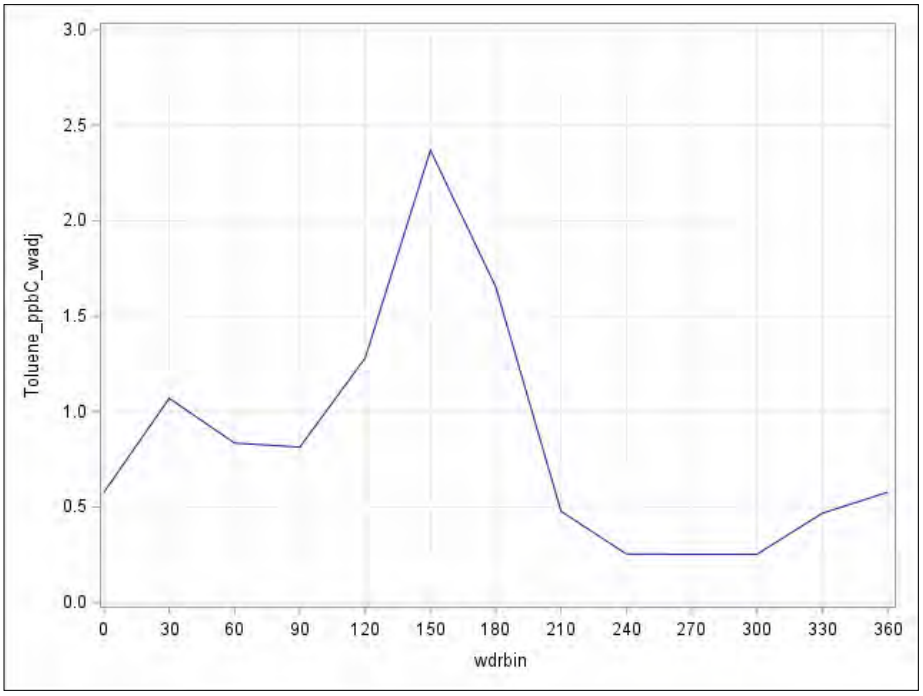

Figure 4.11. Mean wind speed adjusted toluene from June 24 – July 29, 2025 at the UTEP station

The comparison between the total nonmethane hydrocarbon (TNMHC) measurements and the total nonmethane target compounds (TNMTC) measurements was also looked at. A larger difference in these measurements indicates more unidentified species were likely present. Figure 4.12 shows a graph of the difference in ppbC between TNMHC and TNMTC by 30-degree wind bin, and the highest difference value is at the 210 degree (195 to 225 degree) bin.

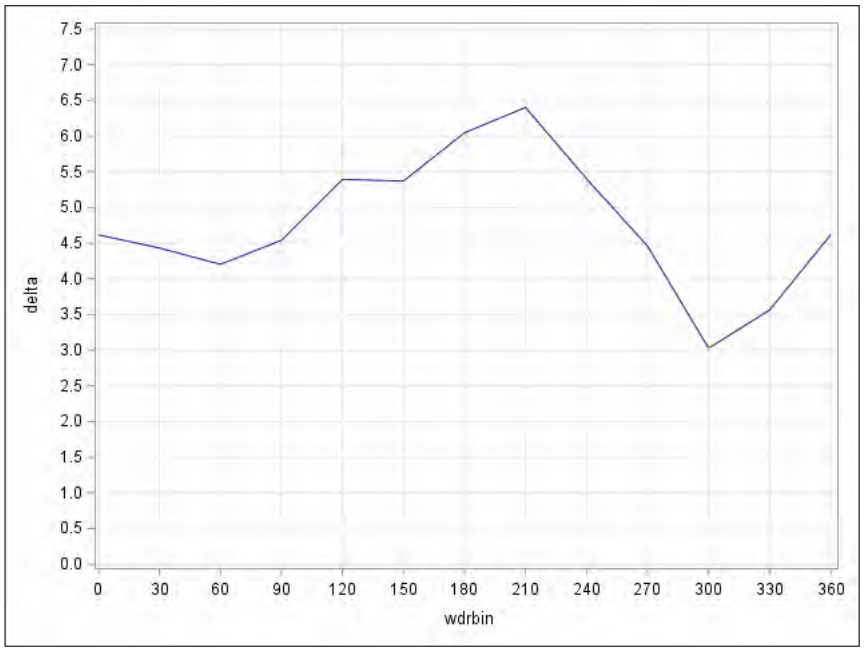

Figure 4.12. Difference between the average TNMHC and TNMTC by wind direction bin.

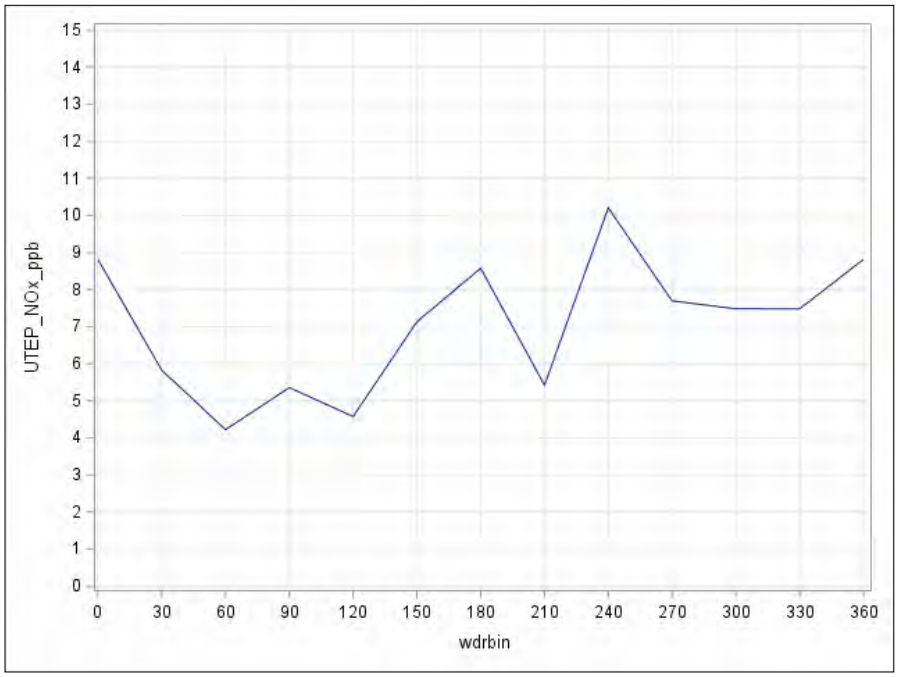

Lastly, total nitrogen oxides ($NO + NO_2$) at the UTEP station were analyzed by wind direction. This appears in Figure 4.13. The data appear to be more or less randomly distributed and do not indicate an explicit upwind source direction though the higher concentrations to the west and north likely point to El Paso, TX.

Figure 4.13. Mean NOx at the UTEP station, June 24 – July 29, 2025, by wind direction bin

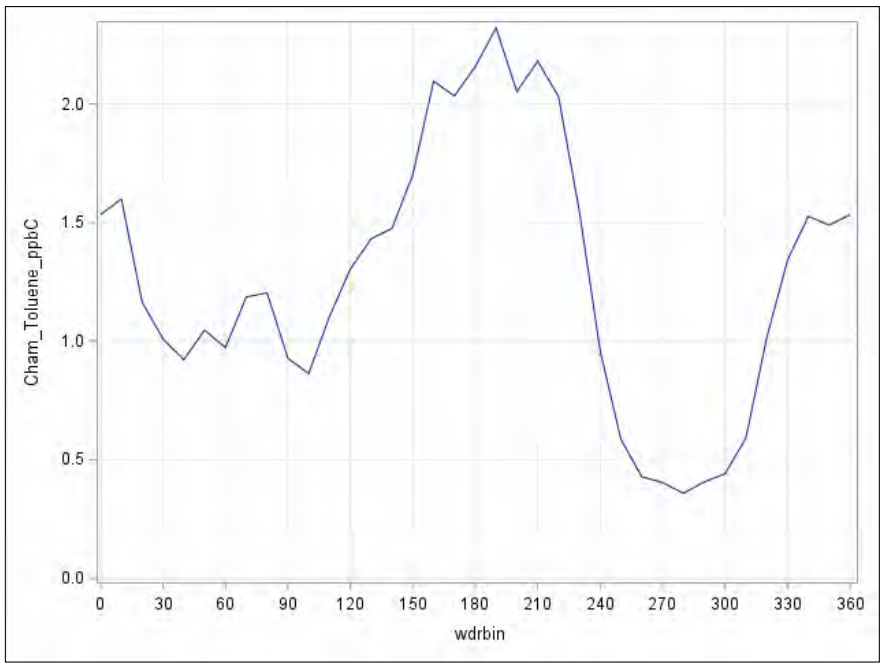

The directionality analysis for toluene was also conducted at the former Delta site and the current Chamizal site. Using data from 2020 to 2024 at Chamizal, a clear picture of directionality is shown in Figure 4.14 below. Two peaks appear, one to the south at 190 degrees and one to the north at 0/360 degrees

Figure 4.14. Mean toluene concentration by 10-degree wind bins at Chamizal for 2020 through 2024.

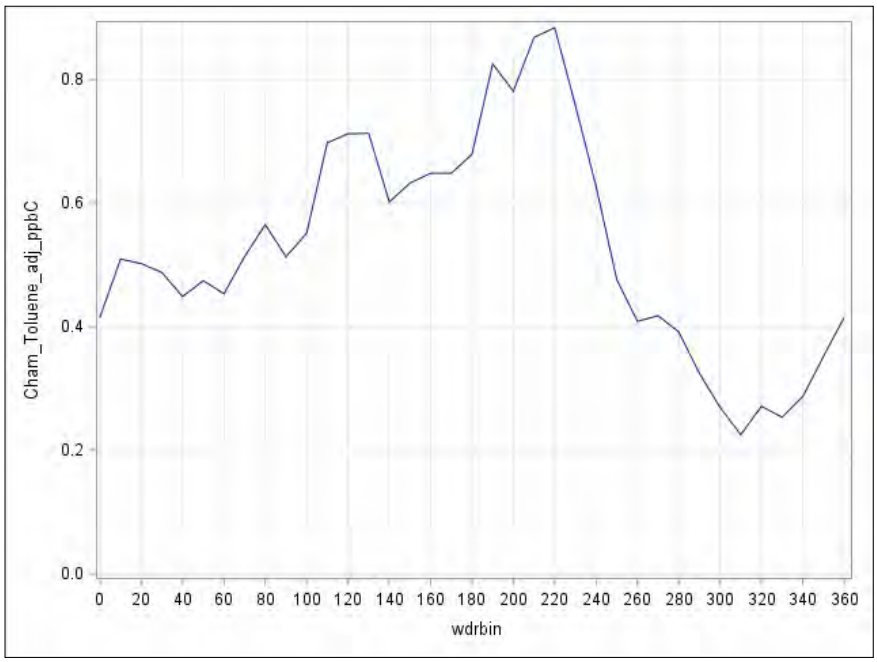

By applying a correction for wind speed, the picture at Chamizal changes considerably. The southerly peak is more pronounced and is centered at 220 degrees, and the northern peak is diminished (Figure 4.15).

Figure 4.15. Mean wind speed-adjusted toluene concentration by 10-degree wind bins at Chamizal for 2020 through 2024.

The CAMS station installed by UT at the Delta Drive site was active over the periods from late 2019 to late 2020, April 2021 to October 2022, and April 2023 to August 2023. Because the station was situated at slightly different locations during each of these three periods, they are broken up in the following six graphs for toluene by wind direction (Figure 4.16). Also, one high outlier value of 113 ppbC on June 7, 2022, has been removed from this analysis. One important conclusion from these graphs is that by adjusting for wind speed, average concentrations point more northerly, perhaps pointing toward the refinery in El Paso.

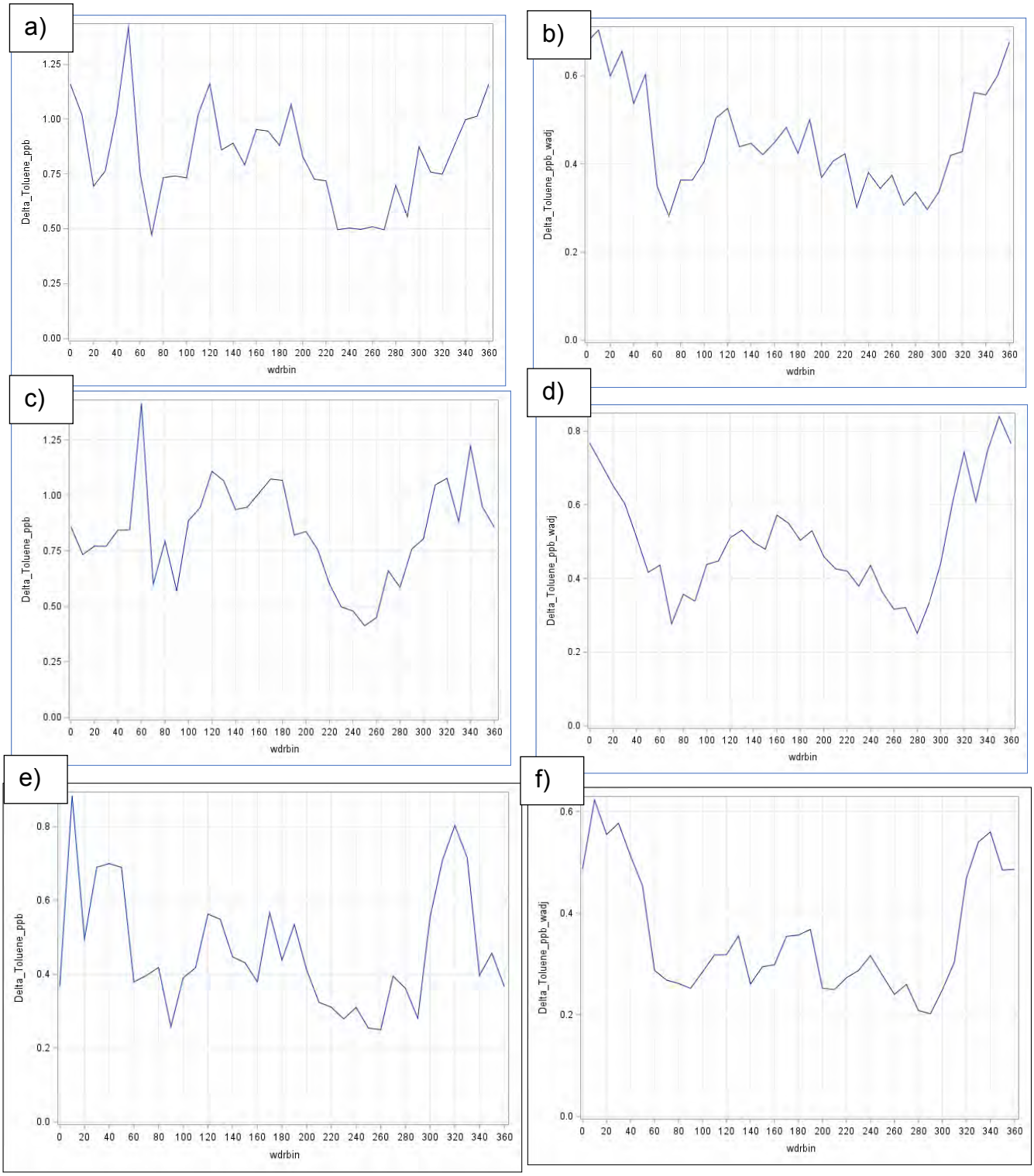

Figure 4.16. (a) Toluene directionality at Delta site in 2020; (b) Wind speed adjusted Toluene directionality at Delta site in 2020; (c) Toluene directionality at Delta site in 2021 – 2022; (d) Wind speed adjusted Toluene directionality at Delta site in 2021 – 2022; (e) Toluene by wind

direction at Delta site in 2023; (f) Wind speed adjusted Toluene by wind direction at Delta site in 2023.

4.2.4 VOC Source Apportionment

4.2.4.1 Winter Campaign

Preliminary multivariate factor analysis was conducted on mobile comprehensive VOC data from the Vocus-PTR-TOFMS and revealed 8 distinct factors (Figure 4.17) which grouped compounds by covariance similarities. Out of 1524 detected ions, 683 VOCs were fed to the factor analysis to aid in source apportionment of individual and groups of VOCs. The preliminary maps for five of these factors are shown in Figure 4.18. For instance, the factor tentatively attributed to "Gasoline and Petrochemical" comprised high loadings of toluene, benzene, C_8 – C_{10} aromatics and other related VOCs. It was distributed across El Paso with different localized enhancements in north and central El Paso. The "Combustion" factor was represented by furanoids, aromatics and nitrogen containing compounds such as C_7H_7NO consistent with benzamide. This factor's hotspot was localized around the burning house (see Section 4.4.1). The factor attributed to "Cooking and VCPs" grouped long-chain fatty acids such as $C_{16}H_{30}O_2$ and long-chain hydrocarbons used in volatile chemical products (VCPs). This factor was spatially expressed close to restaurants and fast-food facilities as well near residences. The "Siloxane factor" was characterized by $C_8H_{24}Si_4O_4$ (D4), $C_{10}H_{30}Si_5O_5$ (D5) and other volatile cyclic siloxanes widely used as lubricants and in personal care products (PCPs). In contrast to primary VOCs directly emitted from different sources, a group of oxygenated VOCs (OVOCs) was represented by "OVOC" Factor which was less localized than other factors indicating mixing across the city. This factor seemed more sensitive to time of day and meteorological conditions affecting photochemical processes. Further data analysis will confirm source apportionment of PM_1 SOA and other markers which will be combined with the wind direction analysis to separate El Paso contributions from those of Juárez. Previous studies and stationary monitoring (Park et al., 2020) apportioned at least 25% of measured total VOCs to mobile sources. The factor analysis can be further analyzed for detailed VOC source apportionment along with the PM_1 source apportionment.

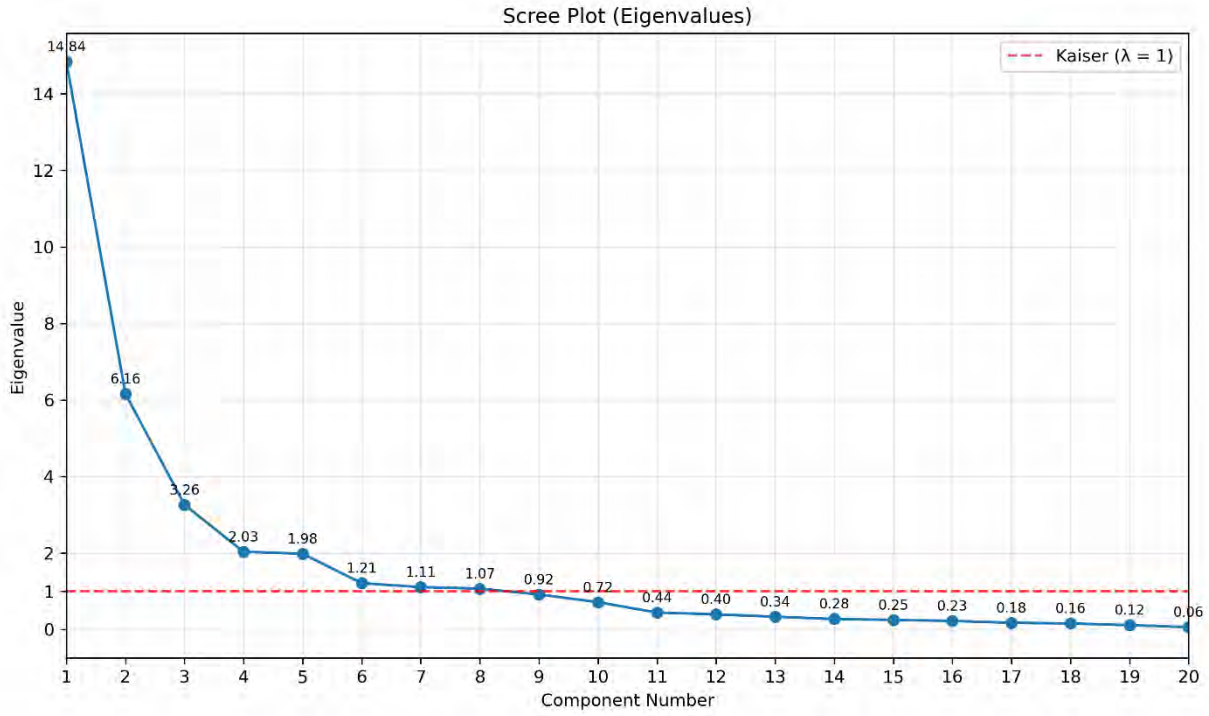

Figure 4.17. The eigenvalue plot conducted on Winter dataset as a rationale for 8-factor solution.

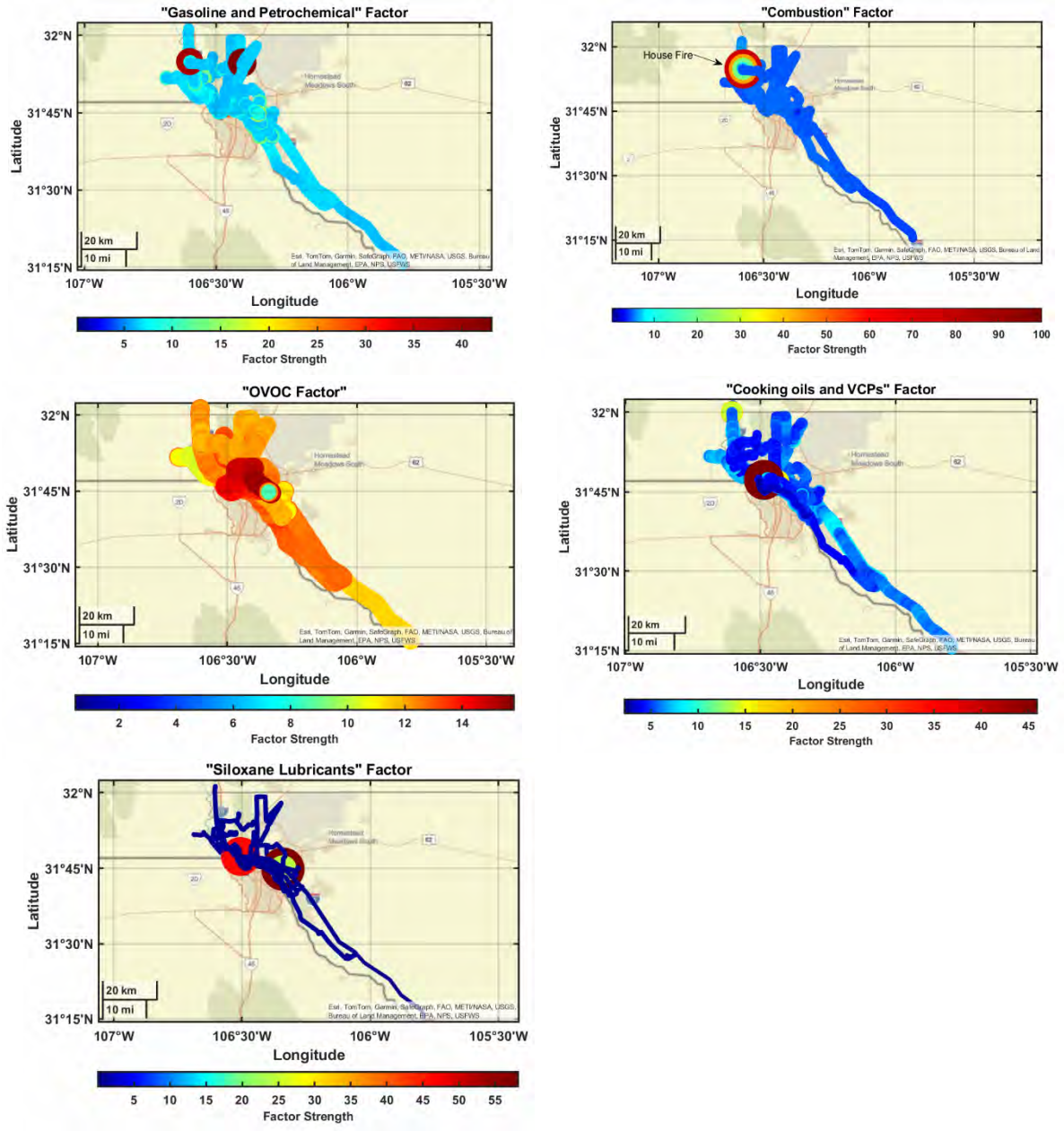

Figure 4.18. Spatial maps of dominant preliminary factors to help source apportionment analysis.

4.3 Particulate Matter Composition and Sources

4.3.1 Mobile measurements of speciated PM_1 concentrations - Overview

Figures 4.19 and 4.20 present the overall spatial distribution maps from the winter and the summer campaign, showing the spatial distribution of total non-refractory PM_1 (NR-PM_1) in units of µg/m^3 (represented by the color bar on the right-hand side of the figures).

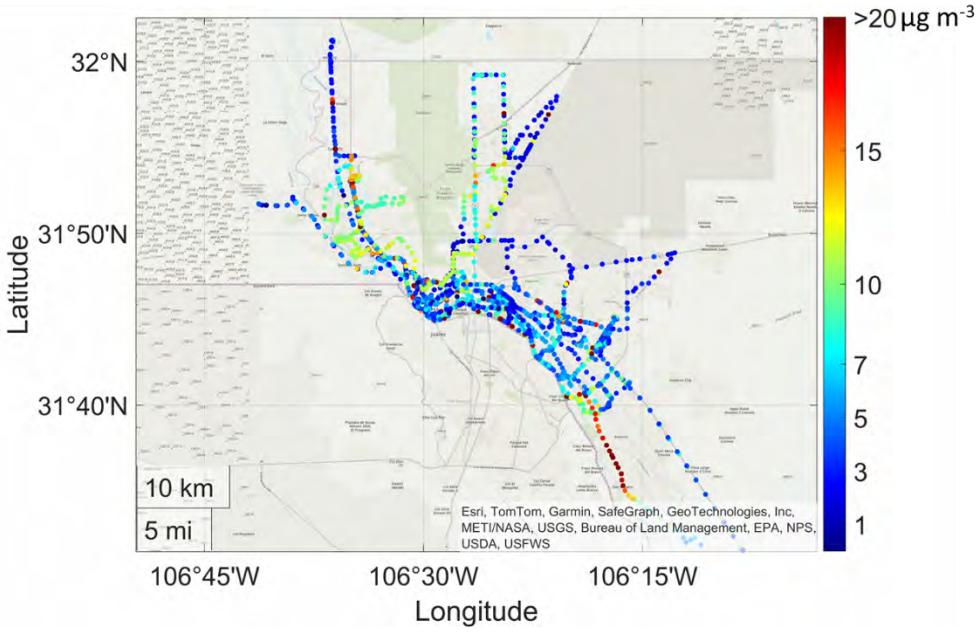

Figure 4.19: Overall Spatial Distribution of PM_1 in January 2025

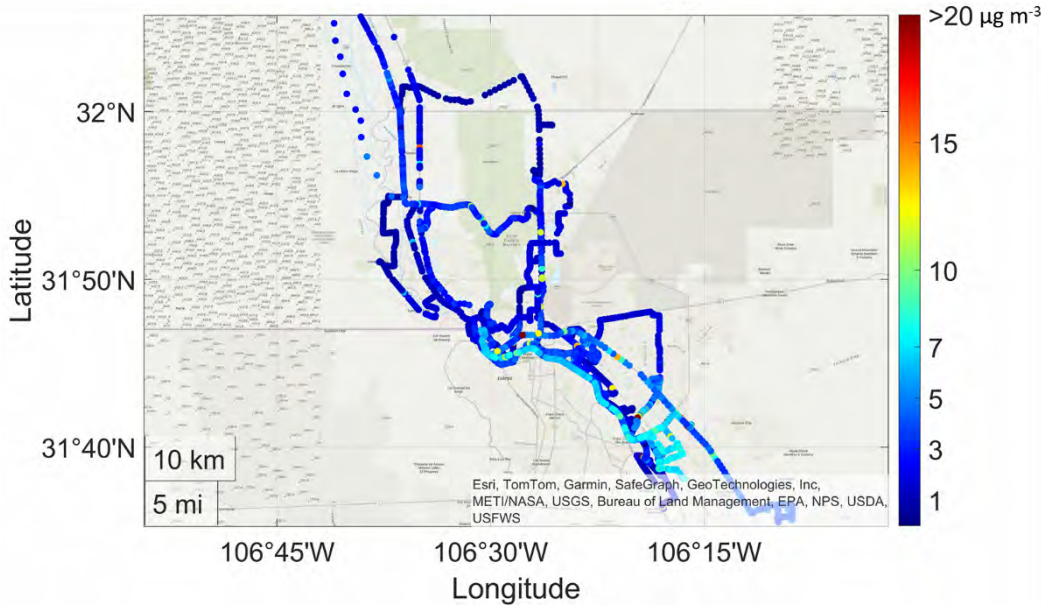

Figure 4.20 Overall Spatial Distribution of PM_1 in May/June 2025

The PM_1 concentrations were generally higher during the winter campaign, likely due to several factors including increased partitioning of ammonium nitrate and organic species to the particle phase at the lower temperatures in the winter, lower boundary layer heights in the winter, and differences in source strengths between the winter and summer campaigns. In addition, during the summer campaign a dust storm in the area led to high concentrations of larger particles that scavenge the smaller particles via coagulation, resulting in low concentrations of PM_1. Concentrations of PM_1 were elevated in the southeastern side of El Paso during both campaigns, near the city of Socorro, TX. During the summer (Figure 4.19) concentrations in this area exceeded 20 µg/m³; in the winter (Figure 4.20), concentrations in this area ranged from 7 and 10 µg/m³.

4.3.2 Observed PM concentration hotspots

Concentrations of PM_1 were sometimes elevated near the US-Mexican border that extends from around downtown El Paso area to the city of San Elizario. For example, Figure 4.21 shows the map of NR-PM_1 measured on January 10, 2025. Using available wind data from the Chamizal TCEQ station, between 14:07 and 21:15 local time (when these mobile measurements took place), the wind direction varies from W, NW and WSW direction, with hourly average wind speeds of 3 mph to 14 mph. Along the highway total PM_1 concentration was over 20 µg/m³. During this high concentrated period, Figure 4.22 shows that most of the PM_1 detected (~16 µg/m³) is organic aerosol. Nitrate and chloride aerosol also increases slightly with organic aerosol. Given the close proximity to the US-Mexican border and the wind direction, the high concentrations observed in Figure 4.22 may originate from sources in Juárez, Mexico.

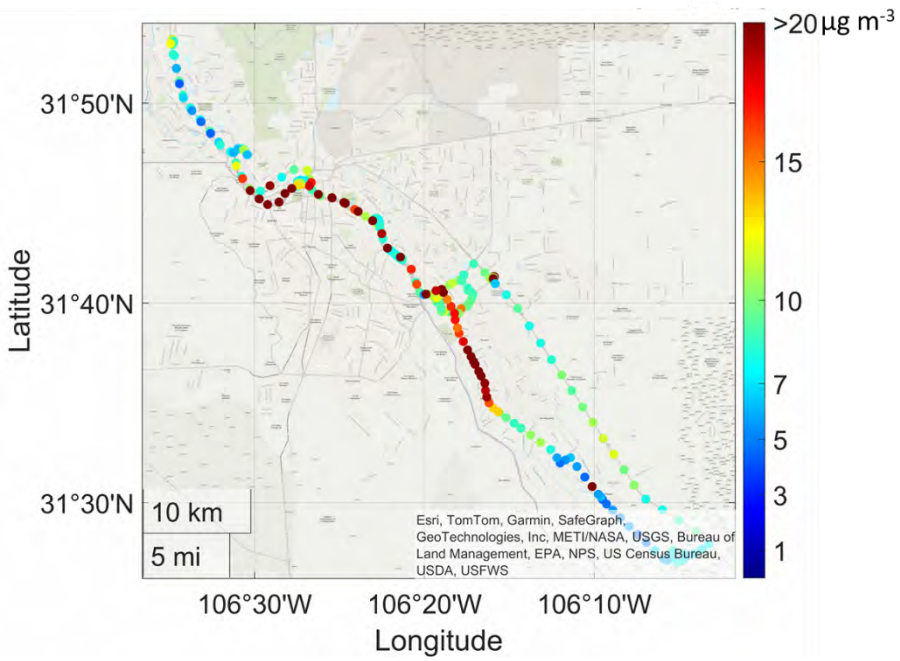

Figure 4.21: Mobile Measurement of PM_1 from 1/10/2025.

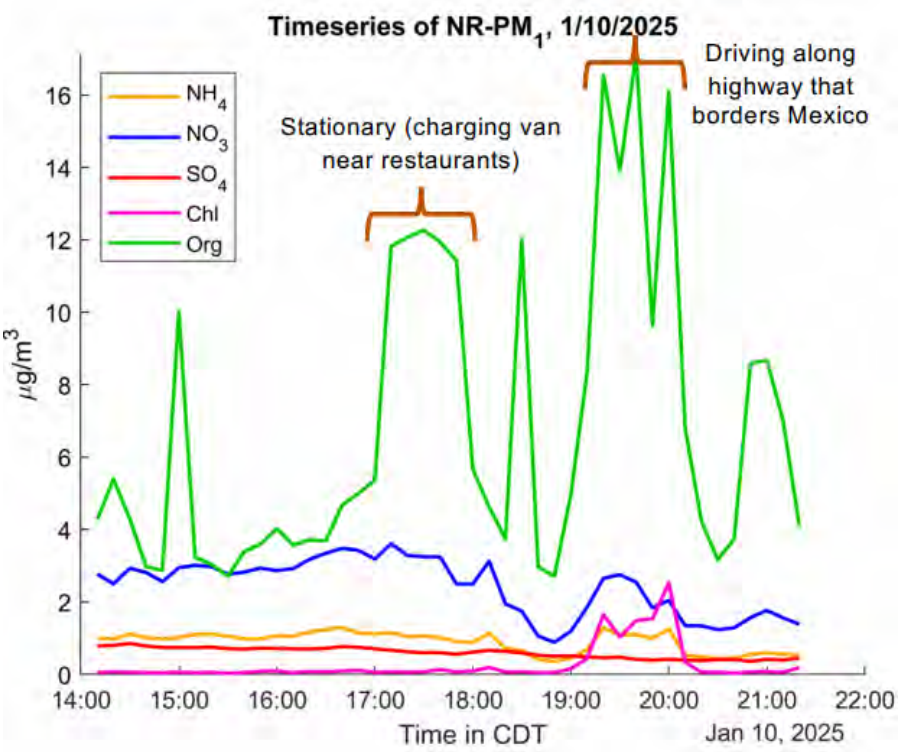

Figure 4.22: Speciated NR-PM_1 during the mobile measurements on 1/10/25.

Figure 4.21 shows a similar mobile route during the summer campaign, during which concentrations along the border stayed relatively constant. Figure 4.23 shows data from this track, which took place on 5/21 between 13:03 and ~22:00 CST. Concentrations of PM_1 along the border highway were around 7 µg/m³. Fires were observed around Gateway Blvd in the Socorro area, which could contribute to the PM_1 concentration hotspots in that area, at around 20 µg/m³. Using available wind data from the Chamizal TCEQ station, the hourly wind direction varies between SSW and W direction, with hourly average speeds of between 4 – 8 mph.

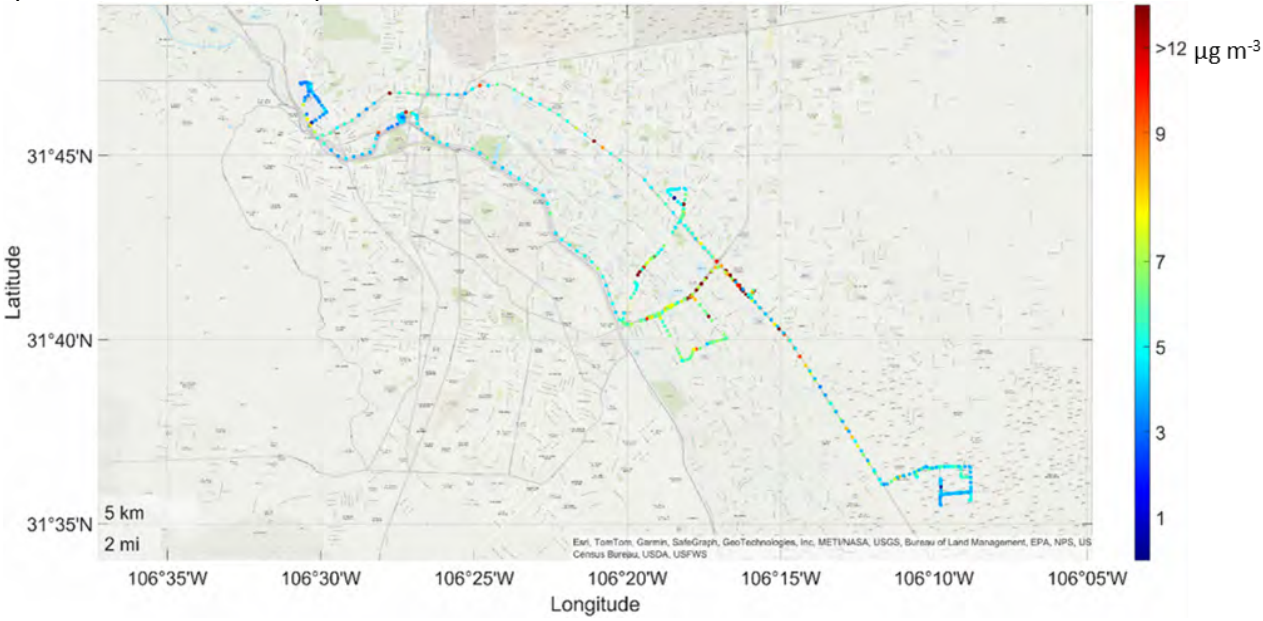

Figure 4.23. Mobile Measurement of PM_1 from 5/21/2025.

Other localized hotspots were also observed. Figure 4.24 shows a mobile track performed during the winter campaign when the background concentration is higher than usual, at around 7 µg/m³. On the western side of the mountain, near the Sunland Park area, the regional PM_1 is elevated to between 10 – 15 µg/m³. In addition, near the downtown El Paso border crossing points, total PM_1 showed spikes of over 20 µg/m³, likely due to increased traffic activities and various cooking emissions.

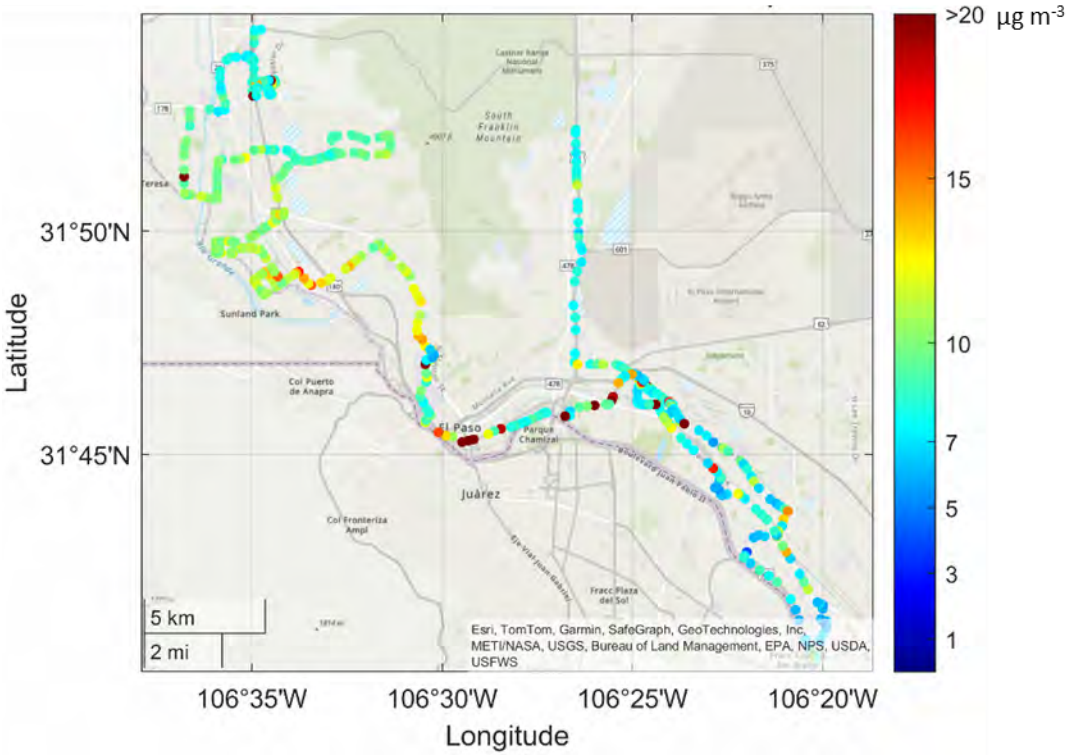

Figure 4.24. Mobile Measurement of PM_1 from 1/13/2025, 12:22 – 19:30 CST

Figure 4.25 below shows a nighttime mobile measurement track conducted from San Miguel, NM to El Paso, TX on 6/5/2025. Interestingly, despite lower planetary boundary layer height at night, the region between San Miguel and Canutillo (western side of mountain range) seems relatively clean, with ambient aerosol concentration around 3 µg/m³. However, as soon as the mobile van begins to cross Transmountain Drive to proceed to the eastern side of the mountain, PM_1 concentrations increase to around 13 µg/m³. This elevated aerosol level continues until the van reaches the UTEP site, demonstrating the elevated PM_1 levels in the El Paso region compared to other nearby regions.

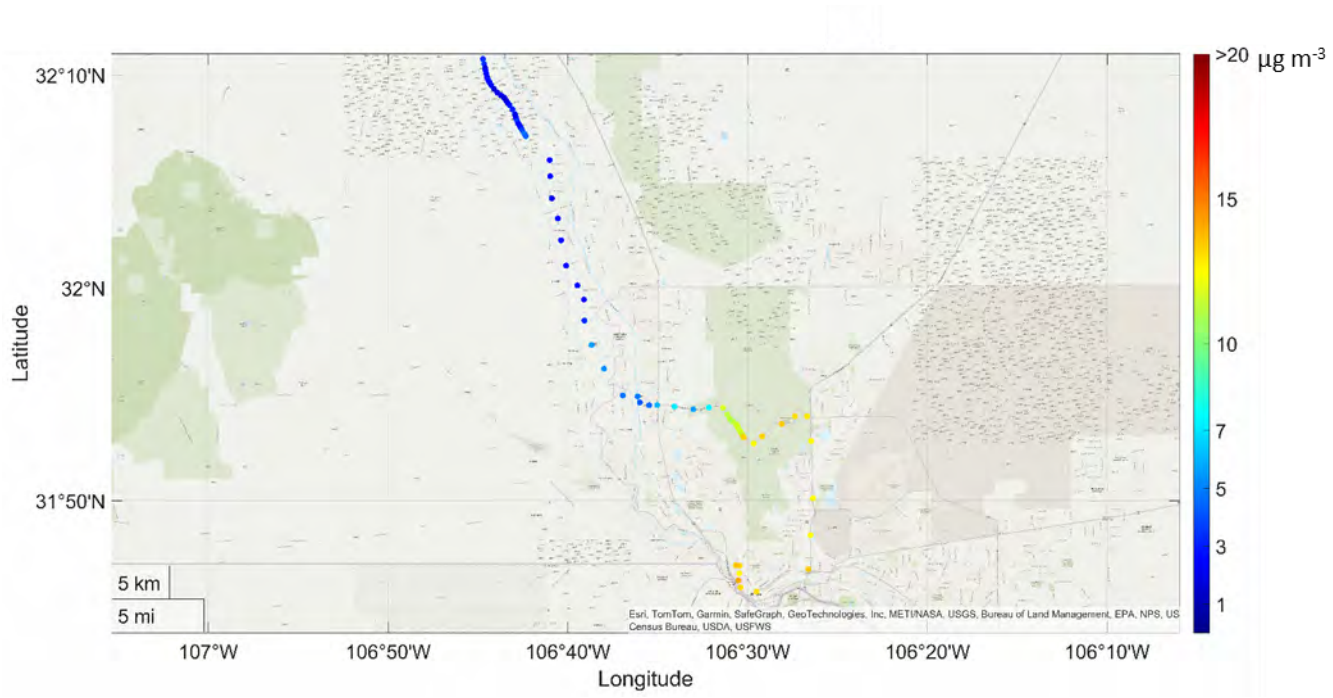

Figure 4.25: Mobile Measurement of PM_1 from 6/5/2025, 00:30 – 1:45 CST.

4.3.3 Stationary Measurements of PM_1

During both the summer and winter campaign, the team performed stationary sampling while the van was not conducting mobile measurements. For the winter campaign, the van was stationary around Bancroft Drive, where the crew stayed in an AirBnB. This location is close to the UTEP site, which was unavailable at that time. During the summer campaign, the van was stationary at the UTEP site (31°46'57.8"N, 106°30'39.3"W), near the UTEP student recreation center.

Figures 4.26, 4.27 and 4.28 below show stacked area plots of all the stationary periods during the winter and summer campaign. During the winter campaign, the highest total PM_1 concentration in this entire study exceeded 60 µg/m³ around 1:00 am CST on January 12th. In addition, the aerosol concentration consistently exceeded 10 µg/m³ between 1/5/2025 and 1/17/2025. In terms of PM composition, in addition to prominent increases in organic aerosol concentrations, inorganic aerosols such as chloride, nitrate and sulfate also periodically increased.

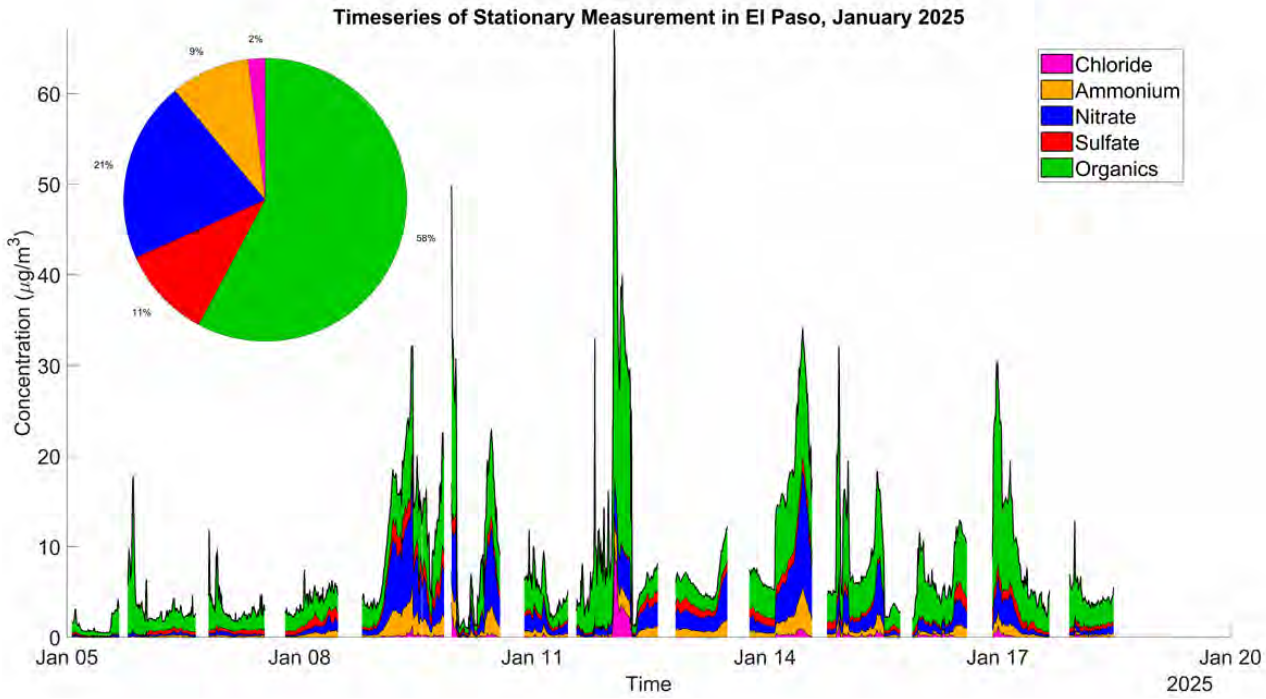

Figure 4.26: Speciated NR-PM_1 stationary measurement in January 2025.

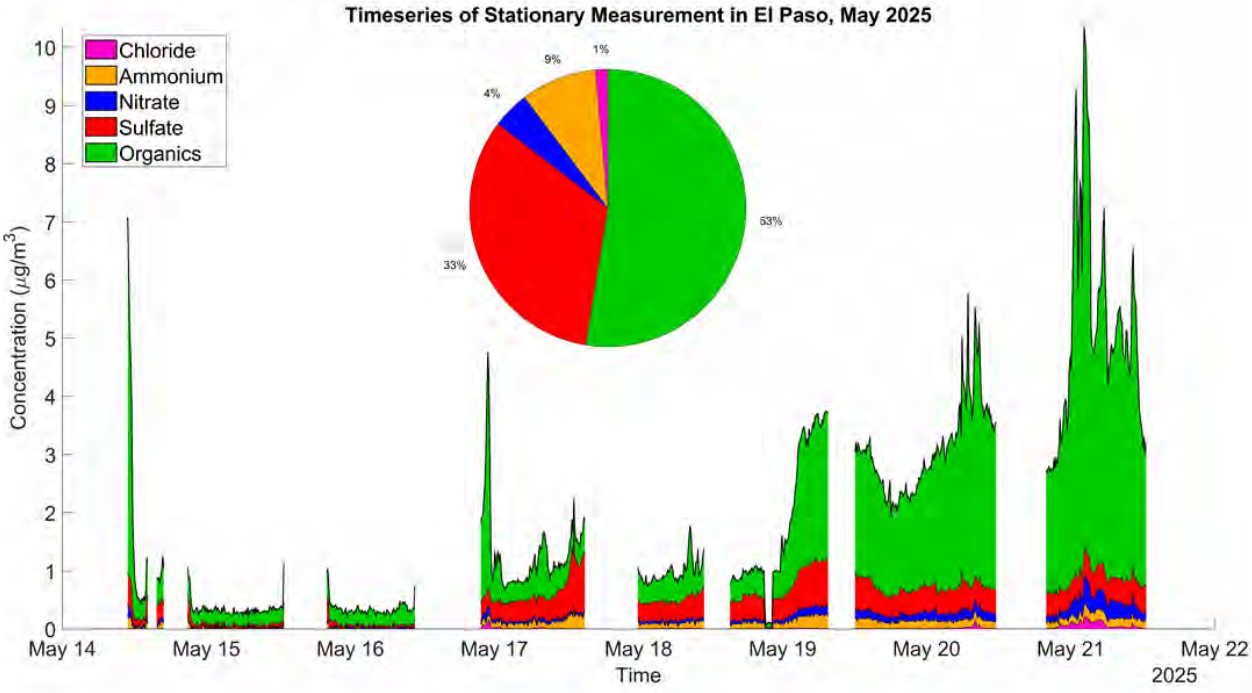

Figure 4.27: Speciated NR-PM_1 stationary measurement in May 2025.

Figure 4.27 above shows the stationary measurements taken during the first phase of the summer campaign. PM concentrations were initially low and gradually increased until the end of the campaign period. One possible explanation for this is the local dust storm during the first few days of the campaign, during which the larger dust particles lead to coagulational scavenging of the smaller particles, causing

the AMS to detect lower concentrations. Even during latter phases of the campaign, PM_1 concentrations during this time period were lower compared to the winter campaign. Sulfate aerosol was more prominent in the summer, and nitrate was more prominent in the winter. This could be due to increased ammonium nitrate evaporation due to higher summer temperatures. Even with the difference in inorganic aerosol concentrations, organic aerosol continues to contribute the majority of PM concentration in the area.

Figure 4.28 shows the stationary measurements taken during the second phase of the summer campaign, when our goal was to focus on capturing continued data with minimal interruptions. During this time period, the highest observed total PM_1 concentration was during the day on 6/5, reaching around 18 µg/m³. The overall trends during this time period seem to agree with the measurements conducted in May. Sulfate is still the major inorganic aerosol in the area, while organics still make the most contribution to the overall PM_1 concentration in the area.

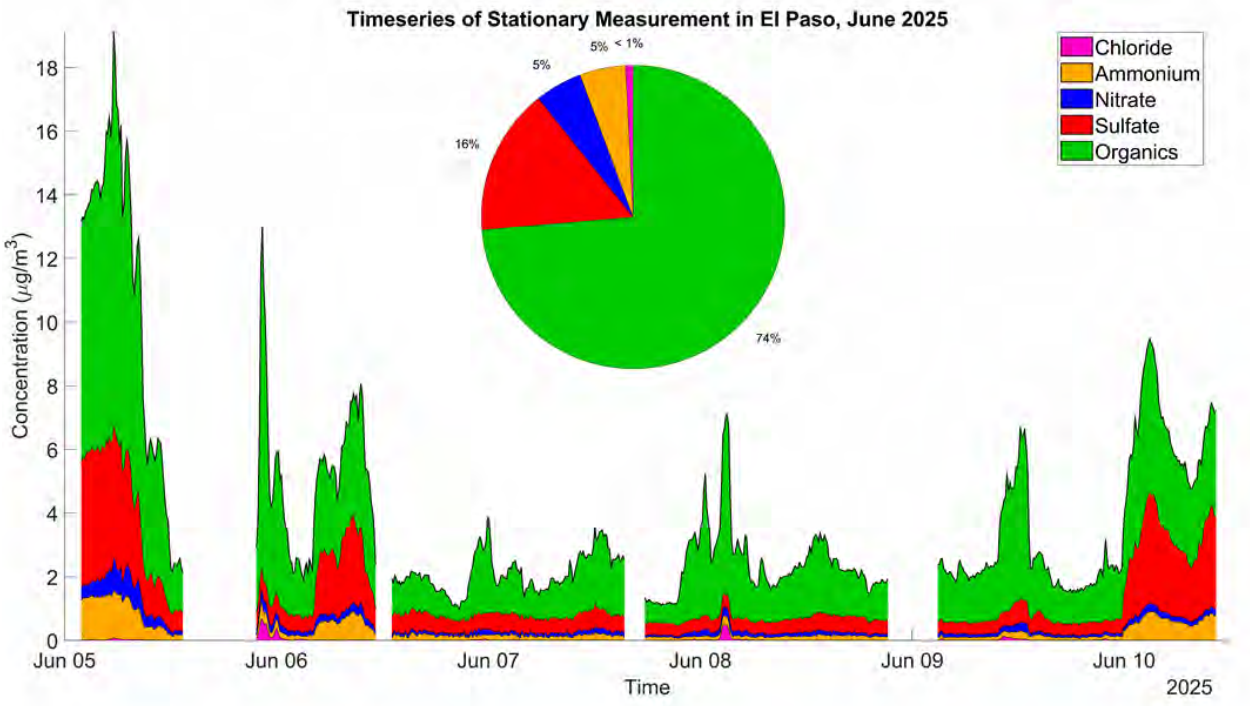

Figure 4.28: Speciated NR-PM_1 stationary measurement in June 2025.

Given the dominance of organics in the El Paso region, as seen in Figure 4.26, 4.27 and 4.28, performing source apportionment on the organic aerosols can offer deeper insights into their possible sources. Full source apportionment of the data would be invaluable and should be completed in future work. Here, the fraction of organic aerosol due to hydrocarbon-like organic aerosol (HOA) and oxygenated organic aerosol (OOA) was approximated according to the method proposed by Ng et al. (2010). This method uses the total organic mass due to ions at mass-to-charge (m/z) 44 and m/z 57 to approximate the concentrations of OOA and HOA, respectively. HOA is generally associated with primary organic aerosol emitted from combustion sources including traffic exhaust, diesel engines, and other fossil fuel sources, while OOA is associated with secondary organic aerosol, formed as a result of oxidation of volatile organic compounds. Figure 4.29 shows the time period when the vehicle was traveling along the border highway, as described in Figure 4.21. During this high-concentration period, organic aerosol has similar contributions from HOA and OOA. This suggests that oxidized secondary organic aerosol contributes as much to the organic aerosol load as local traffic emissions. The average composition analysis, shown in

the pie chart, further confirms that HOA and OOA contribute nearly equally—accounting for approximately 37% and 35% of the organic fraction, respectively.

As a suggestion for future work, full source apportionment should be conducted on the PM_1 data to provide additional insights into the possible sources of PM_1 in the El Paso region.

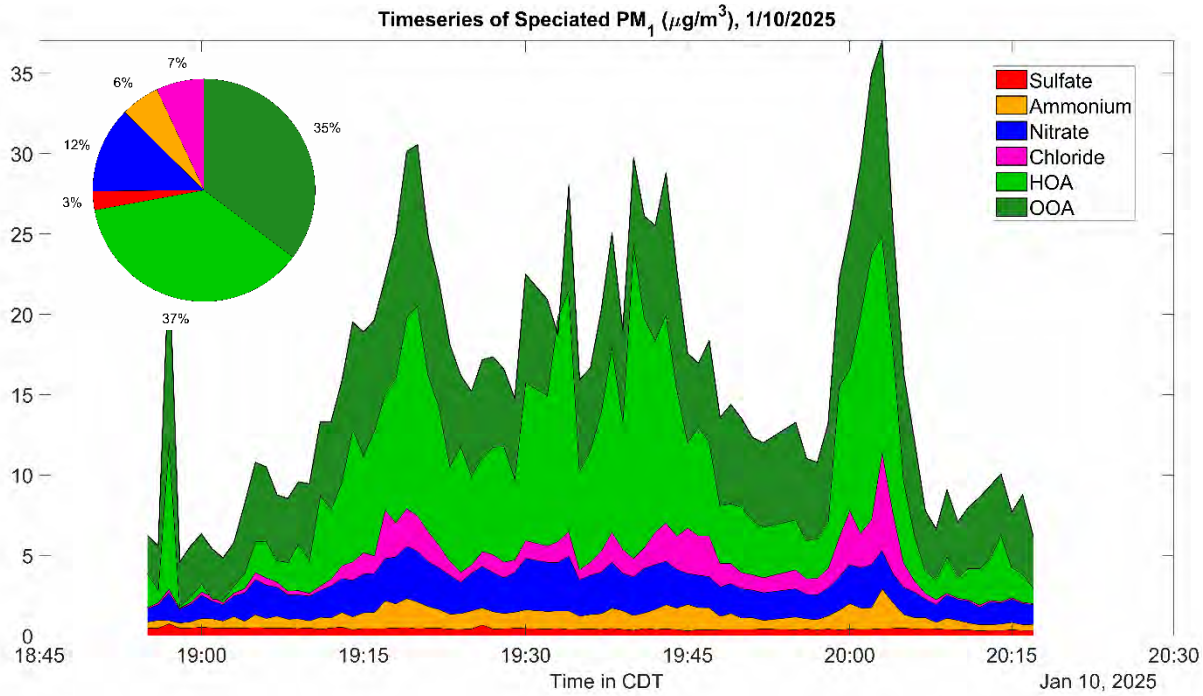

Figure 4.29. Speciated NR-PM_1 during the mobile measurements on 1/10/25, with PMF estimation.

4.3.4 Other Long-term Stationary $PM_{2.5}$ Composition Data (Chamizal Station)

Comprehensive analysis of fine particulate matter in El Paso revealed a multi-faceted mix of sources, with crustal dust emerging as a dominant component of $PM_{2.5}$ mass. To quantify source contributions more rigorously, PMF was applied to speciated $PM_{2.5}$ datasets. One dataset included several years of chemical speciation data (filter-based) from the Chamizal ambient monitoring station (which reports species such as sulfate, nitrate, organic carbon, elemental carbon, metals, etc.). The PMF analysis (using a 6-factor solution) identified the following key source factors (Figure 4.30):

Crustal Dust: This factor was characterized by high loadings of soil elements (e.g., aluminum, silicon, calcium, Fe) and accounted for the largest share of $PM_{2.5}$ mass – over 30% on average. This is consistent with El Paso's desert environment; windblown dust from both local and cross-border (Chihuahuan desert) sources is a major contributor to particulate levels.

Biomass Burning: A factor enriched in potassium (a known tracer for wood smoke) and organic carbon was attributed to biomass burning (wildfires or agricultural burning). This factor also contributed substantially to $PM_{2.5}$, especially during certain episodic events, and was one of the larger contributors after dust. For example, the PMF results suggest that wildfire smoke plumes (likely transported from elsewhere in the region) impacted El Paso at times, reflected in elevated OC and potassium in samples.

Motor Vehicles (Light-duty and Heavy-duty): Two distinct hydrocarbon combustion-related factors were resolved. One was associated with light-duty gasoline vehicle emissions (with markers like elemental carbon and some VOC-related secondary aerosol) contributing on the order of ~15% of $PM_{2.5}$, and another with heavy-duty diesel emissions (characterized by soot carbon and maybe indicators like Zn or Ba from tire/brake wear) contributing roughly 13%. Combined, vehicular emissions (traffic) are a significant source of fine particles (~28%) in the El Paso air, reinforcing that on-road transportation is an important local contributor.

Secondary Ammonium Sulfate: A factor dominated by sulfate (with associated ammonium) was identified, accounting for about 12% of $PM_{2.5}$. Sulfate in this region often originates from regional sulfur dioxide emissions that oxidize in the atmosphere. Likely contributors include coal-fired power generation and other industrial sources; the presence of this factor indicates that transported regional pollution (including possibly from Mexico's coal or oil combustion sources or distant U.S. power plants) adds a non-trivial portion of El Paso's fine PM.

Secondary Ammonium Nitrate: Another smaller secondary factor was ammonium nitrate, contributing around 3 - 4%. Nitrate formation in El Paso is relatively limited by available ammonia and occurs during cooler periods; this small contribution suggests some influence of emissions like agricultural ammonia or vehicle NO_x that form particulate nitrate, but it is a minor fraction except on a few winter days.

Other/Industrial: The 6-factor solution's remaining factor captured various industrial contributions (e.g., trace metals that did not cluster elsewhere). This was less clearly defined but could include emissions from local industries or construction activities. Its contribution was relatively small compared to the main factors above.

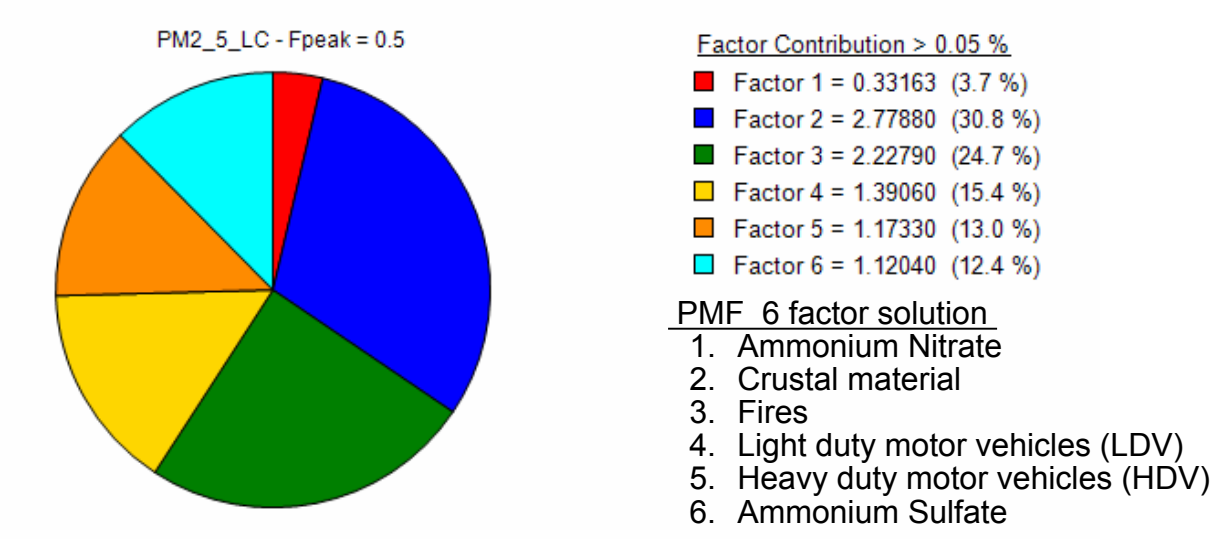

Figure 4.30. Preliminary source apportionment for $PM_{2.5}$ at Chamizal station (6-factor PMF solution).

Overall, the $PM_{2.5}$ composition is dominated by natural crustal material, with major anthropogenic contributions from vehicles and biomass combustion, and lesser contributions from regional industrial sulfate and nitrate. Figure 28 illustrates the source apportionment breakdown at the Chamizal site. These findings emphasize that mitigating $PM_{2.5}$ in El Paso will require addressing dust (which might involve measures like street sweeping, vegetative barriers, or soil stabilization to reduce fugitive dust) as well as controlling combustion sources (vehicles and seasonal burning). Notably, a large fraction of the crustal dust and some of the biomass burning influence is not locally produced but rather transported – for instance, dust events often blow in from the south or west (from Mexico or West Texas/New Mexico desert areas), and wildfire smoke can travel long distances. This means regional cooperation is needed alongside local measures.

4.4 Acute and Chronic Plumes of VOCs and PM

4.4.1 Acute smoke plumes from house fires

During the winter campaign the team observed a burning plume while driving down the transmountain pass (see Appendix Figure C1) and subsequently drove into the plume in the neighborhood. Both VOC and PM concentrations were significantly enhanced representing acute pollution episode. Such unpredictable episodes are difficult to model and their characterization in the field is practically non-existent. We therefore took an opportunity to fingerprint the plumes using our instrumentation. Figure 4.31 shows coincidental house burning plumes encountered by the mobile lab in the winter campaign. Analysis shows that such an acute pollution plume contains orders of magnitude higher concentrations of PM and VOCs than in the average El Paso background. The most enhanced compounds contained acetic acid, furanoids, nitriles and benzenoids which are typical in biomass burning plumes. Guaiacol, an oxygenated VOC is a wood smoke marker while ethylene carbonate was likely emitted from lithium-ion batteries.

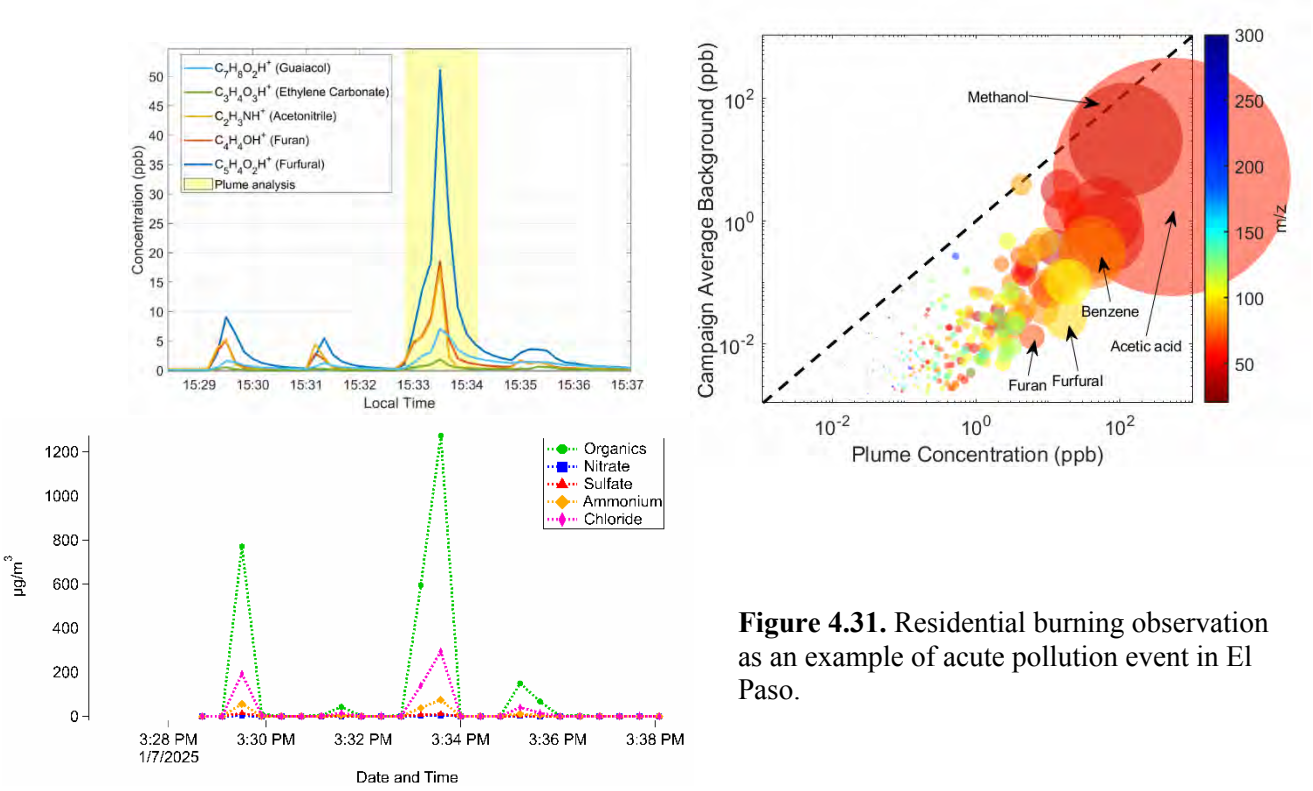

Figure 4.31. Residential burning observation as an example of acute pollution event in El Paso.

Apart from this example, multiple plumes have been fingerprinted, and their deeper analysis would expand the understanding of the sources and their variability in the region. Further analysis can be tailored to TCEQ and others' interest (sterilization facilities, Juárez plumes, train depots, storage facilities, wastewater treatments plants, landfills, etc. The VOC compositional inventory of each plume is novel and could be further analyzed in future work.

4.4.2 Juárez Plume Analysis Example

As an initial assessment to be expanded on in the final report, plumes advected from Juárez were identified for further analysis and fingerprinting of VOC and PM composition. An example of such a plume was presented in the PM Sect. 4.3.1 Figures 4.21 and 4.22. The same plume was also captured by the Vocus, and the analysis carefully dissected the plume through the enhancement fingerprinting testbed (Figure 4.32). The approach takes the bounds of the plume and subtracts the background away from the plume. As shown in the figure, the sum of VOCs was enhanced by more than a factor of 2 from 22 ppb of TVOC El Paso background. The most enhanced VOC was acetic acid (4.6 ppb), followed by methanol (3.1 ppb), ethanol (2.8 ppb), toluene (1.8 ppb), other aromatics and OVOCs pointing to fossil fuel combustion, cooking and other sources such as solvent use. More VOCs can be expanded for this and other plumes.

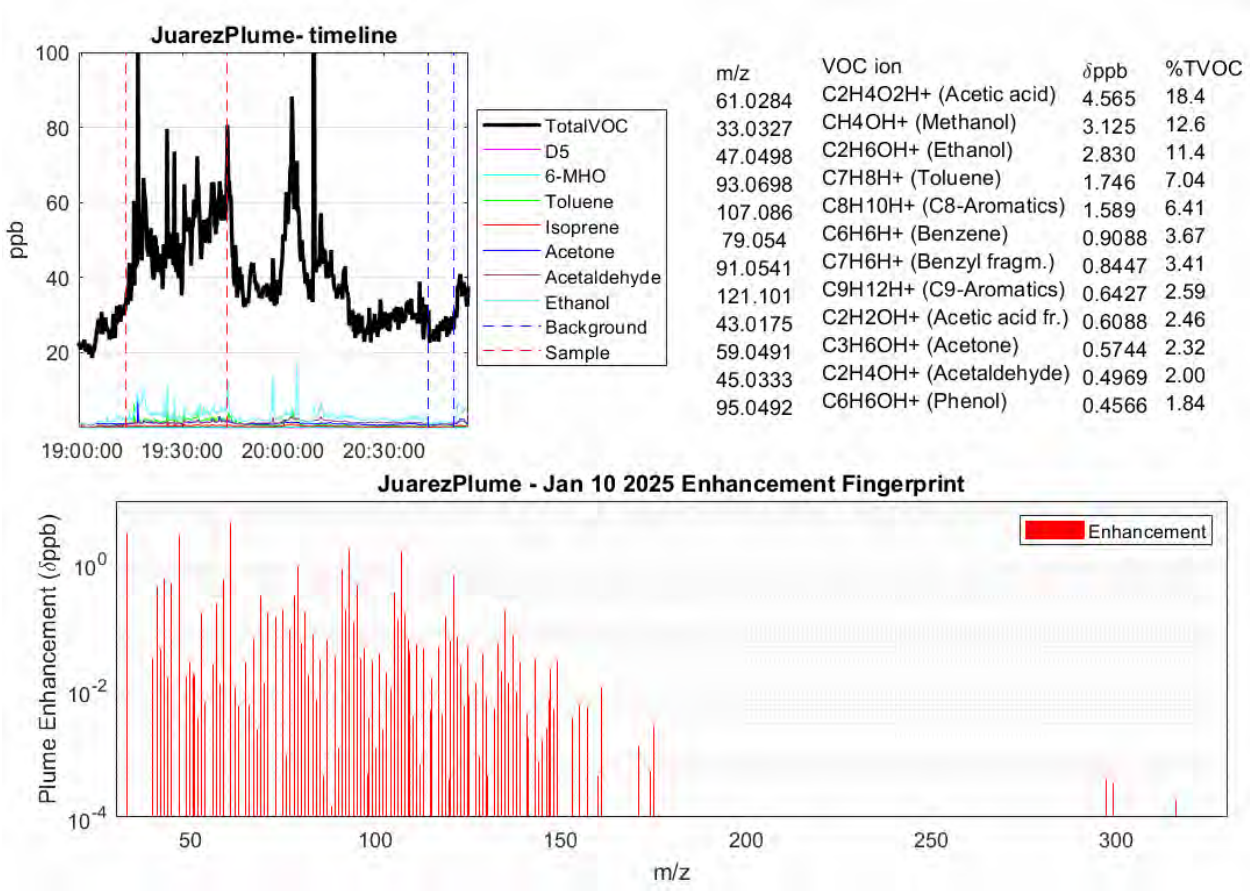

Figure 4.32. Juárez plume fingerprinting example on January 10, 2025 while driving along the border.

4.4.3 Congested Train Areas Analysis Example

The team also conducted measurements near specific sources such as warehouses and train stations/depots. As an initial simple approach, 1-km^2 square areas around the R1, R3, and R4 areas (Figure 4.33) grouped observation points in those areas which were compared to the rest of the campaign. The most enhanced compounds in those areas were consistent with $C_2H_6OH^+$ (Ethanol), $C_2H_6O_2H^+$ (Ethylene glycol), $C_3H_8O_2H^+$ (Propylene glycol), $C_4H_{10}O_2H^+$ (C4-glycol), $C_4H_6O_2H^+$ (Vinyl acetate), $C_5H_{14}O_3Si_3H^+$ (D3-siloxane), and $C_{10}H_{14}H^+$ (C10-aromatics). Some of these compounds are known to be part of cargo while others could come from rail lubricants and creosote which give off a characteristic "rail odor". Furthermore detailed insights could establish the link between evaporative emissions from specific trains stationing or moving while the mobile measurements took place.

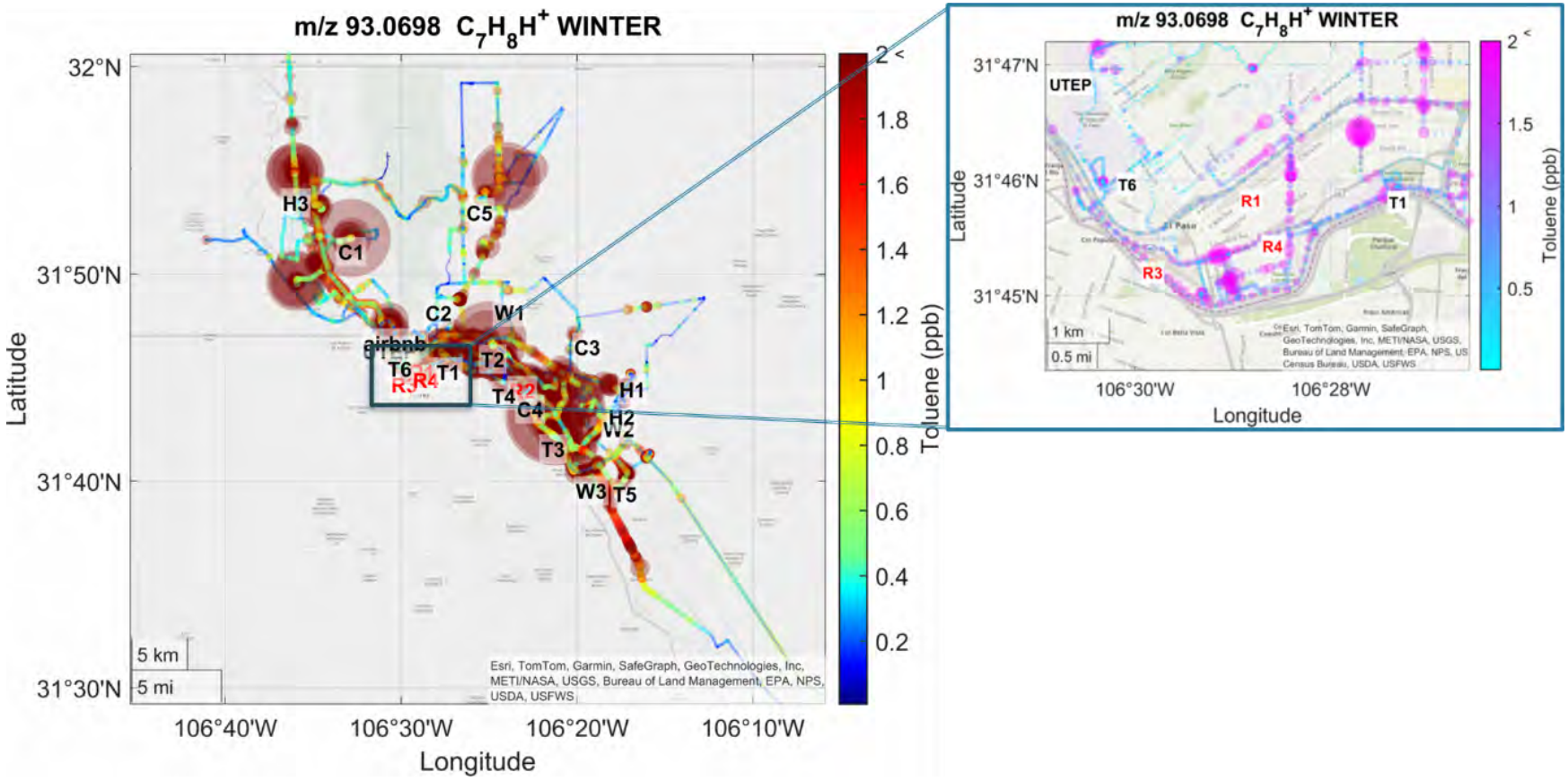

Figure 4.33. Spatial representation of heterogeneity in toluene as an example with a close-up of heavy rail areas which were investigated for prominent VOC contributions

5. CAMx Simulated Concentrations of Air Pollutants and Emission Source Contributions

5.1 Objectives

The Comprehensive Air Quality Model with Extensions (CAMx) was used to conduct air quality modeling for El Paso-Juárez for the 2022 base year. Emissions inventory information for the U.S. and Mexico was obtained from the U.S. Environmental Protection Agency (EPA) 2022v1 emissions modeling platform. Two CAMx simulations were conducted. The objective of the basecase simulation was to characterize spatiotemporal patterns of ozone (O_3), fine particulate matter ($PM_{2.5}$), and other criteria pollutants and contributing precursors. El Paso has historically had among the highest measured concentrations of toluene in Texas (Sullivan, 2023). Novel techniques for the measurement of ethylene oxide have been under development by the project team, and sources of ethylene oxide within the modeling domain were identified in the 2022v1 inventory. A second simulation was conducted for explicit modeling of toluene and ethylene oxide using the CAMx Reactive Tracer (RTRAC) algorithm to track emission source contributions. CAMx predictions were compared with observed concentrations at ambient monitoring sites in El Paso and Juárez as well as with earlier studies in the region.

5.2 CAMx Simulations and Evaluation Methods

The Texas Commission on Environmental Quality (TCEQ) is developing a 2022 modeling platform to support State Implementation Plan (SIP) revisions for ozone and fine particulate matter ($PM_{2.5}$) that will be ready in the future. Based on TCEQ recommendations for this study, a 2022 modeling platform from the EPA's Office of Air Quality Planning and Standards (OAQPS: https://registry.opendata.aws/epa-2022-modeling-platform/) was modified to develop an annual CAMx version 7.20 platform for El Paso-Juárez.

5.2.1 Basecase Simulation of Criteria Pollutants

The EPA modeling platform developed for the Community Multiscale Air Quality (CMAQ) Modeling System had 12-km horizontal resolution over the continental United States and Mexico including Chihuahua and other border states. An outer 12-km domain shown in Figure 5.1 was windowed from the EPA modeling platform and flexi-nested 4-km and 1-km grids were added. The vertical grid structure included 20 layers to an average of 2,144 m above ground level.

Meteorological fields with 12-km resolution from the Weather Research and Forecasting Model (WRF) version 4.4.2 used in the EPA modeling platform were windowed for the 12-km domain. CAMx interpolated the 12-km WRF model fields for the 4-km and 1-km flexi-nested grids during simulations for El Paso-Juárez.

The EPA modeling simulation was repeated to obtain 3-D hourly average concentrations fields from which boundary and initial conditions could be extracted for the 12-km domain.

Carbon Bond version 6 revision 5 (CB6r5) was used as the gas-phase chemical mechanism. The CF2 (coarse-fine) scheme with the SOAP2.2 module for secondary organic aerosol chemistry/partitioning and ISORROPIA for partitioning of inorganic aerosol constituents were used as the aerosol chemistry options. Dry deposition was modeled with the Zhang scheme.

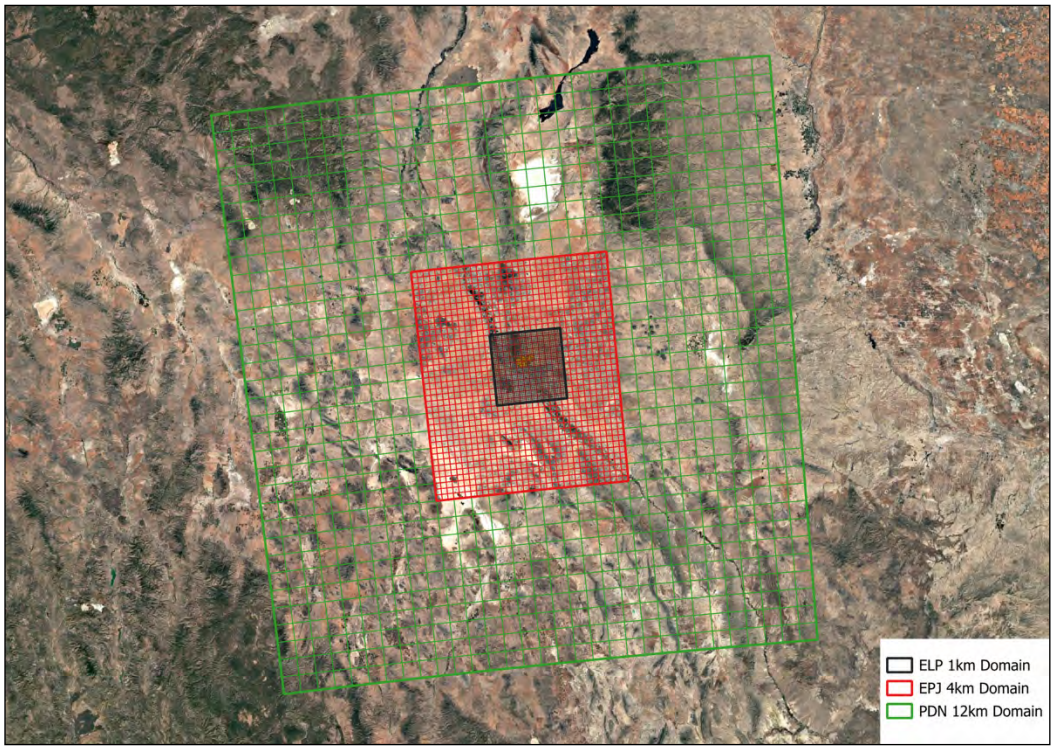

Figure 5.1. CAMx horizontal grid configuration for El Paso-Juárez including a 12-km regional domain (green) and 4-km (red) and 1-km (black) flexi-nested grids.

Emissions for point, nonpoint, on-road and non-road mobile, fire, and biogenic sources were based on the EPA's 2022v1 emissions modeling platform (https://gaftp.epa.gov/Air/emismod/2022/v1/). Methods used by Eyth et al. (2025) to prepare the inventory are summarized in Table A.1. Emissions estimates for most source categories in Chihuahua and other border states were developed in collaboration by the EPA and Mexico's Secretariat of Environment and Natural Resources (SEMARNAT) for the 2018 base year, with the exceptions of emissions from fire and on-road mobile sources. It should be noted that changes in factors such as population and industrial activity (e.g., Maldonado et al., 2025) may have influenced emissions in Juárez between 2018 and 2022.

Emissions for the 12-km domain were windowed from EPA's CAMx-ready emissions files. Ancillary chemical speciation, temporal allocation, and spatial allocation files and scripts for the Sparse Matrix Operator Kernel Emissions (SMOKE) v.5.0 emission processing system provided by EPA were used to prepare model-ready emissions for the 4-km and 1-km grids. It was not necessary to modify the temporal allocations of emissions. Spatial surrogates for processing emissions with 4-km resolution were adopted from the EPA 2022v1 emissions platform. Surrogates for processing emissions with 1-km resolution were generated using the Surrogate Tools DB v1.3 (https://www.cmascenter.org/surrogate_tools_db/). As an alternative to running EPA's MOtor Vehicle Emission Simulator (MOVES), county-level on-road emissions in the U.S. and at the municipality-level emissions in Mexico were allocated within the 4-km and 1-km grids by applying spatial surrogates for roadways. Emissions chemically speciated for the

CB6R7_AE7 chemical mechanism used in CMAQ were mapped to CB6r5_CF2 species used in CAMx. Emission totals for criteria pollutants and precursors for the 4-km and 1-km domains are summarized in Tables 5.1 and 5.2, respectively.

5.2.2 RTRAC Simulation of Toluene and Ethylene Oxide

RTRAC is a probing tool that was implemented in a second CAMx simulation to explicitly model toluene and ethylene oxide, which were not represented explicitly in the CB6r5 chemical mechanism of the core model. RTRAC simulated emissions, dispersion, chemistry, and dry deposition and allowed tagging of emission source contributions to toluene and ethylene oxide concentrations in El Paso and Juárez. Rate constants were provided in RTRAC for the thermal reactions of ethylene oxide (Wallington et al., 1988) and toluene (Yarwood et al, 2022; Tuite et al., 2023) with hydroxyl radical (OH). Dry deposition in RTRAC was based on the Zhang scheme consistent with the core model. The SMOKE processing stream provided in the EPA 2022v1 emissions modeling platform had the capability to generate model-ready toluene and ethylene oxide emissions. Emissions of toluene and ethylene oxide from area and point sources in Mexico were not available. Fire emissions were not reprocessed to separate emissions of toluene and other monoalkyl aromatics in this study. For both cases, the CB6 lumped TOL species was used as a surrogate for explicit toluene (TOLU) emissions. Toluene and ethylene oxide sources and associated emissions used in the RTRAC simulation for the 4-km and 1-km grids are shown in Tables 5.1 and 5.2.

5.2.3 Model Evaluation Methods

5.2.3.1 Ambient Monitoring Networks

CAMx predictions of ozone, $PM_{2.5}$, and toluene were evaluated against measurements at ambient monitoring stations in El Paso and Juárez obtained from the TCEQ and Mexico's SEMARNAT and National Institute for Ecology and Climate Change (INECC). Ethylene oxide is not routinely measured at any of these sites.

Figure 5.2 shows continuous ambient monitoring stations (CAMS) in El Paso operated by the TCEQ or Center for Energy and Environmental Resources (CEER) at The University of Texas at Austin for time periods between 2021 and 2024. An additional site at The University of Texas El Paso (C12) was deactivated on November 16, 2021, prior to the 2022 base year of the CAMx modeling and is not shown. Criteria pollutants measured hourly in the region are shown in Table 5.3 and include ozone (O_3), $PM_{2.5}$ and coarse (PM_{10}) particulate matter, NO_x, SO_2, and CO. Volatile organic compounds (VOCs) have been measured hourly at Chamizal (C41) and until late August 2023 at Delta Drive (C1011) using automated gas chromatographs (auto-GCs) and as 24-hour average concentrations every 6th day at Womble (C123) and Socorro Hueco (C49) by canister sampling and laboratory gas chromatograph-mass spectrometer analysis. Toluene is measured at all auto-GC and canister stations.

Table 5.1. Emissions of selected criteria pollutants/precursors and air toxics (tpd) in 2022 within the El Paso-Juárez 4-km grid.

Source Category and Subcategory (ID) Emissions Totals: 4-km Grid Only	Basecase Simulation Emissions (tpd)					RTRAC Simulation Emissions (tpd)	
	NOx	VOC	$PM_{2.5}$	CO	SO_2	Explicit Toluene (TOLU) or CB6 TOL Surrogate	Ethylene Oxide
Point Total	51.38	6.11	3.47	63.13	0.78	0.365	0.0014
Electric Generating Units (ptegu)	6.68	0.46	0.31	1.75	0.04	0.007	0.0000
Point Source Oil and Gas (pt_oilgas)	1.65	0.02	0.02	0.31	0.01	0.001	0.0000
Aircraft and Ground Support Equipment (airports)	0.67	0.29	0.05	1.78	0.07	0.003	0.0000
Non-IPM Sector (ptnonipm)	2.84	2.05	0.31	2.25	0.45	0.062	0.0014
Canada/Mexico Point Sources (canmex_pt)	39.54	3.30	2.78	57.04	0.20	0.292 (TOL)	0.0000
Nonpoint Total	8.99	93.26	8.96	25.67	1.04	2.071	0.0000
Area Fugitive Dust (afdust)	0.00	0.00	4.22	0.00	0.00	0.000	0.0000
Livestock (livestock)	0.00	0.27	0.00	0.00	0.00	0.000	0.0000
Agricultural Fertilizer (fertilizer)	0.00	0.00	0.00	0.00	0.00	0.000	0.0000
Nonpoint Oil and Gas (np_oilgas)	0.00	0.00	0.00	0.00	0.00	0.000	0.0000
Residential Wood Combustion (rwc)	0.17	1.36	1.61	10.89	0.03	0.019	0.0000
Solvents (np_solvents)	0.00	17.96	0.00	0.00	0.00	0.549	0.0000
Open Burning (openburn)	0.13	0.29	0.55	4.35	0.04	0.004	0.0000
Nonpoint (nonpt)	5.64	4.37	1.21	5.01	0.34	0.043	0.0000
Canada/Mexico Agricultural (canmex_ag)	0.00	0.00	0.08	0.00	0.00	0.000	0.000
Canada/Mexico Area (canmex_area)	3.05	69.02	1.28	5.42	0.62	1.456 (TOL)	0.0000
On-road Total	78.35	30.64	1.51	321.98	1.13	3.111	0.0000
On-road Mobile (on-road)	16.39	5.66	0.20	108.64	0.06	0.888	0.0000
Mexico On-road (mexico_on-road)	61.96	24.98	1.31	213.34	1.06	2.222	0.0000
Non-road Total	6.34	3.21	0.39	61.45	0.01	0.321	0.0000
Rail Locomotives (rail)	3.20	0.07	0.08	0.69	0.00	0.003	0.0000
Non-road Equipment (non-road)	3.14	3.14	0.32	60.76	0.00	0.318	0.0000
Fires: U.S. and Mexico (ptfire-wild, ptfire-rx, ptagfire, ptfire_othna)	0.13	0.73	0.31	3.03	0.03	0.012 (TOL)	0.0000
Biogenic: U.S. and Mexico (beis)	2.64	30.13	0.00	7.15	0.00	0.000	0.0000

Table 5.2. Emissions of selected criteria pollutants/precursors and air toxics (tpd) in 2022 within the El Paso-Juárez 1-km grid.

Source Category and Subcategory (ID) Emissions Totals: 1-km Grid	Basecase Simulation Emissions (tpd)					RTRAC Simulation Emissions (tpd) and Emission Group	
	NOx	VOC	$PM_{2.5}$	CO	SO_2	Explicit Toluene or CB6 TOL Surrogate	Ethylene Oxide
Point Total	23.27	5.48	0.94	26.98	0.65	0.327	0.0001
Electric Generating Units (ptegu)	6.50	0.46	0.24	1.65	0.03	0.007	0.0000
Point Source Oil and Gas (pt_oilgas)	0.77	0.01	0.01	0.11	0.01	0.000	0.0000
Aircraft and Ground Support Equipment (airports)	0.48	0.22	0.03	1.07	0.05	0.001	0.0000
Non-IPM Sector (ptnonipm)	2.77	2.04	0.28	2.21	0.45	0.062	0.0001
Canada/Mexico Point Sources (canmex_pt)	12.74	2.75	0.38	21.94	0.11	0.257 (TOL)	0.0000
Nonpoint Total	6.40	52.13	4.22	13.61	0.36	1.142	0.0000
Area Fugitive Dust (afdust)	0.00	0.00	1.74	0.00	0.00	0.000	0.0000
Livestock (livestock)	0.00	0.02	0.00	0.00	0.00	0.000	0.0000
Agricultural Fertilizer (fertilizer)	0.00	0.00	0.00	0.00	0.00	0.000	0.0000
Nonpoint Oil and Gas (np_oilgas)	0.00	0.00	0.00	0.00	0.00	0.000	0.0000
Residential Wood Combustion (rwc)	0.04	0.28	0.33	2.19	0.01	0.004	0.0000
Solvents (np_solvents)	0.00	13.77	0.00	0.00	0.00	0.391	0.0000
Open Burning (openburn)	0.07	0.18	0.30	2.79	0.03	0.000	0.0000
Nonpoint (nonpt)	4.55	2.06	0.85	4.08	0.25	0.027	0.0000
Canada/Mexico Agricultural (canmex_ag)	0.00	0.00	0.00	0.00	0.00	0.000	0.0000
Canada/Mexico Area (canmex_area)	1.74	35.81	1.00	4.55	0.07	0.719 (TOL)	0.0000
On-road Total	54.52	24.45	0.99	229.85	0.74	2.419	0.0000
On-road Mobile (on-road)	10.00	4.06	0.12	73.94	0.05	0.593	0.0000
Mexico On-road (mexico_on-road)	44.52	20.39	0.87	155.91	0.70	1.826	0.0000
Non-road Total	3.80	2.41	0.26	49.47	0.00	0.243	0.0000
Rail Locomotives (rail)	1.61	0.04	0.04	0.35	0.00	0.001	0.0000
Non-road Equipment (non-road)	2.19	2.37	0.22	49.13	0.00	0.242	0.0000
Fires: U.S. and Mexico (prfire-wild, ptfire-rx, ptagfire, ptfire_othna)	0.02	0.07	0.04	0.51	0.01	0.001	0.0000
Biogenic: U.S. and Mexico (beis)	0.46	4.53	0.00	1.17	0.00	0.000	0.0000
TOTAL	108.46	94.10	9.35	469.49	1.85	4.726	0.0001

Figure 5.2. Ambient monitoring sites in El Paso (blue) and Juárez (red).

Table 5.3. Pollutants measured between 2021-2024 at ambient monitoring stations in El Paso and Juárez.

	Site Name (Abbreviation): CAMS #	O_3	$PM_{2.5}$	PM_{10}	VOC	NO_x	SO_2	CO	H_2S
El Paso	Ojo de Aqua (ojoa): C1021	√		√				√	
	Skyline Park (skln): C72	√							
	Van Buren (vbur): C693			√					
	Womble (wmbl): C123				√§				
	Ivanhoe (ivho): C414	√		√					
	Chamizal (chmz): C41	√	√	√	√¥	√	√	√	
	Ascarate Park SE (ascr): C37	√	√			√			
	Mimosa (mmsa): C418			√					
	Lower Valley (lval): C36								√
	Socorro Hueco (shuc): C49	√		√	√§				
	Delta Drive (dlt): C1011*				√¥	√			
Juárez	Institute for Engineering and Technology (IIT)	√	√	√		√	√	√	
	North Wastewater Treatment Plant (PTN)	√							

* Operated from April 2021-Sept. 2022 and May 2023-Aug. 2023; Deactivated on August 29, 2023
§ Canister sampling with laboratory gas chromatograph-mass spectrometer (GC-MS) analysis
¥ Auto-GC sampling

The Municipio de Juárez and the Institute for Engineering and Technology (IIT) at the Autonomous University of Ciudad Juárez (UACJ) conduct ambient monitoring. Data are reported to Mexico's SEMARNAT and INECC. Near real-time unvalidated data for Juárez can be viewed via the National Air Quality Information System (SINAICA) platform (https://sinaica.inecc.gob.mx). The Air Quality Indicator Consultation System (SCICA) portal was identified in Mexico's 2022 national air quality report (INECC, 2022) as the source for validated data: http://scica.inecc.gob.mx/exec/addl. Hourly measurements of ozone, $PM_{2.5}$, and other criteria pollutants shown in Table 5.3 were available for the Institute for Engineering and Technology site (ref. Figure 5.2) in Juárez during 2022. Only hourly ozone observations were available for the North Wastewater Treatment Plant (PTN) site during 2022. The national air quality report for 2022 does not indicate any VOC measurements are made in Chihuahua. Observational datasets for Juárez were not found for years beyond 2022.

5.2.3.2 Statistical Performance Measures and Benchmarks

CAMx predicted maximum daily 8-hour average (MDA8) O_3 and 24-hour average $PM_{2.5}$ concentrations for the 2022 base year were evaluated against observations using three statistical metrics, normalized mean bias (NMB), normalized mean error (NME), and correlation coefficient, and associated performance goals and criteria from Emery et al. (2016) shown in Table 5.4. Model predictions of hourly average toluene concentrations at the Chamizal and Delta Drive auto-GC sites were also evaluated, but performance benchmarks have not been established for toluene and other air toxics.

Table 5.4. Statistical metrics used in the evaluation of CAMx predicted ozone and $PM_{2.5}$ concentrations.

Statistical Measure	Equation	Performance Goal	Performance Criteria
Normalized Mean Bias (%), NMB		MDA8 O_3 $< \pm$ 5% 24-hr $PM_{2.5} < \pm$ 10%	MDA8 O_3 $< \pm$ 15% 24-hr $PM_{2.5} < \pm$ 30%
Normalized Mean Error (%), NME		MDA8 O_3 $< \pm$ 15% 24-hr $PM_{2.5} < \pm$ 35%	MDA8 O_3 $< \pm$ 25% 24-hr $PM_{2.5} < \pm$ 50%
Correlation Coefficient		MDA8 O_3 > 0.75 24-hr $PM_{2.5} > 0.70$	MDA8 O_3 > 0.50 24-hr $PM_{2.5} > 0.40$

5.2.3.3 Distributions of Base Year Modeled and Multiyear Observed Concentrations

Box and whisker plots examined CAMx predicted MDA8 ozone, 24-hour average $PM_{2.5}$, and 1-hour average toluene concentrations for the 2022 base year as well as observations at individual sites from 2021 through 2024. The plots show statistics for the 5th, 25th, 50th, 75th, 95th, 99th percentile and maximum concentrations. They were evaluated for consistency with and additional understanding of trends in the statistical performance benchmarks for the model described above and were also used to assess

interannual trends in measured concentrations. Contour plots were developed to show spatial patterns of selected CAMx predicted and observed percentile concentrations.

5.3 Results and Discussion

5.3.1 Ozone

Table 5.5 indicates that statistical performance measures for CAMx predicted MDA8 ozone concentrations are in relatively good agreement with observations in El Paso and Juárez. Annual NMB statistics were within ±8.5%, achieving the performance criteria of ±15%; three sites, Chamizal, Ascarate Park, and Skyline Park also achieved the performance goal of ±5%. With the exception of the annual NME at IIT (16.4%), all sites achieved the NME performance goal of ± 15%. Annual correlation coefficients at six of the eight sites achieved the performance goal of 0.75, and all sites achieved the performance criteria of 0.50.

Quarterly statistics varied for individual sites as well as between different sites. Quarterly NMB statistics across all sites, with the exceptions of Q3 at Socorro Hueco (-15.7%) and Ojo de Aqua (-18.4%) and Q3 (-20.6%) and Q4 (-18.0%) at IIT, achieved the performance criteria of ±15%. Quarterly NME and r statistics across all sites achieved the performance criteria of ± 25% and 0.5, respectively, with many also achieving the performance goals.

Distributions of CAMx predicted and observed MDA8 ozone percentile concentrations during 2022 shown in the box and whisker plots in Figure 5.3 were consistent with the evaluation of the statistical performance measures. Contour plots of observed and model simulated 75th and 99th percentile ozone concentrations are shown as examples in Figure 5.4. The model tends to underestimate 75th and 95th percentile MDA8 ozone concentrations at Socorro Hueco, Ojo de Agua, and IIT during 2022. This is primarily during Q3 as shown in Table 5.5 as well as time series for the three sites in Appendix B.

Distributions of observed MDA8 ozone concentrations for stations operating between 2021-2024 in El paso and Juárez are shown in Figure 5.3 to examine interannual trends. Median (50th percentile) MDA8 ozone concentrations ranged between 40 to 50 ppb and did not show substantial interannual variability at individual sites. Between 2021 and 2024, measured 99th percentile and maximum MDA8 exhibited upward trends. At Chamizal (74 ppb), Ascarate Park (73 ppb), Socorro Hueco (76 ppb), Skyline Park (77 ppb), and Ojo de Aqua (75 ppb), 99th percentile concentrations exceeded 70 ppb in 2024, and maximum observed values were among the highest of the four years. Sullivan (2023) also found increases in measured 4th highest MDA8 ozone concentrations at Ascarate Park, Socorro Hueco, Skyline Park, and Ojo de Aqua between 2021 and 2022. In an earlier study, Ramboll (2021) noted an upward trend in the El Paso County maximum ozone design value between 2016-2020.

Table 5.5. Annual and quarterly model performance metrics for MDA8 ozone concentrations at El Paso and Juárez sites in 2022.

Site	2022 Time Period	Number	NMB MDA8 Ozone Goal < ± 5% Criteria < ± 15%	NME MDA8 Ozone Goal < ± 15% Criteria < ± 25%	r MDA8 O_3 Goal > 0.75 Criteria > 0.5
Ivanhoe	**Annual**	**360**	**8.2**	**13.2**	**0.82**

(El Paso)	Q1 (Jan - Mar)	90	12.5	15.4	0.55
	Q2 (Apr - June)	90	15.0	16.5	0.74
	Q3 (July - Sept)	89	0.3	10.6	0.78
	Q4 (Oct - Dec)	91	5.1	9.8	0.84
Chamizal (El Paso)	**Annual**	**348**	**-3.7**	**10.8**	**0.85**
	Q1 (Jan - Mar)	89	-3.5	11.0	0.61
	Q2 (Apr - June)	87	2.5	8.4	0.75
	Q3 (July - Sept)	82	-8.2	11.7	0.81
	Q4 (Oct - Dec)	90	-6.6	13.0	0.80
Ascarate Park (El Paso)	**Annual**	**313**	**3.0**	**12.1**	**0.83**
	Q1 (Jan - Mar)	48	1.0	10.1	0.40
	Q2 (Apr - June)	89	9.9	14.2	0.65
	Q3 (July - Sept)	88	-5.4	10.6	0.82
	Q4 (Oct - Dec)	88	6.9	12.6	0.83
Socorro Hueco (El Paso)	**Annual**	**362**	**-6.5**	**11.8**	**0.82**
	Q1 (Jan - Mar)	90	-0.9	8.8	0.67
	Q2 (Apr - June)	90	-0.9	9.1	0.73
	Q3 (July - Sept)	91	-15.7	17.0	0.77
	Q4 (Oct - Dec)	91	-7.4	11.1	0.86
Skyline Park (El Paso)	**Annual**	**319**	**-2.4**	**12.7**	**0.68**
	Q1 (Jan - Mar)	83	-0.1	10.8	0.47
	Q2 (Apr - June)	91	6.3	14.3	0.46
	Q3 (July - Sept)	91	-9.4	12.1	0.73
	Q4 (Oct - Dec)	54	-9.0	13.8	0.70
Ojo de Aqua (El Paso)	**Annual**	**330**	**-7.3**	**13.0**	**0.78**
	Q1 (Jan - Mar)	67	-0.1	7.7	0.50
	Q2 (Apr - June)	83	-0.1	10.9	0.46
	Q3 (July - Sept)	91	-18.4	18.5	0.77
	Q4 (Oct - Dec)	89	-4.7	11.4	0.85
North Wastewater Treatment Plant (Juárez)	**Annual**	**327**	**-5.7**	**12.1**	**0.85**
	Q1 (Jan - Mar)	75	-4.3	11.2	0.65
	Q2 (Apr - June)	84	-3.5	9.8	0.71
	Q3 (July - Sept)	89	-11.9	14.9	0.77
	Q4 (Oct - Dec)	79	-0.3	12.1	0.78
Institute for Engineering and Technology (Juárez)	**Annual**	**297**	**-8.4**	**16.4**	**0.67**
	Q1 (Jan - Mar)	70	1.5	9.5	0.53
	Q2 (Apr - June)	90	4.6	14.1	0.54
	Q3 (July - Sept)	85	-20.6	20.7	0.81
	Q4 (Oct - Dec)	52	-18.0	19.1	0.67

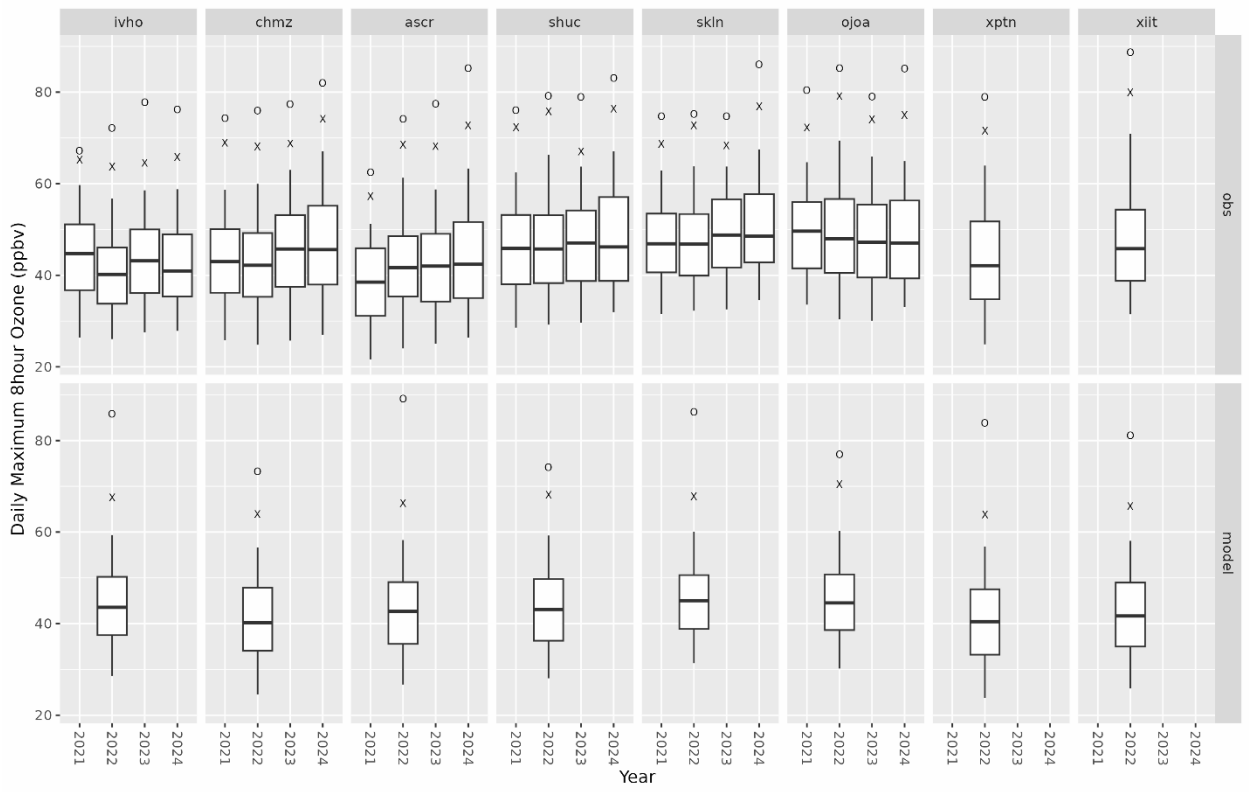

Figure 5.3. Observed and CAMx simulated MDA8 ozone concentrations by year at Chamizal, Ojo de Agua, Skyline, Ivanhoe, Ascarate Park, and Socorro Hueco in El Paso, and North Wastewater Treatment Plant and Institute for Engineering and Technology in Juárez. The box shows the median and interquartile range, whiskers extend to 5th and 95th percentiles, x indicates 99th percentile, and o indicates maximum concentration.

(a) (b)

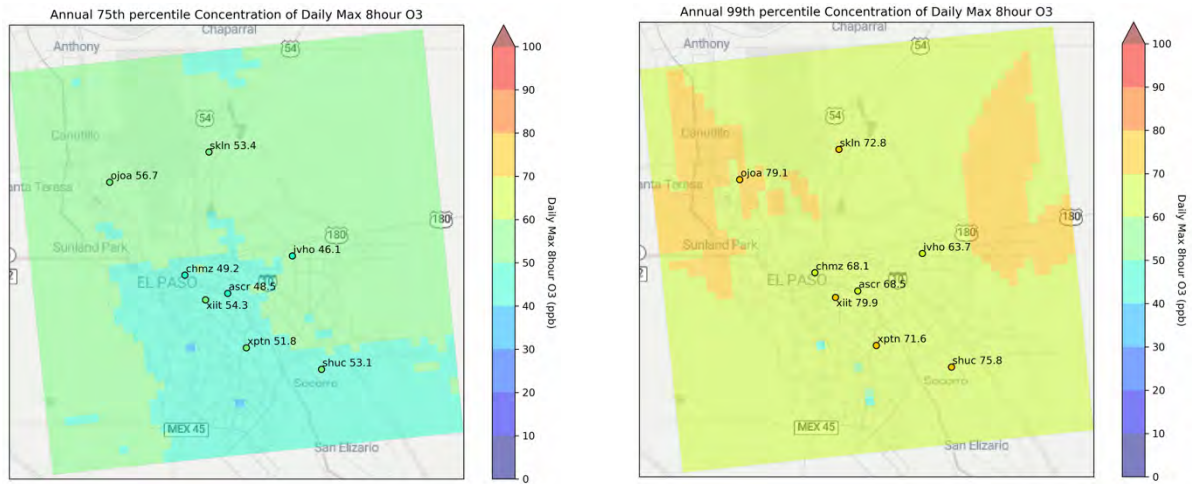

Figure 5.4 Observed and CAMx simulated (a) 75th and (b) 99th percentile MDA8 ozone concentrations within the 1-km domain.

Maximum observed MDA8 concentrations at IIT (89 ppb) and PTN (79 ppb) during 2022, shown in Figure 5.3, matched those reported by INECC (2022). The regulatory limit in Mexico in 2022 was based on the annual maximum MDA8 concentration ≤ 65 ppb and currently is ≤60 ppb. Neither site in Juárez was in compliance with the levels of these standards in 2022.

Ozone pollution roses in Figure 5.5 show the magnitude and associated wind direction occurrence for non-exceedance (< 70 ppb) versus exceedance (≥ 70 ppb) days based on measured concentrations from 2021 through 2024 and CAMx predictions for the 2022 base year at El Paso CAMS stations. Both modeled and observed pollution roses indicate that exceedance days are frequently associated with prevailing easterly (90º) through west-southwesterly (240º) winds in contrast to more pronounced westerly winds on non-exceedance days at most sites. Results for Skyline Park and Chamizal in this study were consistent with those of Ramboll (2022) during September 2016 through 2020. Karle et al. (2021) found that synoptic and local winds influenced ozone enhancements in El Paso. Radar wind profiler data at Socorro Hueco during 2016 through 2018 suggested high ozone episodes were largely associated with surface winds between ~55º through 185 º from channeling along local topography of the Rio Grande Valley; westerly winds were the predominant climatological direction aloft attributed to synoptic conditions to the west and northwest of El Paso-Juárez. HYSPLIT back trajectories initiated from central of El Paso on high ozone days showed greater densities from the southeast and east (Karle et al, 2021).

5.3.2 $PM_{2.5}$

Only two sites, Chamizal in El Paso and IIT in Juárez, had $PM_{2.5}$ measurements available in 2022 for evaluation of CAMx simulated concentrations. NMB statistics in Table 5.6 show that the model underestimated observed 24-hour average $PM_{2.5}$ concentrations at Chamizal. NMB statistics achieved the performance criteria of ± 35% during Q1 (-26.5%) and Q4 (-33.4%) but not during other quarters or annually. The annual NME statistic (47.1%) at Chamizal met the performance criteria of ± 50%. This criterion was met by NME statistics for Q1 (35.8%) and Q4 (40.8%) but not during the spring (Q2) and summer (Q3) months. Annual and quarterly correlation coefficients all achieved the performance criteria of 0.40.

Modeled distributions of 24-hour $PM_{2.5}$ concentrations across all percentiles underestimated measured concentrations during 2022. Similar to ozone, observed 95th and 99th percentile and maximum 24-hour average $PM_{2.5}$ concentrations at Chamizal in Figure 5.6 showed an upward trend between 2022 and 2024. Fiftieth and 75th percentile observed concentrations at Ascarate Park were higher than at Chamizal in 2024 with relatively comparable 95th (~ 25 μg/m^3) and 99th (~37 μg/m^3) percentile concentrations.

Model performance was particularly challenged at the IIT site in Juárez, exhibiting a strong underprediction bias. The regulatory limit in Mexico for 24-hour average $PM_{2.5}$ concentrations in 2022 was based on the 99th percentile concentration ≤ 41 μg/m^3 and is currently ≤ 33 μg/m^3. The observed value of 60 μg/m^3 during 2022 shown in Figure 5.6 was substantially above these levels.

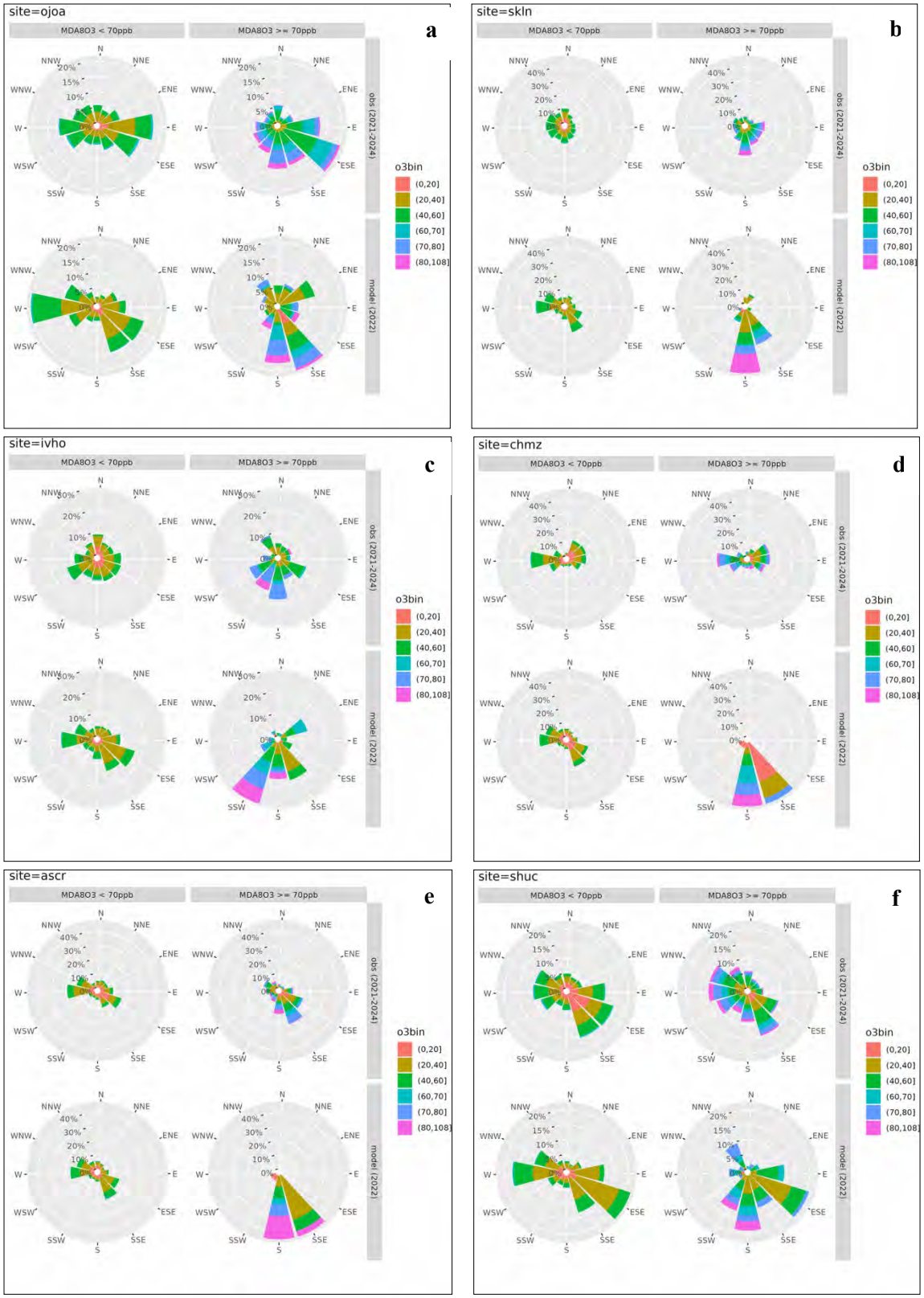

Figure 5.5 Ozone pollution roses at (a) Ojo de Aqua, (b) Skyline Park, (c) Ivanhoe, (d) Chamizal, (e) Ascarate Park, and (f) Socorro Hueco for (left) non-exceedance (< 70 ppb) and (right) exceedance (≥ 70 ppb) days from (top) observations during 2021-2024 and (bottom) CAMx predictions for 2022.

Table 5.6. Annual and quarterly model performance metrics for 24-hour average $PM_{2.5}$ concentration at El Paso and Juárez sites in 2022.

Site	Time Period	n	NMB 24-hour $PM_{2.5}$ Goal < ± 10% Criteria < ± 35%	NME 24-Hour $PM_{2.5}$ Goal < ± 10% Criteria < ± 50%	r 24-Hour $PM_{2.5}$ Goal > 0.70 Criteria > 0.40
Chamizal (El Paso)	**Annual**	**326**	**-41.3**	**47.1**	**0.41**
	Q1 (Jan - Mar)	90	-26.5	35.8	0.50
	Q2 (Apr - June)	83	-56.1	57.2	0.42
	Q3 (July - Sept)	77	-44.5	51.7	0.55
	Q4 (Oct - Dec)	76	-33.4	40.8	0.45
Institute for Engineering and Technology (Juárez)	**Annual**	**364**	**-87.2**	**87.6**	**0.07**
	Q1 (Jan - Mar)	89	-82.5	82.5	0.39
	Q2 (Apr - June)	91	-88.1	88.1	0.20
	Q3 (July - Sept)	92	-90.9	90.9	0.45
	Q4 (Oct - Dec)	92	-85.7	87.3	0.04

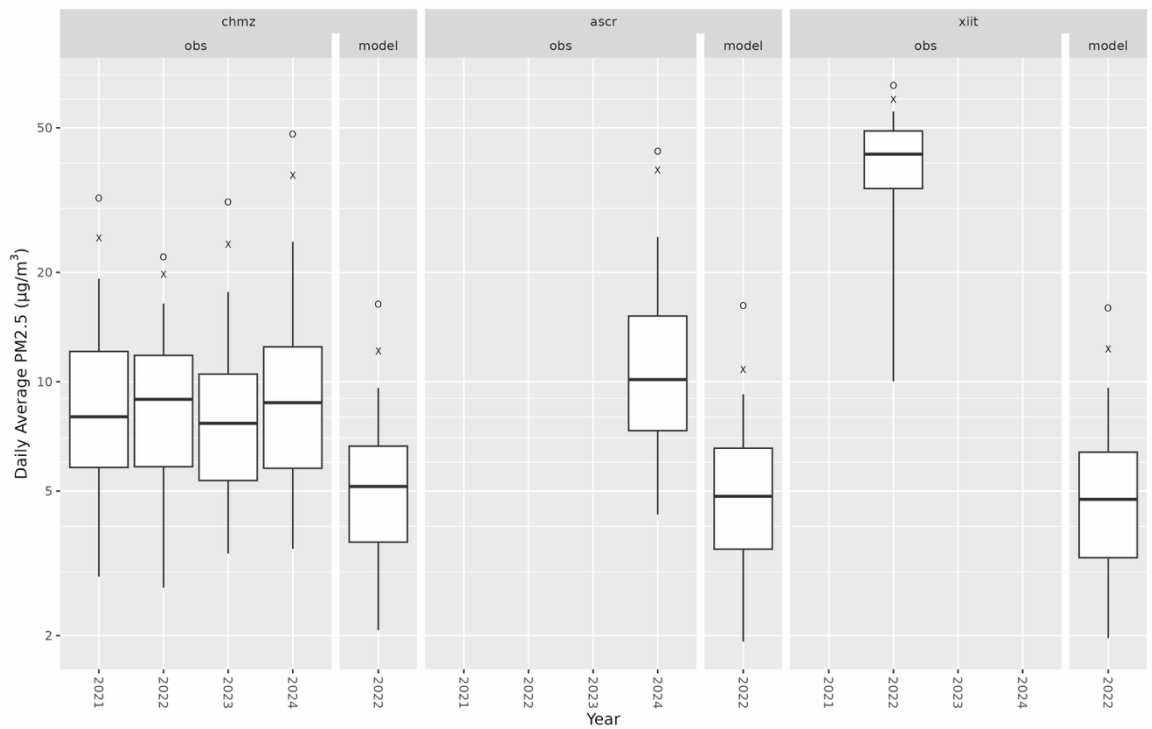

Figure 5.6. Observed and CAMx simulated 24-hour average $PM_{2.5}$ concentrations by year at Chamizal and Ascarate Park in El Paso and Institute for Engineering and Technology in Juárez. The box shows the median and interquartile range, whiskers extend to 5th and 95th percentiles, x indicates 99th percentile, and o indicates maximum concentration.

Windblown dust (WBD) was not included in the EPA 2022v1 emissions inventory for El Paso County or the Municipio de Juárez. The TCEQ (2025) issued an exceptional event demonstration for 2023 and 2024 $PM_{2.5}$ exceedances at El Paso County (2025) on August 5, 2025 for public comment; many events are associated with windblown dust. Ramboll (2025) recently completed WBD emissions estimates for the TCEQ's 2022 photochemical modeling platform, which will be important to incorporate for the El Paso-Juárez airshed in the future.

Table 5.7. Unadjusted $PM_{2.5}$ emissions (tpy) from area fugitive dust (afdust) sector sources in El Paso County and the Municipio de Juárez by SCC in the EPA 2022v1 emissions modeling platform. Adjustments accounting for near-source deposition and reductions due meteorological conditions (i.e., precipitation or snow cover) were applied by the EPA for the U.S., including El Paso County. Total $PM_{2.5}$ emissions from the afdust sector are shown for the Municipio de Juárez as well as before and after adjustments for El Paso County.

Source Classification Code (SCC)	**Description**	**$PM_{2.5}$ Emissions (tpy)**	
		El Paso (Unadjusted)	**Juárez**
2294000000	Mobile Sources; Paved Roads; All Paved Roads; Total: Fugitives	332.56	15.324
2296000000	Mobile Sources; Unpaved Roads; All Unpaved Roads; Total: Fugitives	967.37	-
2311010000	Industrial Processes; Construction: SIC 15 - 17; Residential; Total	22.47	1.425
2311020000	Industrial Processes; Construction: SIC 15 - 17; Industrial/Commercial/Institutional; Total	389.38	-
2311030000	Industrial Processes; Construction: SIC 15 - 17; Road Construction; Total	33.99	-
2325000000	Industrial Processes; Mining and Quarrying: SIC 14; All Processes; Total	59.463	-
2801000003	Miscellaneous Area Sources; Agriculture Production - Crops; Agriculture - Crops; Tilling	111.73	14.969
2801000005	Miscellaneous Area Sources; Agriculture Production - Crops; Agriculture - Harvesting	-	2.415
2805100010	Miscellaneous Area Sources; Agriculture Production - Livestock; Dust kicked up by Livestock; Beef cattle - finishing operations on feedlots (drylots)	40.142	0.7506
2805100020	Miscellaneous Area Sources; Agriculture Production - Livestock; Dust kicked up by Livestock; Dairy Cattle	0.5345	-
2805100030	Miscellaneous Area Sources; Agriculture Production - Livestock; Dust kicked up by Livestock; Broilers	0.00018429	-
2805100040	Miscellaneous Area Sources; Agriculture Production - Livestock; Dust kicked up by Livestock; Layers	0.010572	-
2805100050	Miscellaneous Area Sources; Agriculture Production - Livestock; Dust kicked up by Livestock; Swine	0.0020518	-
2805100060	Miscellaneous Area Sources; Agriculture Production - Livestock; Dust kicked up by Livestock; Turkeys	0.24006	-
	Total Unadjusted:	**1957.89**	**37.30**

	Total Adjusted:	**1343.03**	**NA**

$PM_{2.5}$ emissions in El Paso County from the area fugitive dust (afdust) sector in the 2022v1 inventory, shown in Table 5.7, were considerably greater in magnitude and originated from many more sources than in the Municipio de Juárez. The EPA separated afdust emissions from other nonpoint sources in the U.S. in the 2022v1 inventory to apply adjustments accounting for near-source dry deposition and reductions due to meteorological conditions (i.e., precipitation or snow cover) using SMOKE. Adjustments were sensitive to grid resolution. The team was not able to identify adjustments applied across individual SCCs for El Paso County. However, comparisons between $PM_{2.5}$ emissions from the afdust sector in El Paso County before and after the adjustment showed a 31.4% reduction (1958 tpy versus 1343 tpy). The adjustments reduced the $PM_{2.5}$ emissions total for El Paso County from 2900 tpy to 2285 tpy as well as the overall contribution of the afdust sector, but it remained the dominant source of emissions. Adjusted afdust sector emissions in the U.S. were used in CAMx simulations conducted for this study. The 12-km resolution of afdust emissions developed by EPA was interpolated for the 1-km and 4-km grids.

Table 5.7 shows unadjusted $PM_{2.5}$ emissions by SCC as well as total unadjusted and adjusted $PM_{2.5}$ emissions for the afdust sector in El Paso County. In addition to afdust, commercial and residential cooking (264 tpy); on-road mobile sources (118 tpy); open burning of land clearing debris (117 tpy); non-road vehicles and equipment, e.g. construction and mining, lawn and garden, recreational, agricultural, commercial, rail (98 tpy); power generation utilizing natural gas (83 tpy); and residential wood combustion (69 tpy) were among the key sources of $PM_{2.5}$ emissions in El Paso County in the 2022v1 inventory.

Total $PM_{2.5}$ emissions for the Municipio de Juárez in the 2021v1 inventory were 2281 tpy. Electric power generation accounted for 1099 tpy (~ 48%) of total emissions. Although individual facilities in Mexico were not identified, nearly all emissions appeared to be geographically aligned in Google Earth Pro with the Samalayuca power station located within the 4-km grid domain. On-road vehicles, particularly short and long haul diesel trucks and diesel transit buses but also gasoline passenger cars and trucks, accounted for 482 tpy. Other notable sources included brick kilns (234 tpy), commercial cooking-charbroiling (101 tpy), secondary metal and fabricated metal products production (95 tpy), and woodstoves (60 tpy). Afdust sector emissions of $PM_{2.5}$ were approximately 37 tpy in the 2022v1 inventory.

Afdust sources in the Municipio de Juárez may be less extensive and/or $PM_{2.5}$ emissions may be smaller in magnitude than in El Paso, but a working hypothesis is these sources are underrepresented or missing in the inventory. Positive Matrix Factorization analysis at Chamizal (Section 4.3.4) identified crustal material as the dominant factor (30.8%) contributing to $PM_{2.5}$ mass. Together these analyses emphasize the importance of accurate characterization of dust emissions in inventories for the region to support air quality modeling and development of binational mitigation strategies.

5.3.3 Toluene

Chamizal had the second highest mean measured toluene concentration for 2021-2024 among approximately 42 auto-GC sites in Texas; Delta Drive ranked fifth. Hourly observed toluene concentrations exhibited a large range at each of these sites, shown in the box and whisker plots in Figure 5.7. For example, modeled versus observed 50th percentile concentrations were 0.29 ppb and 0.37 ppb, respectively, at Chamizal, with 99th percentile concentrations of 2.5 and 7.0 ppb and maximum concentrations of 5.4 ppb and 16.7 ppb. Distributions of observed toluene concentrations at Chamizal showed little interannual variability from 2021 through 2024 with the exception of observed maximum concentrations. Observed concentrations at Delta Drive declined between 2022 and 2023. Modeled and observed 24-hour average toluene concentrations for Chamizal and Delta Drive as well as at the Womble and Socorro Hueco canister sites are shown in Figure 5.8. The lack of chemically speciated VOC measurements precluded assessments of model performance and interannual trends in observed toluene concentrations in Juárez.

Statistical performance measures in Table 5.8 indicated that CAMx predictions underestimated hourly average toluene concentrations at Chamizal and Delta Drive during 2022. The underprediction bias is most evident during time periods with relatively higher observed toluene concentrations during the 2022 base year, as shown in Figure 5.8 and time series in Appendix B. The annual inventory for El Paso and Juárez may underestimate routine emissions and/or does not capture episodic emission events that could contribute to observed enhancements in toluene concentrations.

Contour plots of mean and 99th percentile CAMx predicted toluene concentration by grid cell within the 1-km domain are shown in Figure 5.9. Emission sources in the U.S. and Mexico were tagged in RTRAC to identify their contributions to CAMx predictions of elevated toluene concentrations during 2022. This information could be used to prioritize emission source categories that warrant further investigation. Figure 5.10 is an enlarged map of the four VOC measurement sites: Chamizal, Delta Drive, Womble, and Socorro Hueco, for reference. Figure 5.11 shows the annual top 10% of simulated toluene concentrations by wind direction as well as associated wind direction frequency (number of hours) and emissions source contributions during 2022 at each of these sites.

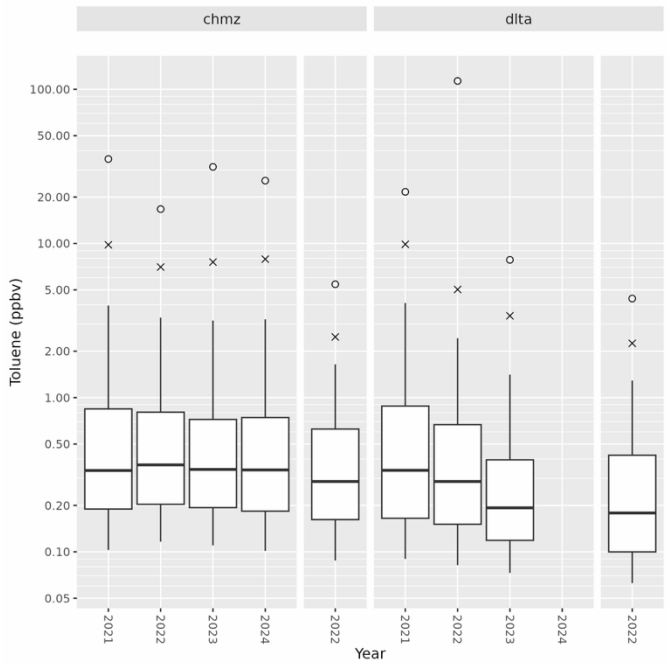

Figure 5.7. (a) Hourly observed and CAMx simulated toluene concentrations at Chamizal and Delta Drive auto-GC sites. The box shows the median and interquartile range, whiskers extend to 5th and 95th percentiles, x indicates 99th percentile, and o indicates maximum concentration.

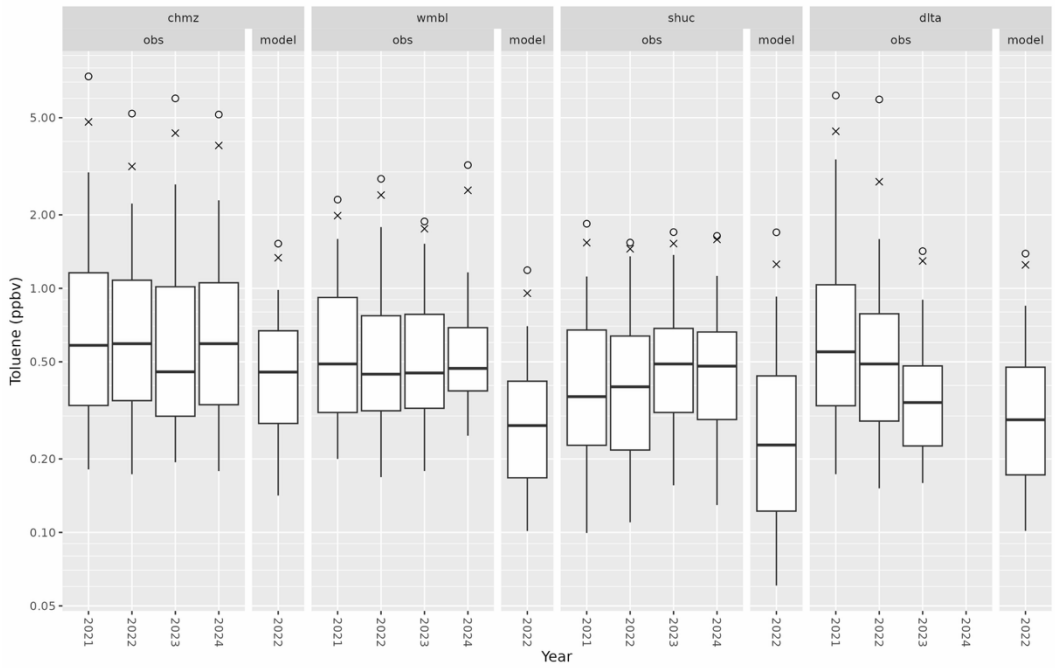

Figure 5.8. Observed and CAMx simulated 24-hour average toluene concentrations at Chamizal and Delta Drive (all days with available data) and Womble and Socorro Hueco canister sampling sites every sixth day. The box shows the median and interquartile range, whiskers extend to 5th and 95th percentiles, x indicates 99th percentile, and o indicates maximum concentration.

Table 5.8. Annual and quarterly model performance metrics for 1-hour average toluene concentrations at El Paso auto-GC sites in 2022.

Auto-GC Site: Toluene	Time Period	n	NMB	NME	r
Chamizal (El Paso)	**Annual**	**7369**	-39.9	64.7	0.47
	Q1 (Jan - Mar)	1798	-34.1	63.0	0.56
	Q2 (Apr - June)	1917	-39.9	65.0	0.42
	Q3 (July - Sept)	1875	-17.1	60.2	0.46
	Q4 (Oct - Dec)	1779	-55.8	68.0	0.44
Delta Drive* (El Paso)	**Annual**	**5727**	-48.9	67.0	0.32
	Q1 (Jan - Mar)	1924	-49.4	64.7	0.59
	Q2 (Apr - June)	1849	-51.5	69.5	0.19
	Q3 (July - Sept)	1954	-45.8	68.4	0.39
	Q4 (Oct - Dec)	0	NA	NA	NA

*In operation Jan.-Sept. 2022

(a) (b)

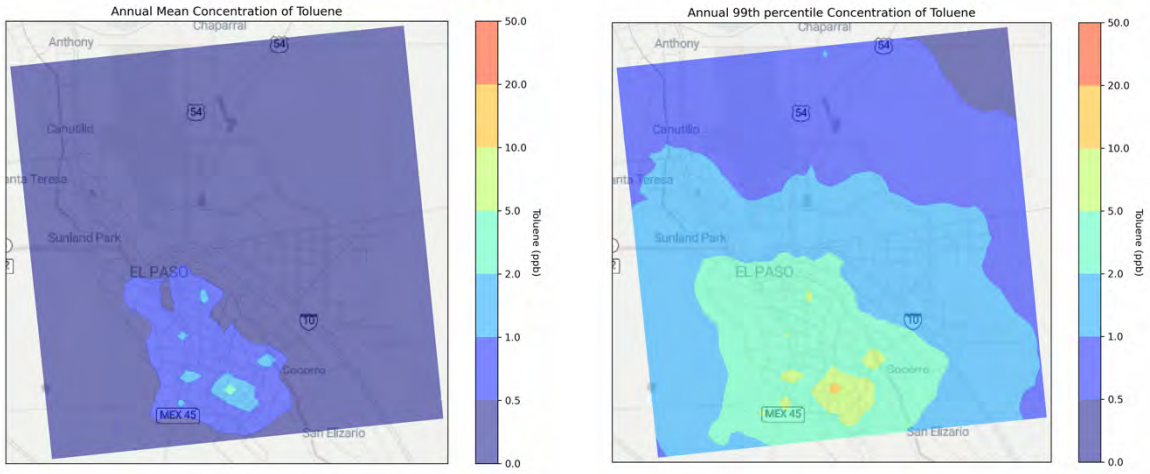

Figure 5.9 CAMx simulated (a) mean and (b) 99th percentile toluene concentrations within the 1-km domain.

Figure 5.10 VOC measurement sites (blue pins) within the TCEQ CAMS network in El Paso.

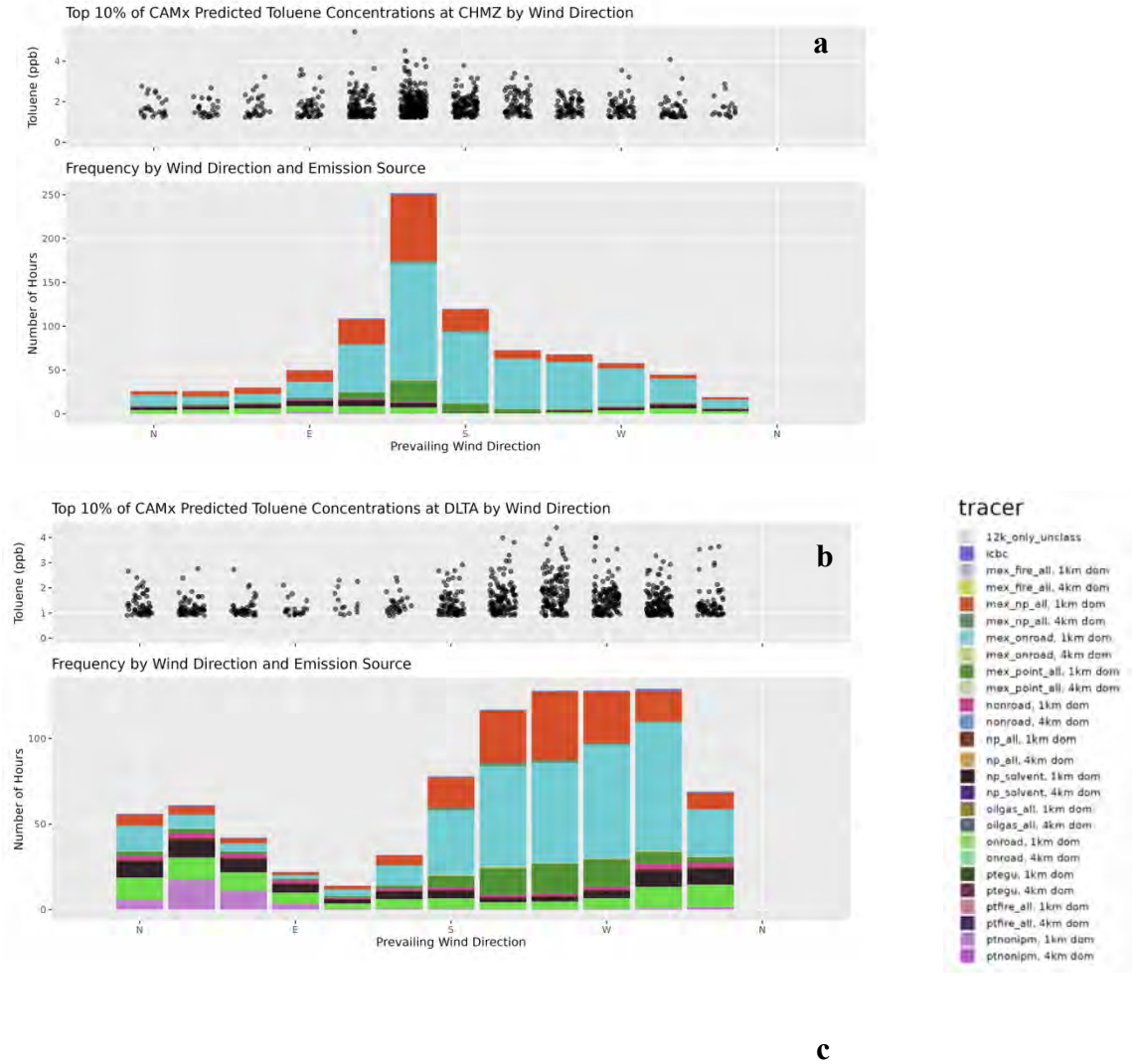

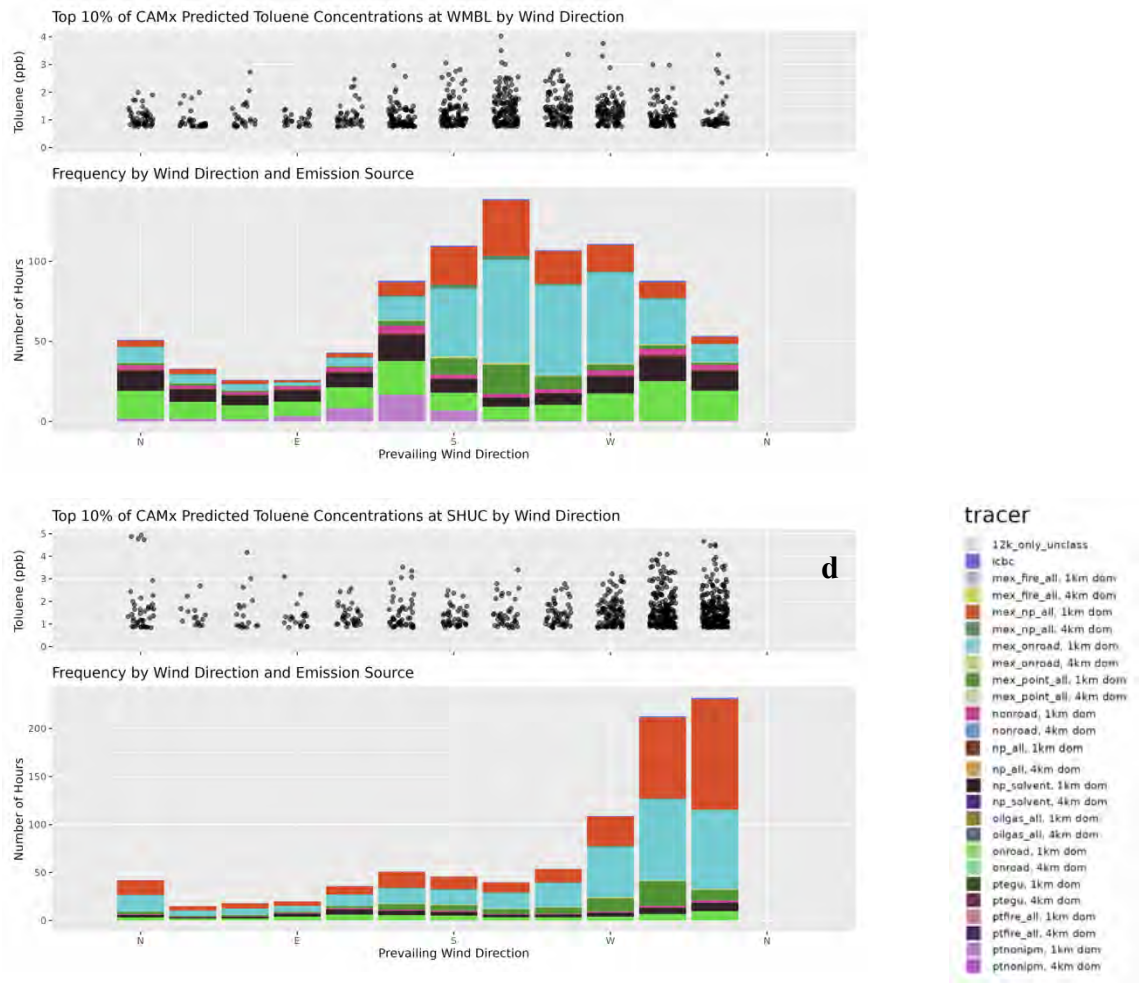

Figure 5.11. (Top) Annual top 10% of RTRAC simulated toluene concentrations (ppb) by wind direction and (Bottom) associated wind direction frequency (number of hours) and emissions source contributions during 2022 from the U.S. and Mexico at (a) Chamizal, (b) Delta Drive, (c) Womble, and (d) Socorro Hueco. Note differences in scales between plots.

Prevailing wind directions associated with elevated toluene concentrations varied between the four sites. Chamizal was more frequently affected when winds were from the east-southeast (ESE) to south-southeast (SSE) in contrast to the influences with winds from the west-southwest (WSW) to west (W) at Socorro Hueco. Common to all four sites, and broadly consistent with findings from the field intensives (Section 4.2), were contributions by Mexican on-road, nonpoint, and point source emissions within the 1-km domain to elevated toluene concentrations. Delta Drive and particularly Womble had complex variations in emission sources with wind direction, with nonpoint solvent usage, on-road, and point sources in El Paso, in addition to sources from Mexico, predicted to contribute to elevated toluene concentrations.

The 2022v1 inventory was examined for the purpose of identifying anthropogenic sources that accounted for the majority of toluene (TOLU) and toluene and monoalkyl aromatics emissions (TOL) in the

Municipio de Juárez. As described in Section 5.2.2, explicit toluene emissions estimates were available for the on-road sector in the 2022v1 inventory, but emissions from point, nonpoint/non-road, and fires represented toluene and monoalkyl aromatics as in the CB6 chemical mechanism. Total annual emissions from all sources were 1435 tpy. On-road mobile sources accounted for 800 tpy (56%) of this total with the largest contributions from gasoline passenger cars, trucks, and motorcycles on urban unrestricted access roads or off network. Nonpoint sources (527 tpy or 37% of total emissions) in Juárez were diverse and included wastewater treatment; solvent utilization from surface coating for the automobile, graphic arts, metal, and wood furniture industries; gasoline service stations; commercial and consumer products; and residential woodstoves and fireplaces. Point source emissions contributed 106 tpy. Plastics manufacturing facilities accounted for approximately 50% of emissions from point sources. Other sources, accounting for approximately 5%-11% of point emissions each, included warehousing and storage facilities, electric power generation, electrical equipment and component manufacturing, vehicle parts manufacturing, alumina/aluminum production and processing, and fabricated metal parts manufacturing facilities.

Explicit toluene emission estimates were included for all sectors except fires, which as for Juárez represented toluene and monoalkyl aromatics, in El Paso County. Total annual toluene emissions were 490 tpy in the 2022v1 inventory. On-road mobile sources contributed 221 tpy (45%) primarily from gasoline passenger cars, trucks, and motorcycles on urban unrestricted access roads, off network or refueling. Nonpoint sources accounted for 152 tpy (31%) with solvent utilization primarily from surface coating operations (e.g., textile products, traffic markings, industrial maintenance, plastics products, electronic and other electrical products, wood furniture, motor vehicles) and commercial and consumer products (e.g., adhesives and sealants, household, personal care) contributing to most emissions (142 tpy). Non-road sources (92 tpy or 19% of total emissions) included commercial, industrial, lawn and garden, construction and mining, recreational, and railway maintenance equipment, as well as locomotives. Point source accounted for approximately 4% of total emissions primarily from industrial manufacturing, petroleum industry fugitives, and leather and leather product production.

5.3.4 Ethylene Oxide

Three point sources, of ethylene oxide emissions in the 2022v1 inventory, all associated with commercial sterilization, in El Paso County and Dona Ana County (Santa Theresa), New Mexico, were located within the modeling domain (Figure 5.12). Wastewater treatment (nonpoint source) also contributed to ethylene oxide emissions in El Paso (0.00297219 tpy) and Dona Ana (0.000424464 tpy). Juárez has an important and growing medical equipment industry (Maldonado et al., 2025). Although ethylene oxide sterilization occurs at U.S. facilities such as in Dona Ana County, the team could not confirm at the time of writing if and to what extent it is used within Juárez. Information regarding ethylene oxide emissions was not available for Mexico.

Figure 5.13. shows CAMx simulated mean and 99th percentile concentrations (ppb) of ethylene oxide within the 1-km domain. Ethylene oxide is not routinely measured in the El Paso-Juárez region. Novel techniques to distinguish ethylene oxide concentrations using the Vocus have been under development by the measurement team for this study.

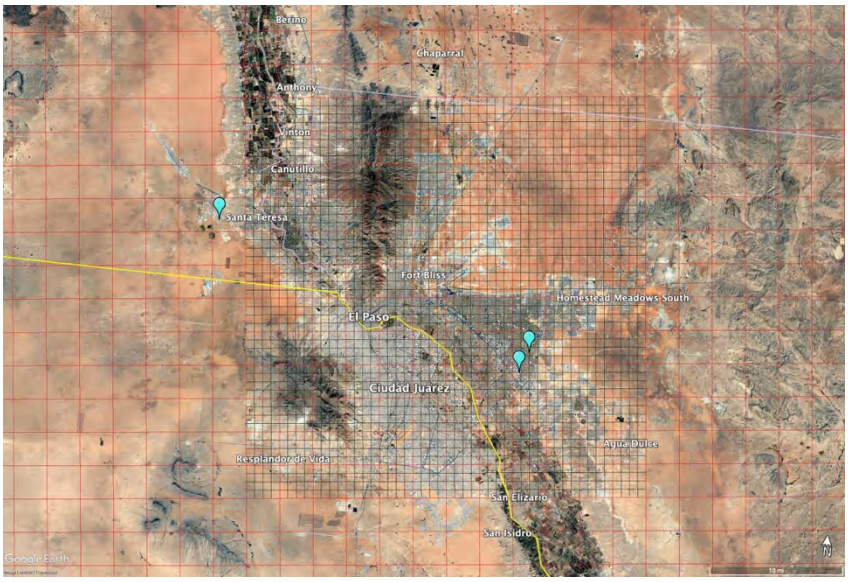

Figure 5.12 Ethylene oxide emission point sources within El Paso (0.02320 tpy) and Dona Ana (0.4815 tpy) Counties in the EPA 2022v1 emissions inventory. Portions of the CAMx 1-km (black) and 4-km (red) grid domains are shown for reference.

(a) (b)

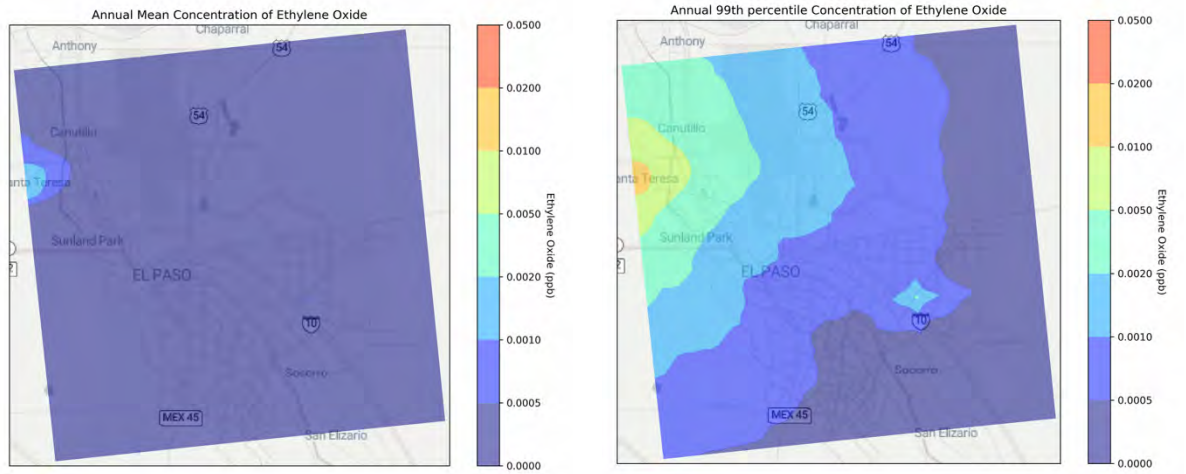

Figure 5.13 CAMx simulated (a) mean and (b) 99th percentile ethylene oxide concentrations within the 1-km domain.

6 Discussion

The findings from AQRP Project 24-024 have several important implications for air quality planning processes in the El Paso- Juárez region:

6.1 Air Quality Improvements in El Paso-Juárez Require Collaborative Solutions

Analyses of ambient monitoring data for ozone, particulate matter, and precursors in El Paso and Juárez suggests that both cities will face continued challenges in meeting their respective national air quality standards. Air pollution in El Paso, including ozone precursors such as aromatic VOCs and particulate matter, originates from local sources as well as sources along the border of and within Mexico that are outside of local jurisdiction. Dust is a dominant contribution to $PM_{2.5}$ in El Paso and can be regional in nature from surrounding desert lands as well as driven by anthropogenic sources of area fugitive emissions. Achieving compliance with more stringent air quality standards will likely depend on joint cooperation between state and federal agencies in the U.S. and Mexico and regional stakeholders. The La Paz Agreement in 1983 and subsequent implementation efforts such as the Border 2025 environmental program offer a foundation to build further collaboration. Binational efforts aimed at improving data to support air quality planning and management processes could include coordinated development of emissions inventories, enhanced VOC and $PM_{2.5}$ monitoring in both cities, joint development and assessment of emission control strategies (e.g., retrofit or replacement programs for older high-emitting vehicles and industrial equipment, area fugitive dust, real-time data sharing for air quality episodes, as well as improved archiving and accessibility of air quality data for Juárez. This project provides a quantitative basis for engaging in these discussions by improving the understanding of the magnitude and spatiotemporal patterns of air pollution in the El Paso-Juárez airshed.

6.2 Addressing Traffic and Area Sources in El Paso

Local sources in El Paso have important contributions to air quality in the region. Source apportionment showed that light- and heavy-duty vehicles collectively are a major contributor to $PM_{2.5}$ (nearly 30%) and are also sources of NO_x and selected VOC emissions that drive ozone formation. The correlation of afternoon C8 aromatics with traffic patterns indicated that vehicular emissions within El Paso contribute substantially to the urban hydrocarbon pool. Additionally, local area sources such as restaurants, small industries, and residential heating can add to organic gas and aerosol loads. Controlling these emissions through for example, policies to expedite the turnover of older vehicles and/or improve public transit could have direct benefits for reducing locally generated NO_x and VOC emissions. Likewise, implementation of dust containment measures (e.g., street cleaning, enforcement of tarping systems in trucks), may help mitigate crustal contributions to $PM_{2.5}$. Overall, integrated control strategies are needed that address local emissions while accounting for transboundary components to air quality in El Paso.

6.3 Importance of Advanced Monitoring and Analysis

This project demonstrated the value of deploying advanced monitoring technologies, such as the PTR-TOFMS and HR-AMS, in urban airsheds. These instruments provided high-resolution insights into pollutant composition and dynamics that traditional monitors cannot capture. For example, the ability to continuously measure a wide range of VOCs allowed identification of source-specific tracers (e.g., methanethiol for sewage/landfills, or unique aromatic ratios for traffic vs. solvent sources) in near real-time. Moreover, the mobile laboratory approach helped to create detailed pollution maps, revealing hotspots that might be missed by fixed stations. The successful use of an electric mobile lab is also notable, by avoiding self-contamination from the vehicle's own exhaust, cleaner measurements can be obtained, setting a precedent for sustainable monitoring practices. A recommendation is that agencies consider maintaining such advanced monitoring capabilities in El Paso (e.g., establishing a permanent supersite with some advanced instruments, or periodic mobile monitoring campaigns) to continue capturing data that can verify the effectiveness of control measures and address emerging issues such as industrial shifts or vehicle technologies and fuel composition.

6.4 Multiscale Modeling and Observation Integration

Integrating modeled and observed high-resolution observations for different pollutants has the potential to lead to greater understanding of spatiotemporal variability in criteria pollutant precursors and air toxics in the El Paso-Juárez region. As an example, Figure 6.1 illustrates observed 0.5 km aggregated toluene concentrations in winter and summer seasons overlaid on annual CAMx predictions. During the winter season, cold weather and calm winds resulted in higher concentrations close to the border and overall, relative to the summer campaign when PBL heights and wind speeds were greater. Spatial patterns of observations and modeled toluene concentrations show general consistency, indicating the potential importance of contributions from Juárez to air quality experienced by local residents as well within El Paso.

Previous studies, such as Sullivan (2023), have shown that significant air quality improvements have been achieved over the past three decades. For example, Seila et al. (2001) documented toluene as the second highest VOC in Juárez (31 ppb at Juárez Police station) and the highest VOC at the El Paso site (15 ppb at Campbell site), attributed to solvents and vehicular emissions. During the 1996 Paso del Norte study, median toluene concentrations were 3.6 ppb at Campbell site (Seila et al., 2001).

Overall, contemporary modeling and observations from this project show substantially lower concentrations with similar trends observed at ambient monitoring sites within the TCEQ network. The average observed concentration of toluene during the winter campaign was 0.68 ppb and 0.25 ppb during the summer season - approximately 5 to 10 times lower than three decades ago. However, observed maxima of 37 ppb and 25 ppb during winter and summer campaigns, respectively, indicate that localized hotspots persist despite overall improvements. This multiscale approach demonstrates good spatial correspondence between modeled and observed patterns while highlighting the importance of high-resolution mobile measurements for capturing local-scale variability.

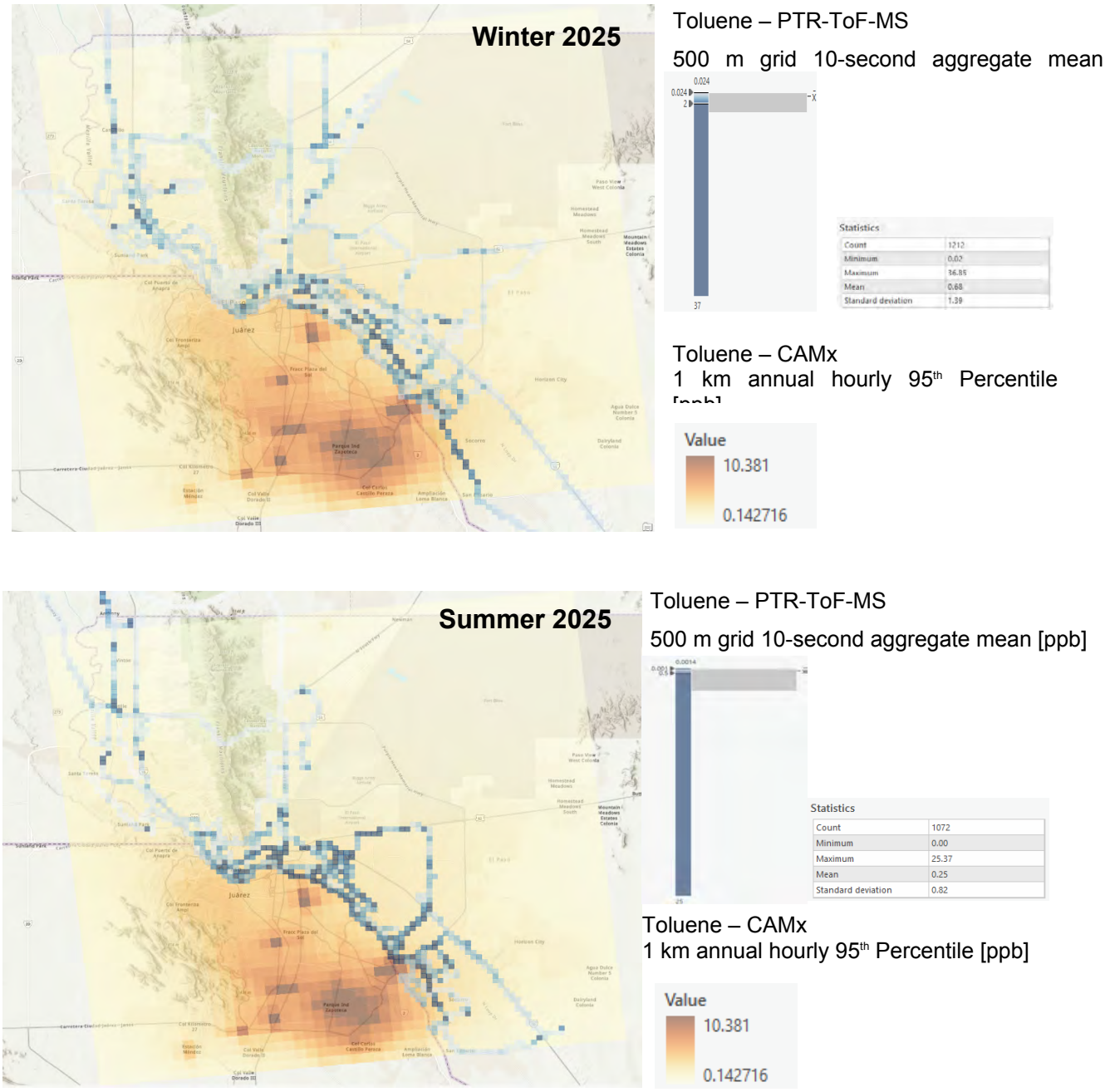

Figure 6.1. Observed spatiotemporal distribution of toluene concentrations for two seasons: (a) Winter and (b) Summer, overlaid on CAMx annual average concentrations (background color scale). Observations are aggregated in 0.5 km bins, whereas CAMx model is gridded at 1 km (see Sect 6.3 on the important limitations of multi-scale comparisons).

6.5 Secondary Pollution Formation and Health Implications

The project provided insights on secondary pollutant formation in the El Paso region. Diurnal and spatial patterns of ozone were consistent with a VOC-limited regime, which suggests that controlling VOC emissions could yield ozone reductions. Many VOCs also form secondary organic aerosol (SOA) after oxidation. HR-AMS data indeed showed that a portion of the organic particulate matter in El Paso is secondary in nature (oxidized organics), likely stemming from these VOC precursors. Thus, strategies

targeting VOC reductions, such as better containment of solvent use, industrial emissions, and vehicle hydrocarbons, have the co-benefit of reducing both ozone and particulate matter as SOA. Additionally, the identification of significant ammonium sulfate aerosol points to regional SO_2 sources, where continued efforts to cut sulfur emissions, such as cleaner fuels and emission controls on smelters or power plants in the region, will help reduce this component of $PM_{2.5}$. Reducing fine particulate matter is especially critical given the new health-based standard; $PM_{2.5}$ is linked to cardiovascular and respiratory health risks, so the predominance of crustal material in El Paso's $PM_{2.5}$ raises questions about its health impact. Crustal PM might be less toxic than combustion PM, but at high concentrations it can still affect respiratory health and visibility. Our findings stress the need for health studies or exposure assessments in El Paso to determine the impact of these various PM components on the local population.

6.6 Achieving More Stringent National Standards

The study suggests that achieving and /or maintaining compliance with a $PM_{2.5}$ standard of 9 $\mu g/m^3$ in El Paso will be challenging but possible with concerted action. Annual average $PM_{2.5}$ concentrations at Chamizal in recent years has ranged between 8 - 10 $\mu g/m^3$; the source composition particularly indicates the importance dust and motor vehicles. Although windblown dust may be partially beyond immediate control (driven by weather), but incremental dust mitigation strategies in addition to aggressive vehicle emissions reductions may contribute to reductions in $PM_{2.5}$ concentrations. Both El Paso and Juárez face challenges for compliance with the federal standards of their respective countries. El Paso alone likely cannot completely solve its ozone challenges. Therefore, future work should involve critical cross-border emissions strategy development and reduction assessments. These could take the form of binational air quality management districts or projects, similar to what has been done in other border regions (e.g., Bergin et al., 2005).

In conclusion, the study provides a timely scientific foundation for air quality planning and management in El Paso. Integrating field observations with modeling has helped to provide a more comprehensive understanding El Paso's ozone and $PM_{2.5}$ pollution. A combination of local action and regional cooperation will be required to ensure cleaner air for El Paso and Juárez residents under the stricter standards. The methods and findings here can also serve as a template for other border regions facing similar air quality issues.

6.7 Limitations

6.7.1 Temporal and Spatial Sampling Constraints

The primary limitations of this study are the relatively short sampling periods across the year and region. Mobile observations were conducted during specific time windows and should not be extrapolated to other temporal periods. This temporal constraint is particularly important when comparing mobile measurements with annual model estimates, as large spatiotemporal variability can impact the statistical uniformity of reported results.

Spatial coverage also presents limitations. While our track planning captured high-resolution data along the border, it resulted in oversampling of some areas, predominantly during daytime hours. Conversely, areas further from the border and nighttime conditions received less representation, potentially introducing spatial bias due to uneven sampling distribution.

6.7.2 Scale and Comparison Challenges

The model-observation comparison maps presented in this report should be interpreted as preliminary showcases demonstrating spatial correspondence between two distinct measurement scales. Due to differences in spatial and temporal resolution, as well as inherent uncertainties in both approaches, quantitative spatial interpretations should be limited to the specific conditions encountered during sampling. The current analysis presents data without additional transformations or manipulations to maintain transparency.

1. Conclusions

This project successfully met its objectives of improving the understanding of ozone and fine particulate matter formation in the El Paso region through novel observations and analysis. Over the course of 2024 - 2025, the team conducted two field measurement campaigns and complementary air quality modeling using a CAMx platform developed for the El Paso-Juárez region, yielding the following overarching conclusions about dominant pollution sources, secondary ozone and aerosol formation, and transboundary influences of pollutant contributions and precursors:

- Fine particulate pollution ($PM_{2.5}$) in El Paso is primarily driven by crustal dust and vehicular emissions, with notable contributions from biomass burning and secondary aerosols (sulfate and nitrate). Ozone formation is strongly influenced by VOC emissions, many of which originate in or are transported through the El Paso-Juárez metropolitan area, such that ozone episodes are strongly associated with periods of high anthropogenic VOC presence under sunny conditions.

- Significant fractions of both O_3 precursors and $PM_{2.5}$ in El Paso originate from outside local boundaries, including from Ciudad Juárez and broader regional sources. Toluene and other VOC enhancements along the border and at night illustrated the impact of Juárez. Air quality modeling identified the potential importance of international on-road, area, and industrial point source emissions to elevated toluene concentrations in El Paso. Ambient monitoring data indicated that measured ozone and $PM_{2.5}$ concentrations in Juárez during the 2022 base year exceeded Mexico's national air quality standards. These finding underscore that air quality in El Paso and Juárez is a binational issue.

- The deployment of an electric mobile lab with advanced instrumentation provided insights into spatial and temporal pollution trends, offering the capability to capture “hotspots” of pollution (e.g., localized sulfur plumes, border-zone VOC spikes) and to observe fine-scale temporal patterns (diurnal cycles at the UTEP site) that together inform source attribution. Integration of these observations with existing ambient monitoring and modeling information enhanced information for the region.

- The project’s results will directly aid air quality strategy development. For $PM_{2.5}$, controlling dust and tailpipe emissions emerged as priorities. For ozone, reducing VOC emissions (both locally and in Juárez) is likely the most effective approach in a VOC-sensitive regime. Data support considering collaborative programs with Mexico to target industrial and mobile source emissions that impact both sides of the border. Importantly, any attainment plan for the new $PM_{2.5}$ standard will need to account for natural and transported contributions; regulatory mechanisms (such as exceptional event exclusions for dust storms, or assessment of international contributions for ozone) may be necessary to address the portions of pollution beyond local control.

While this project has advanced the understanding of El Paso’s air quality, it also pointed to areas for further research. Continued monitoring efforts, possibly establishing a permanent supersite in El Paso with advanced instruments to track progress are recommended. Additional studies could explore wintertime dynamics (e.g., temperature inversions and domestic heating contributions not fully captured in the project campaigns) and expand analyses of air toxics, i.e., PTR-TOFMS data contain information on hundreds of VOCs that could be further analyzed for such assessments. Improving emission inventories in El Paso and Juárez, particularly for windblown and area fugitive dust, on-road vehicle fleets, and industrial sources, as well as the spatial resolution of the meteorological modeling used to support air quality modeling efforts would be important ongoing refinements. Including future-year projections and control strategy simulations will be necessary to translate these findings into effective

policy decisions. Novel comprehensive data (>1000 VOC ions and markers) and real-time speciated PM_1 data from this project and have been archived and could support further in-depth analyses in the future.

In terms of the opportunities and future directions, this study represents the first mobile measurements in the El Paso region using an electric, non-tailpipe emission platform, providing proof of concept for future applications. The extensive dataset generated has significant potential for further exploration beyond this project's scope. Particularly promising is the opportunity for deeper analysis of source plume fingerprinting for chemicals not typically monitored in routine air quality networks and comprehensive combined source apportionment. Further analysis of the VOC dataset could focus on deeper understanding of VOC reactivity and elucidate those most important for ozone formation, for example, by analysis of maximum incremental reactivity (MIR) concentrations by location/time to further enhance conceptual models of ozone formation in El Paso.

Future research could build on the approaches and data from this project, implementing around-the-clock mobile measurements to capture diurnal variations, developing more representative model-observation comparisons using PBL height normalizations and wind directionality with appropriate weighting schemes, and establishing regular mobile monitoring programs. The combination of mobile and stationary measurements employed here has improved both spatial and temporal representativeness, but continuous mobile monitoring would further enhance our understanding of regional air quality patterns.

AQRP Project 24-024 provided new observations, air quality modeling, and analyses that addressed the priority research questions for the state of Texas. The study highlights the potential benefits of a dual approach of local action and cross-border cooperation to improve air quality. Project deliverables serve as a resource for TCEQ and the community in crafting informed, effective air quality planning and management strategies for the El Paso region

2. References

Bergin, M.S., West, J.J., Keating, T.J. and Russell, A.G., 2005. Regional atmospheric pollution and transboundary air quality management. Annu. Rev. Environ. Resour., 30(1), pp.1-37.

Emery, C., Liu, Z., Russell, A.G., Odman, M.T., Yarwood, G., Kumar, N., 2017. Recommendations on statistics and benchmarks to assess photochemical model performance, Journal of the Air & Waste Management Association, 67(50), pp. 582–598. http://dx.doi.org/10.1080/10962247.2016.1265027

Eyth, A., Vukovich, J., Farkas, C., Godfrey, J., Seltzer, K. Dayton, L, and Dietrich, Y., Technical Support Document (TSD) Preparation of Emissions Inventories for the 2022v1 North American Emissions Modeling Platform, U.S. Environmental Protection Agency, Office of Air Quality Planning and Standards, EPA-454/B-25-001, May 2025.

Holzinger, R., 2015. PTRwid: A new widget tool for processing PTR-TOF-MS data. Atmospheric Measurement Techniques, 8(9), pp.3903-3922.

Instituto Nacional de Ecología y Cambio Climático, Informe Nacional Calidad del Aire México 2022. https://sinaica.inecc.gob.mx/pags/informes.php

Karle, N.N., Fitzgerald, R.M., Sakai, Sullivan, D.W., Stockwell, W.R., Multi-Scale Atmospheric Emissions, Circulation and Meteorological Drivers of Ozone Episodes in El Paso-Juárez Airshed, Atmosphere 2021, 12, 1575. https://doi.org/10.3390/atmos12121575

Lara, P., Fitzgerald, R.M., Karle, N.N., Talamantes, J., Miranda, M., Baumgardner, D, Stockwell,W.R., 2022. Winter andWildfire Season Optical Characterization of Black and Brown Carbon in the El Paso-Ciudad Juárez Airshed. Atmosphere, 13, 1201. https://doi.org/10.3390/atmos13081201

Maldonado, M., González, N, and Gutiérrez Zubiate, A.P., Employment Shifts in Ciudad Juárez: Beyond the Numbers, Hunt Institute for Global Competitiveness at The University of Texas at El Paso, March 2025.

Ng, N. L., Canagaratna, M. R., Zhang, Q., Jimenez, J. L., Tian, J., Ulbrich, I. M., Kroll, J. H., Docherty, K. S., Chhabra, P. S., Bahreini, R., Murphy, S. M., Seinfeld, J. H., Hildebrandt, L., Donahue, N. M., DeCarlo, P. F., Lanz, V. A., Prévôt, A. S. H., Dinar, E., Rudich, Y., and Worsnop, D. R.: Organic aerosol components observed in Northern Hemispheric datasets from Aerosol Mass Spectrometry, Atmos. Chem. Phys., 10, 4625–4641, https://doi.org/10.5194/acp-10-4625-2010, 2010.

Ng, N.L., Canagaratna, M.R., Jimenez, J.L., Zhang, Q., Ulbrich, I.M. and Worsnop, D.R., 2011. Real-time methods for estimating organic component mass concentrations from aerosol mass spectrometer data. Environmental Science & Technology, 45(3), pp.910-916.

Park, E.S., Sullivan, D., Kang, D., Ying, Q., and Spiegelman C.H., 2020. Assessment of mobile source contributions in El Paso by PMF receptor modeling coupled with wind direction analysis, Science of the Total Environment 720 (2020) 137527. https://doi.org/10.1016/j.scitotenv.2020.137527

Reconsideration of the National Ambient Air Quality Standards for Particulate Matter; Correction, 40 CFR Parts 50 and 58 (2024). https://www.govinfo.gov/content/pkg/FR-2024-12-19/pdf/2024-29223.pdf

Ramboll, Dust Emissions Inventory Support for Particulate Matter Modeling, Final Report submitted to the Texas Commission on Environmental Quality, Contract No. 582-23-45978, Work Order No. 10, Tracking No. 2025-06, Task 5.2, June 18, 2025.

Ramboll, Federal Clean Air Act El Paso County §179B Demonstration: El Paso-Las Cruces, Texas-New Mexico Nonattainment Area, submitted to the Texas Commission on Environmental Quality, Work Order No. 582-22-30580-022, Contract No. 582-19-90500, Tracking No. 2022-01, February 28,

2022.https://www.tceq.texas.gov/downloads/air-quality/modeling/international-transport/179b-demonstration-for-el-paso-county.pdf

Seila, R.L., Main, H.H., Arriaga, J.L., Martínez, G. and Ramadan, A.B., 2001. Atmospheric volatile organic compound measurements during the 1996 Paso del Norte Ozone Study. Science of the total environment, 276(1-3), pp.153-169.

Stark, H., Yatavelli, R.L., Thompson, S.L., Kimmel, J.R., Cubison, M.J., Chhabra, P.S., Canagaratna, M.R., Jayne, J.T., Worsnop, D.R. and Jimenez, J.L., 2015. Methods to extract molecular and bulk chemical information from series of complex mass spectra with limited mass resolution. International Journal of Mass Spectrometry, 389, pp.26-38.

Sullivan, D. Ambient VOC Monitoring in El Paso, TX, Project Report submitted to the Texas Commission on Environmental Quality (TCEQ), GAD Number 582-17-72921, TCEQ Project 582-23-43395-10, Tracking Number: 2023-14, August 31, 2023.

Texas Commission on Environmental Quality (TCEQ), Exceptional Events Demonstration for 2023 and 2024 PM2.5 Exceedances at El Paso County, August 5, 2025. https://www.tceq.texas.gov/downloads/air-quality/air-monitoring/pm/2023-2024_elpaso_pm2-5_ee_demonstration_final-4aug2025.pdf

Tuite, K., Akherati, A., and Yarwood, G., Comparing Ozone Precursor Responses and Volatile Organic Compound (VOC) Reactivity of Carbon Bond Version 7 Revision 1 (CB7r1) to Other Mechanisms, Final Report submitted to the Texas Commission on Environmental Quality, Work Order No. 582-23-42327-033, Contract No. 582-19-90500, Tracking No. 2023-04, Task 6.2, June 29, 2023.

U.S. EPA (2025), Air Quality Design Values for Criteria Pollutants, https://storymaps.arcgis.com/stories/86cc46a9348c48289c718f06cae93b1d, accessed 20 August 2025.

U.S. EPA (2024). Reconsideration of the National Ambient Air Quality Standards for Particulate Matter: Lowering the primary annual PM . standard to 9.0 µg m ³. Federal Register, Docket No. EPA HQ OAR 2015 0072. EPA final rule summary document, Feb. 7, 2024.

Wallington, T.J., Liu, R., Dagaut, P. and Kurylo, M.J., 1988. The gas phase reactions of hydroxyl radicals with a series of aliphatic ethers over the temperature range 240–440 K. International Journal of Chemical Kinetics, 20(1), pp. 41-49.

Yarwood, G., Fianna L., Shi, Y., and Beardsley, R. Develop Carbon Bond Version 7 Revision 1 (CB7r1) for CAMx Ozone Modeling, Final Report submitted to the Texas Commission on Environmental Quality, Work Order No. 582-22-31131-025, Contract No. 582-19-90500, Tracking No. 2022-16, Task 6.2, June 24, 2022.

6. ACKNOWLEDGMENTS

We thank Weining Zhao and Beata Czader of the TCEQ and Greg Yarwood of Ramboll for their recommendations about the El Paso-Juárez air quality modeling configuration, Jiaoyan Huang of the EPA for assistance with the EPA OAQPS 2022 modeling platform, and Doug Boyer of the TCEQ for insights about El Paso emissions sources.

We appreciate the support and assistance of Vince Torres (AQRP Project Manager), Jocelyn Mellberg (TCEQ Project Manager), Celinda Vallejo-Rodriguez (TCEQ Project Liaison), Joseph Rabago (TCEQ Project Liaison Backup), and RoseAnna Goewey (AQRP Grant & Program Manager) throughout the project.

Appendix A

Table A1. Emission sources* and inventory preparation methods for the EPA 2022v1 emissions modeling platform by Eyth et al. (2025).

Emission Sector (ID)	Description	EPA Methodology for the Preparation of Emissions Inventories for the 2022v1 North American Emissions Modeling Platform
U.S. Point		
Electric Generating Units (ptegu)	Electric generating units (EGUs) in the U.S. National Electric Energy Database System (NEEDS) v6	• 2022 hourly NOx and SO_2 for units matched with Continuous Emissions Monitoring System (CEMS); other pollutant emissions from these units allocated hourly by CEMS heat input • 2022 annual emissions for units not matched with CEMS data • Inventory does not include EGUs closed in 2022
Point Source Oil and Gas (pt_oilgas)	Oil and gas, natural gas, or crude petroleum extraction, drilling oil and gas wells, support activities for oil and gas operations, natural gas distribution, oil and gas pipeline and related structures construction, pipeline transportation of crude oil or natural gas, offshore oil platforms	• 2022 annual emissions data submitted by states or projected from 2020 NEI or 2021 NEI
Aircraft and Ground Support Equipment (airports)	All aircraft types for public, private, and military purposes and aircraft ground support equipment	• Federal Aviation Administration (FAA) Aviation Environmental Design Tool (AEDT) 2022 annual emissions for 51 largest airports • Smaller airport emissions projected from 2020 NEI to 2022 using factors from 2023 Terminal Area Forecast (TAF) •
Non-IPM Sector (ptnonipm)	Non-EGU point sources and rail yards; potentially low-emitting EGUs not matched to NEEDS database or CEMS data; fugitive dust PM emissions from vehicular traffic on paved/unpaved roads at industrial facilities, coal handling at coal mines, grain elevators	• 2022 annual emissions submitted by states or projected from 2020 NEI
U.S. Nonpoint		
Area Fugitive Dust (afdust)	Annual county-level $PM_{2.5}$ and PM_{10} emissions from paved roads, unpaved roads and airstrips, construction (residential, industrial, road and total), agriculture production, mining and quarrying	• Paved and unpaved road emissions projected from 2020 NEI based on 2020 and 2022 differences in vehicle miles traveled (VMT) • Agricultural dust from livestock projected from 2020 NEI based on 2020 and 2022 differences in animal counts • Emissions from other sources held constant at 2020 NEI values • Adjustments applied to account for reduction in emissions due to transportable fraction and for precipitation processes

Livestock (livestock)	Annual county-level emissions (except $PM_{2.5}$) from beef and dairy cattle, poultry production and waste, swine production, waste from horses and ponies, production and waste for sheep, lambs, and goat.	• U.S. Department of Agriculture (USDA) animal populations and 2022 meteorological data from Weather Research and Forecasting (WRF) in Carnegie Mellon Farm Emissions Model (FEM) simulation
Agricultural Fertilizer (fertilizer)	Ammonia (NH_3) emissions from agricultural soils	• Fertilizer Emission Scenario Tool for CMAQ (FEST-C) landuse and agricultural activity data with CMAQ (v5.4) bidirectional NH_3 flux modeling
Nonpoint Oil and Gas (np_oilgas)	Annual county-level emissions from offshore and onshore oil and gas activity including from drill rigs, workover rigs, artificial lift, hydraulic fracturing engines, pneumatic pumps and other devices, storage tanks, flares, truck loading, compressor engines, dehydrators; pipeline blowdowns and pigging; abandoned wells	• 2020 NEI version of Nonpoint Oil and Gas Emission Estimation Tool with 2022 county-level activity from Enverus and state agencies and Subpart W updates • Volatile organic compound (VOC), ethylbenzene, toluene, benzene, xylene (BTEX) emissions from pipeline blowdowns and pigging estimated from EPA Greenhouse Gas Reporting Program data and data submitted by states • VOC and BTEX from abandoned wells based on Inventory of U.S. Greenhouse Gas Emissions and Sinks data for 2022
Residential Wood Combustion (rwc)	Annual county-level emissions from residential wood burning devices including fireplaces, fireplaces with inserts, free standing woodstoves, pellet stoves, outdoor hydronic heaters, indoor furnaces, outdoor burning in firepots and chimeneas	• 2022 emissions projected from 2020 NEI with state-level adjustment factors derived from State Energy Data System (SEDS). 2020 NEI estimates developed from national county-level survey of wood burning activity in 2018. • Specific adjustments for California and Idaho
Solvents (np_solvents)	Annual county-level emissions from residential, commercial, institutional, and industrial use of volatile chemical products (VCPs)	• 2022 was data unavailable; VCPy model used to estimate 2021 emissions and source classification code (SCC)-specific ratios for 2021/2020 applied to 2020 NEI
Open Burning (openburn)	Annual county-level emissions from yard waste, land clearing, and residential household waste burning	• Emissions from 2020 NEI without updates
Nonpoint (nonpt)	Annual county-level emissions from stationary nonpoint sources not subdivided into other sectors	• 2022 base year emissions from portable fuel containers, asphalt paving, commercial cooking, charcoal grilling, landfills and publicly-owned treatment works (POTWs) held constant at 2020 NEI levels • Emissions from Stage I gasoline unloading at service stations and bulk terminals and plants, aviation gasoline Stage I and II, pipeline gasoline, all other nonpoint source fuel combustion from 2020 NEI adjusted for 2022 using Energy Information Agency (EIA) State Energy Data System (SEDS) consumption ratios • Cremation emissions from 2020 NEI adjusted using Center for Disease Control (CDC) and National Funeral Directors Association data for human cremation in 2022
U.S. On-road		
On-road Mobile (on-road)	Emissions from motorized vehicles that operate on public roadways including parked vehicle and on-network processes. Vehicle source types include motorcycles; passenger cars and trucks; light commercial trucks; transit, school, and other buses; refuse trucks; single unit	• 2022 emissions developed using SMOKE-MOVES for representative U.S. counties based on year-specific emission factors from MOVES4 and county-level activity data • Activity data included vehicle miles traveled (VMT) from Federal Highway Administration data and some state and local agency submissions, vehicle population, starts, hoteling hours, off-network idling hours.

	short-haul trucks and long-haul trucks; motor homes, combinations short-haul trucks and long-haul trucks. Vehicles are further distinguished by fuel use including diesel, gasoline, E-85, compressed natural gas (CNG).	• Texas submitted 2022 VMT and hoteling activity • MOVES emission factor development applied year-specific hourly meteorological data • Vehicle age distributions in MOVES4 were held constant between 2020 and 2022 except for Georgia. 2020 age distributions were based on vehicle registration data from IHS Markit.
U.S. Non-road		
Rail Locomotives (rail)	Annual county-level emissions from all locomotives in nonpoint data category including line haul locomotives on Class I,II, and III railroads and commuter rail lines and Amtrak. Excludes railway maintenance locomotives and point source yard locomotives.	• 2022 emissions projected from 2020 NEI • Emissions from Class I line haul rail locomotives projected based on R-1 fuel use from Surface Transportation Board. Link-level line-haul activity for 2020 NEI from Federal Railroad Administration data • Emissions from Class II and III locomotives projected using activity data from U.S EIA's Annual Energy Outlook. Nationwide data for locations of short-line and regional railroads operation. • Emissions from Amtrak rail lines followed approach for Class II and III locomotives with downward adjustment of 2020 fuel use and emissions based on Amtrak's FY22 Sustainability Report. Even distribution of fuel use across all diesel-powered route miles in 2020 NEI continued for 2022. • Commuter rail emissions based on approach for Class II and III railroads with fuel use estimate based on National Transit Database from Federal Transit Administration. • Texas submitted locomotive emissions to SCCs (not specifically identified)
Non-road Equipment (non-road)	Monthly county-level emissions from all mobile sources that do not operate on roads, excluding CMVs, railways, and aircraft.	• For all states except California, 2022 emissions developed using MOVES4 that incorporated NON-ROAD model (MOVES-NON-ROAD) • Texas submitted county-level database for 2020 NEI. County databases used to run MOVES-NON-ROAD were consistent with 2020 NEI state submissions
U.S. Fires		
Wildfires (ptfire-wild)	Emissions from forest wildfires from smoldering and flaming combustion phase	• 2022 day-specific emissions at point locations • Satellite Mapping Automated Reanalysis Tool for Fire Incident Reconciliation version 2 (SMARTFIRE2) applied to obtain fire location coordinates, daily acres burned by fire type • Day-specific emissions from Bluesky Modeling Pipeline • Texas provided activity data for wildfires
Prescribed Fires (ptfire-rx)	Emissions from prescribed burning: pile burns, forest burning flaming smoldering combustion phases, rangeland burning	• 2022 day-specific emissions at point locations modeled using similar approach as for wildfires • Texas provided activity data for prescribed burns but not pile burns
Agricultural Fires (ptagfire)	Emissions from agricultural production; agricultural field burning of crops (bean, corn, cotton, rice, wheat, sugar cane, winter wheat and soybeans, unspecified; rangeland burning: flaming)	• Area sources in NEI modeled as day-specific fires in 2022v1 emissions modeling platform using Hazard Mapping System (HMS) activity data filtered using 2022 U.S. Department of Agriculture (USDA) cropland data layer (CDL) and similar approach as for ptfire emissions

U.S. Biogenic		
Biogenic Emissions (BEIS)	Emissions from vegetation and soils	• 2022 hourly gridded emissions developed using year-specific meteorological data, Biogenic Emission Landcover Database version 6 (BELD6) and Biogenic Emission Inventory System version 4 (BEIS4) within CMAQ
Mexico		
Point Sources (canmex_point)	Emissions from stationary point sources in Mexico	• Emissions representing 2018 developed for six border states (Chihuahua, Baja California, Sonora, Coahuila, Nuevo Leon, Tamaulipas) by EPA and Mexico's Secretaría de Medio Ambiente y Recursos Naturales (SEMARNAT) • Emissions for all other states from Inventorio Nacional de Emisiones de Mexico 2016 (SEMARNAT) projected to 2019 (EPA 2019ge platform) • Annual and monthly point resolution
Agricultural Sources (canmex_ag)	Emissions from agricultural activity in Mexico and Canada	• Emissions representing 2018 for six border states: Chihuahua, Baja California, Sonora, Coahuila, Nuevo Leon, Tamaulipas • Emissions for all other states projected from 2016 to 2019 (EPA 2019ge platform) • Annual municipio resolution
Nonpoint and Non-road Sources (canmex_area)	Emissions from nonpoint and non-road sources in Mexico and Canada	• Emissions representing 2018 for six border states: Chihuahua, Baja California, Sonora, Coahuila, Nuevo Leon, Tamaulipas • Emissions for all other states projected from 2016 to 2019 (EPA 2019ge platform) • Annual municipio resolution
On-road Sources (mexico_on-road)	Emissions from on-road mobile sources in Mexico	• 2020 and 2023 emissions from MOVES-Mexico interpolated to 2022 • VOC HAPs and speciated VOCs consistent with U.S. MOVES model (included naphthalene, benzene, acetaldehyde, formaldehyde, methanol as well as toluene, xylene, ethylbenzene, and others; particulate HAPs and diesel particulate matter not included) • Monthly municipio resolution
Fires (ptfire_othna)	Emissions from fires in Mexico, Central America, and Caribbean	• Daily 2022 fire emissions from wildfires and agricultural burning at point locations from the Fire Inventory from the National Center for Atmospheric Research (NCAR) version 2.5 (FINN v2.5)

*Commercial marine vehicles (CMV) and emissions from Canada were not within the El Paso-Juárez CAMx domain and are not included.

Appendix B

(a)

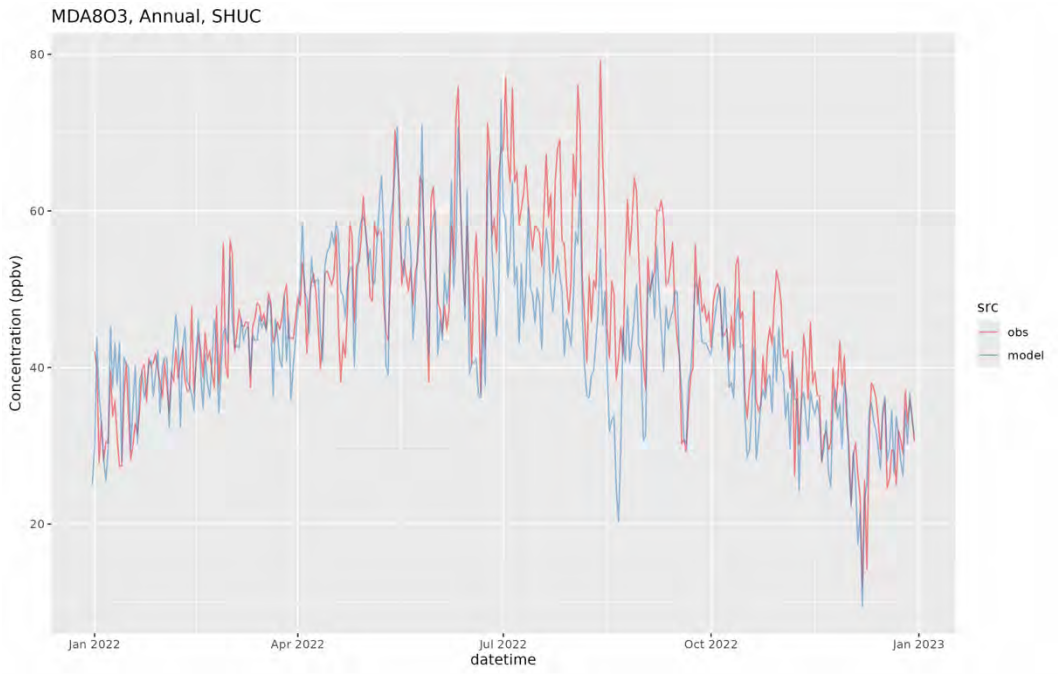

(b)

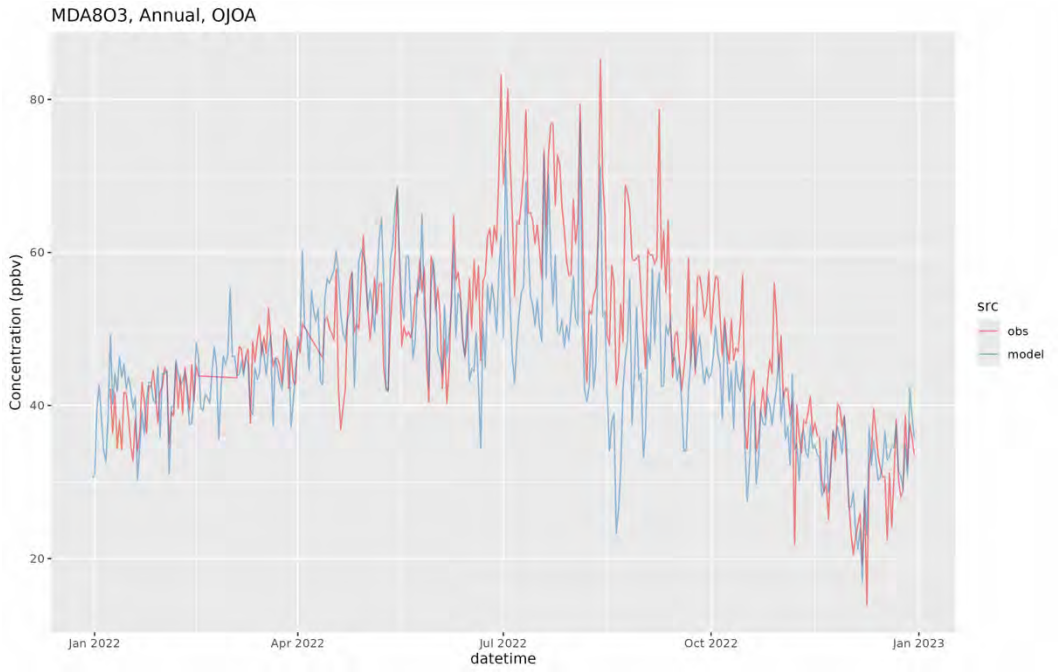

(c)

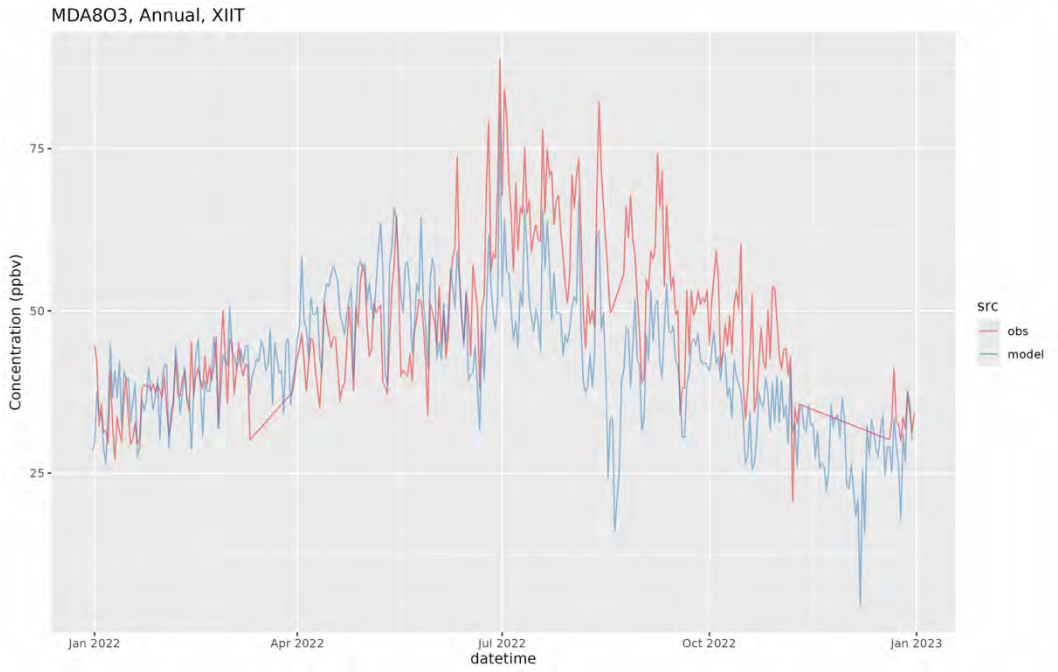

Figure B.1 Time series of observed (red) and modeled (blue) MDA8 ozone concentrations in 2022 at (a) Socorro Hueco (El Paso), (b) Ojo de Aqua (El Paso), and (c) Institute for Engineering and Technology (Juárez). Note differences in scales between plots.

(a)

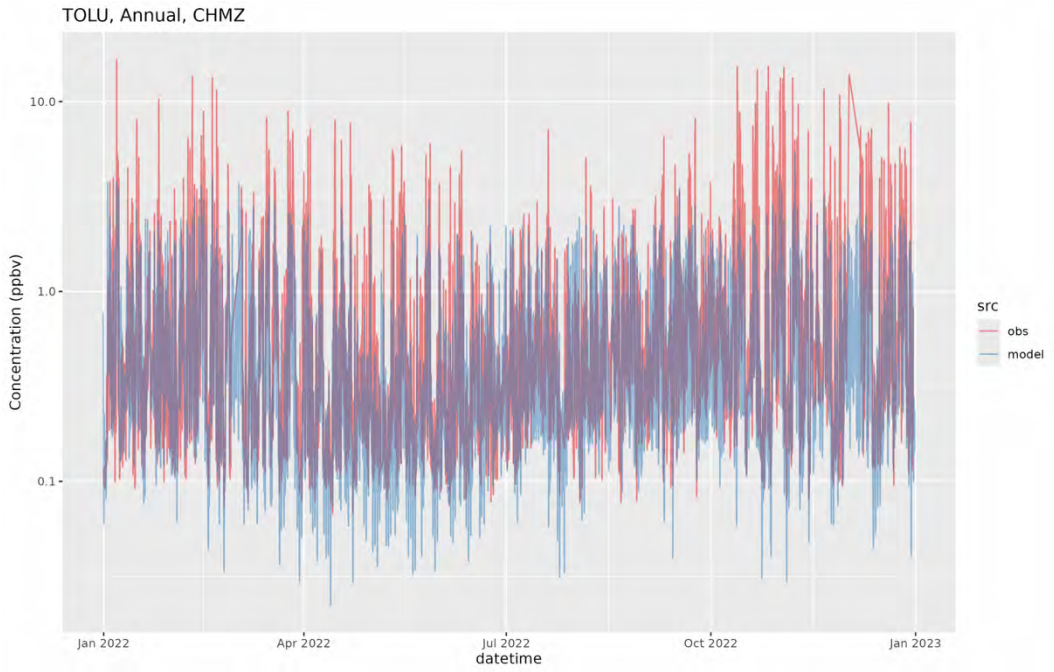

(b)

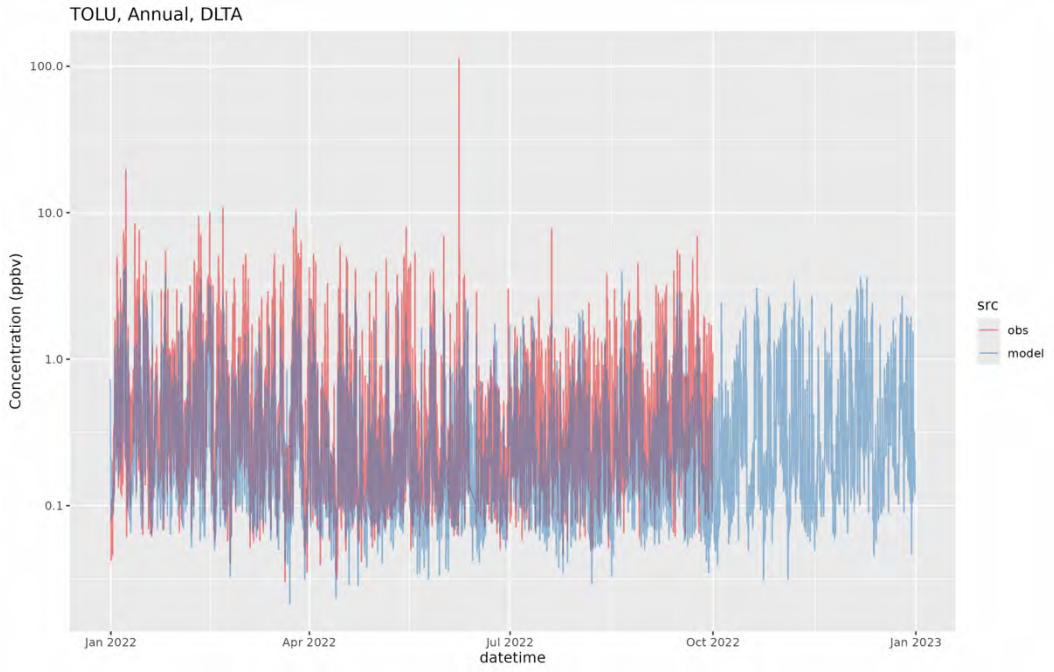

Figure B.2 Time series of observed (red) and modeled (blue) hourly toluene concentrations (ppb) in 2022 at (a) Chamizal (El Paso) and (b) Delta Drive. Note differences in scales between plots.

Appendix C

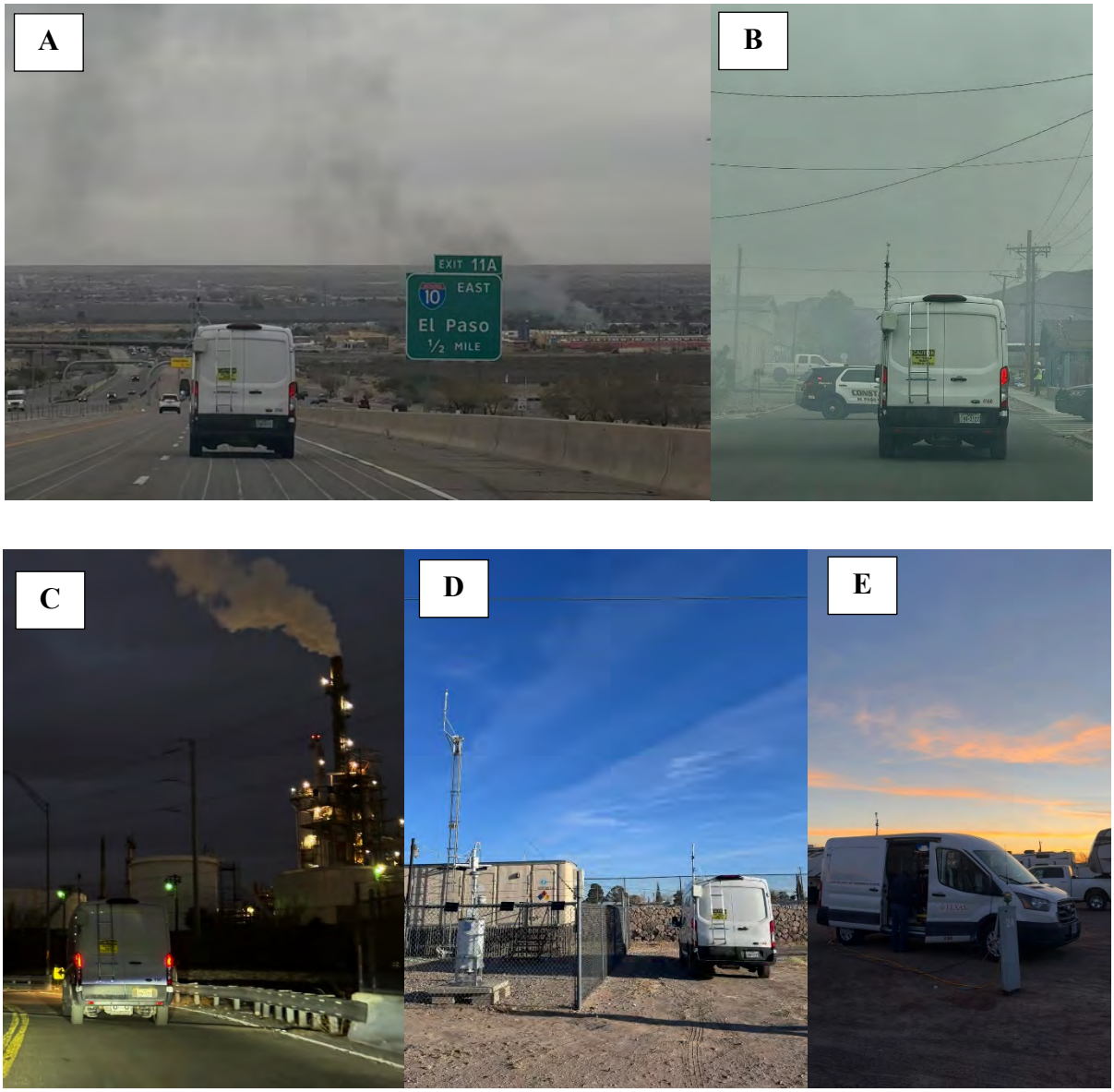

Figure C.1 Photographs showing the UT mobile lab during Winter campaign in (A) driving down the trans mountain drive; (B) near the house fire; (C) near refineries; (D) colocation with Chamizal TCEQ station; (E) charging and measurement at Roadrunner RV.

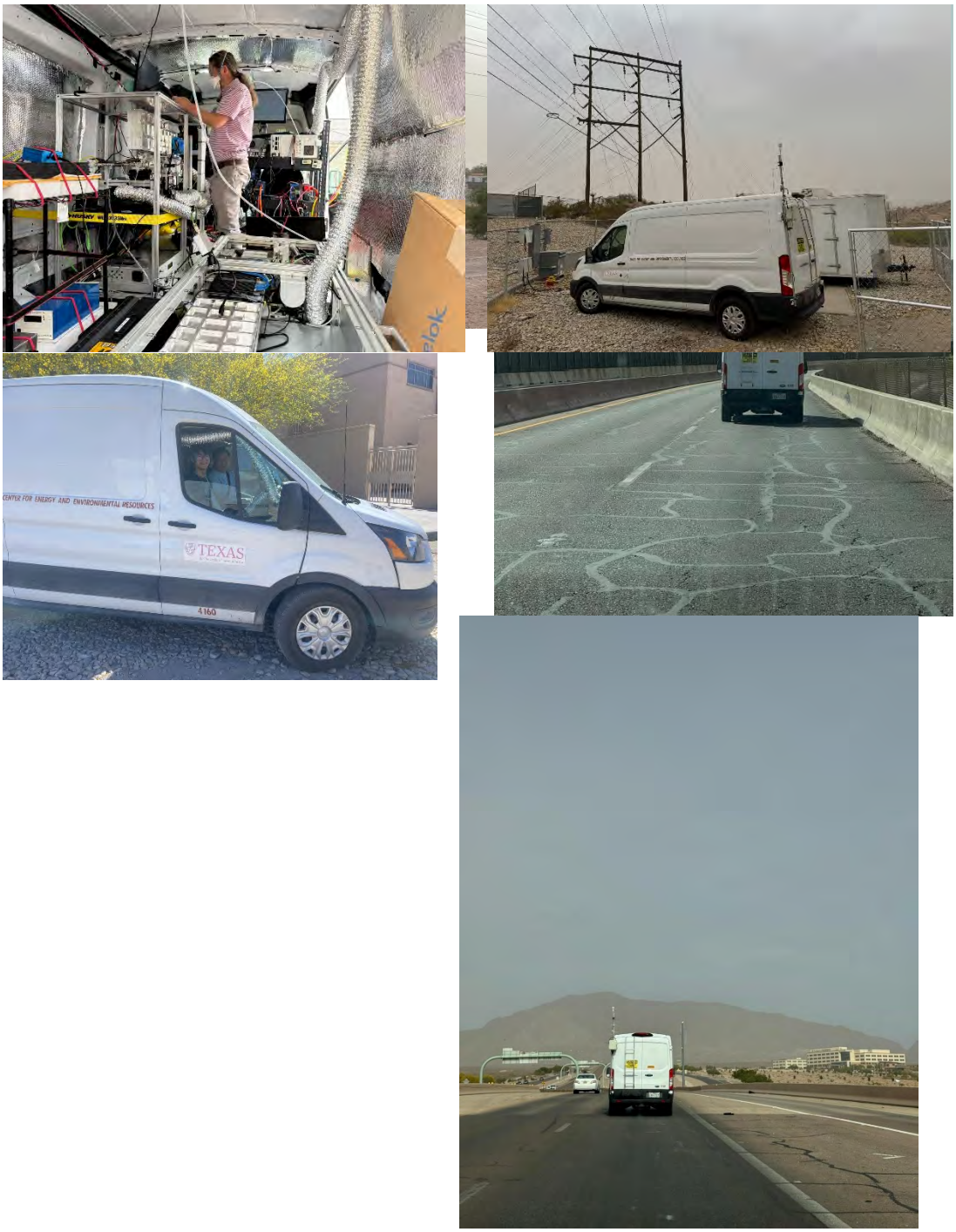

Figure C.2 Select photographs from the May/June field campaign. **Top left:** Interior van layout with visible instrumentation and active cooling ducts. **Top right:** Van during co-location at the UTEP stationary monitoring site. **Middle left:** Research team preparing for mobile deployment. **Middle right:** Measurement activities near the wastewater treatment plant. **Bottom left:** Mobile sampling conducted near the U.S. – Mexico border. **Bottom right:** Measurement during a mild dust storm with reduced visibility.

Appendix D.

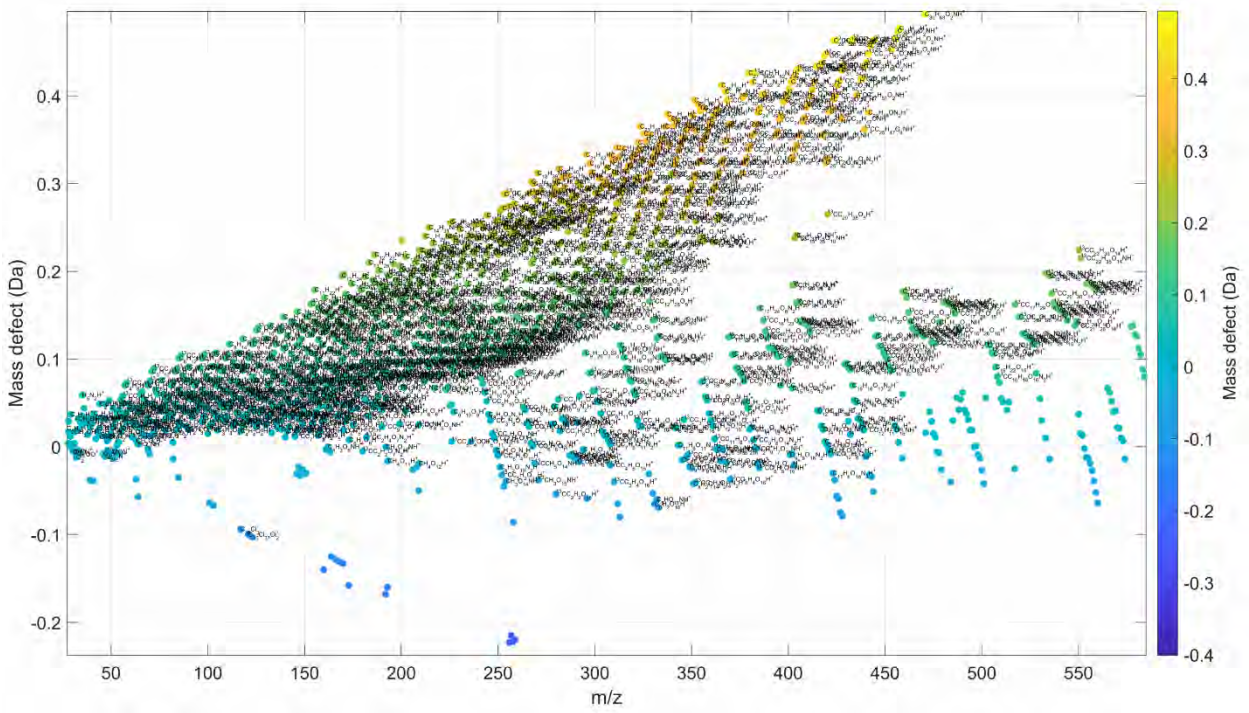

Figure D.1 Mass defect plot for the unified mass list with more than 1500 ions detected in the El Paso Winter Campaign (the identified formulas shown are preliminary).

Appendix E.

Figure E1. Spatial observation maps (percentile and ppb) for 40 prominent VOC ions in the summer and winter field campaigns.

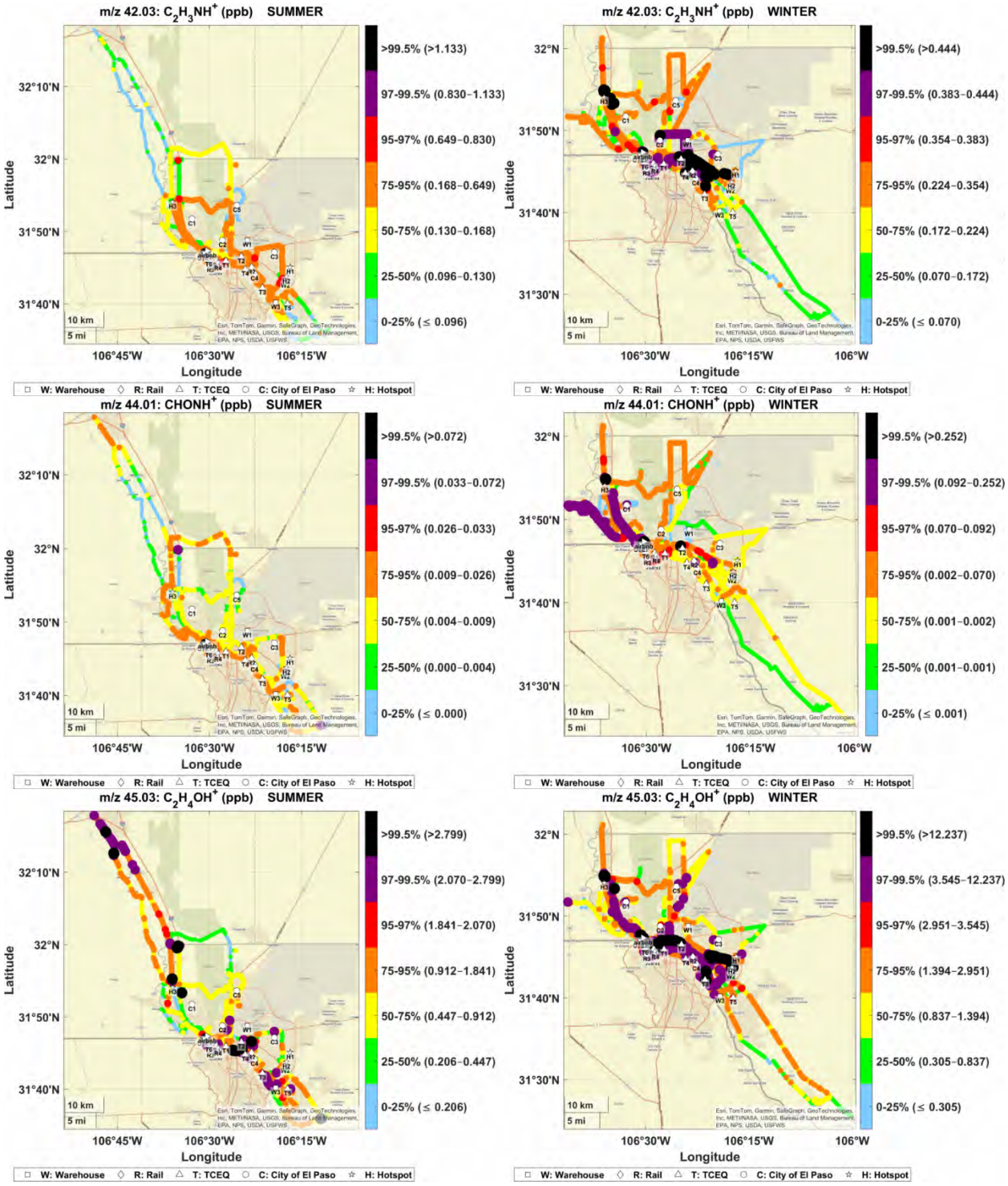
m/z 42.03: C2H3NH+ (ppb) SUMMER
>99.5% (>1.133)
97-99.5% (0.830-1.133)
95-97% (0.649-0.830)
75-95% (0.168-0.649)
50-75% (0.130-0.168)
25-50% (0.096-0.130)
0-25% (≤ 0.096)
m/z 42.03: C2H3NH+ (ppb) WINTER
>99.5% (>0.444)
97-99.5% (0.383-0.444)
95-97% (0.354-0.383)
75-95% (0.224-0.354)
50-75% (0.172-0.224)
25-50% (0.070-0.172)
0-25% (≤ 0.070)
m/z 44.01: CHONH+ (ppb) SUMMER
>99.5% (>0.072)
97-99.5% (0.033-0.072)
95-97% (0.026-0.033)
75-95% (0.009-0.026)
50-75% (0.004-0.009)
25-50% (0.000-0.004)
0-25% (≤ 0.000)
m/z 44.01: CHONH+ (ppb) WINTER
>99.5% (>0.252)
97-99.5% (0.092-0.252)
95-97% (0.070-0.092)
75-95% (0.002-0.070)
50-75% (0.001-0.002)
25-50% (0.001-0.001)
0-25% (≤ 0.001)
m/z 45.03: C2H4OH+ (ppb) SUMMER
>99.5% (>2.799)
97-99.5% (2.070-2.799)
95-97% (1.841-2.070)
75-95% (0.912-1.841)
50-75% (0.447-0.912)
25-50% (0.206-0.447)
0-25% (≤ 0.206)
m/z 45.03: C2H4OH+ (ppb) WINTER
>99.5% (>12.237)
97-99.5% (3.545-12.237)
95-97% (2.951-3.545)
75-95% (1.394-2.951)
50-75% (0.837-1.394)
25-50% (0.305-0.837)
0-25% (≤ 0.305)
Latitude
Longitude
W: Warehouse R: Rail T: TCEQ C: City of El Paso H: Hotspot

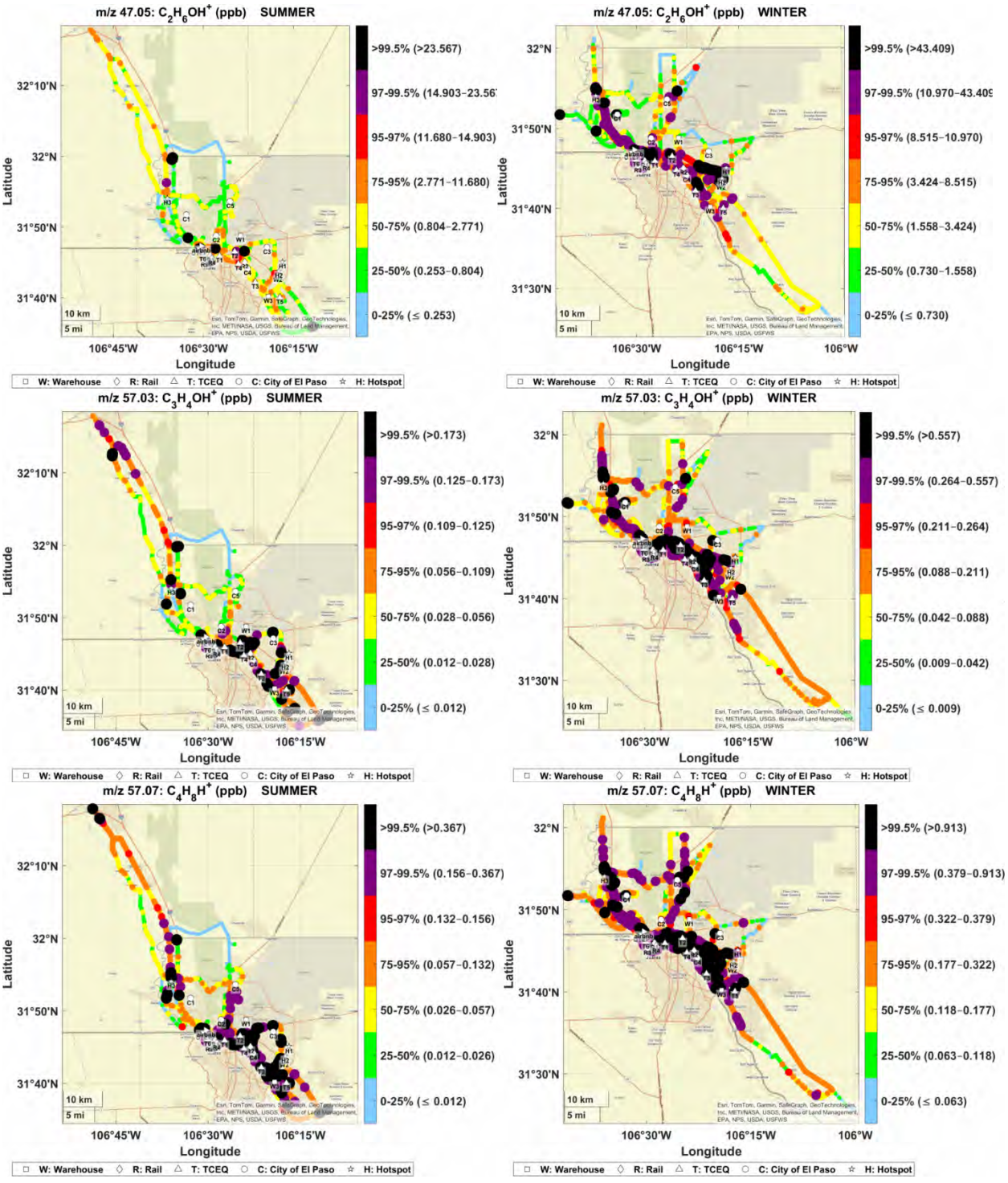
m/z 47.05: C2H6OH+ (ppb) SUMMER
>99.5% (>23.567)
97-99.5% (14.903-23.56
95-97% (11.680-14.903)
75-95% (2.771-11.680)
50-75% (0.804-2.771)
25-50% (0.253-0.804)
0-25% (≤ 0.253)
m/z 47.05: C2H6OH+ (ppb) WINTER
>99.5% (>43.409)
97-99.5% (10.970-43.409
95-97% (8.515-10.970)
75-95% (3.424-8.515)
50-75% (1.558-3.424)
25-50% (0.730-1.558)
0-25% (≤ 0.730)
m/z 57.03: C3H4OH+ (ppb) SUMMER
>99.5% (>0.173)
97-99.5% (0.125-0.173)
95-97% (0.109-0.125)
75-95% (0.056-0.109)
50-75% (0.028-0.056)
25-50% (0.012-0.028)
0-25% (≤ 0.012)
m/z 57.03: C3H4OH+ (ppb) WINTER
>99.5% (>0.557)
97-99.5% (0.264-0.557)
95-97% (0.211-0.264)
75-95% (0.088-0.211)
50-75% (0.042-0.088)
25-50% (0.009-0.042)
0-25% (≤ 0.009)
m/z 57.07: C4H8H+ (ppb) SUMMER
>99.5% (>0.367)
97-99.5% (0.156-0.367)
95-97% (0.132-0.156)
75-95% (0.057-0.132)
50-75% (0.026-0.057)
25-50% (0.012-0.026)
0-25% (≤ 0.012)
m/z 57.07: C4H8H+ (ppb) WINTER
>99.5% (>0.913)
97-99.5% (0.379-0.913)
95-97% (0.322-0.379)
75-95% (0.177-0.322)
50-75% (0.118-0.177)
25-50% (0.063-0.118)
0-25% (≤ 0.063)
Latitude
Longitude
32°10'N
32°N
31°50'N
31°40'N
31°30'N
106°45'W
106°30'W
106°15'W
106°W
10 km
5 mi
W: Warehouse
R: Rail
T: TCEQ
C: City of El Paso
H: Hotspot

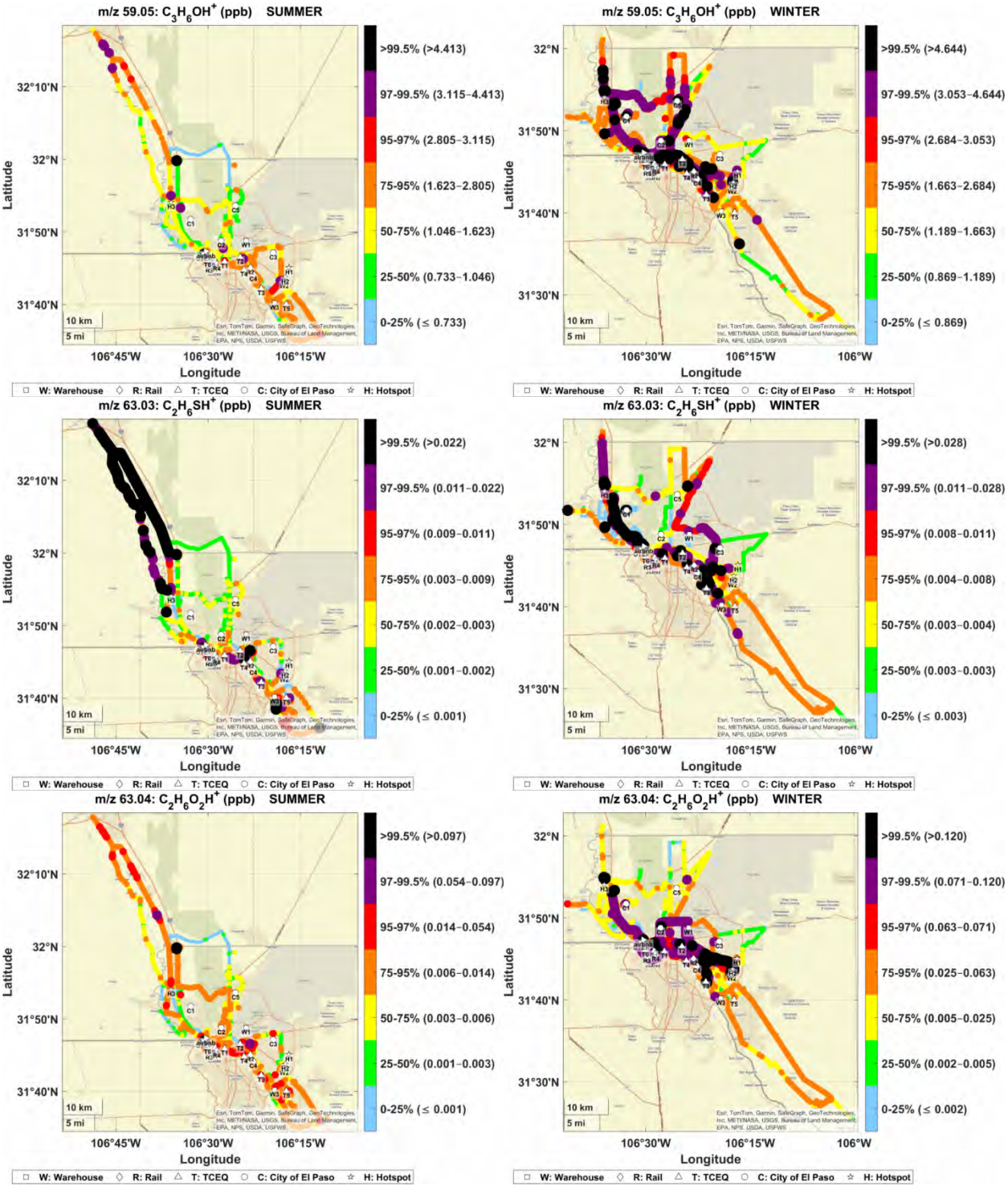
m/z 59.05: C3H6OH+ (ppb) SUMMER
>99.5% (>4.413)
97-99.5% (3.115-4.413)
95-97% (2.805-3.115)
75-95% (1.623-2.805)
50-75% (1.046-1.623)
25-50% (0.733-1.046)
0-25% (≤ 0.733)
m/z 59.05: C3H6OH+ (ppb) WINTER
>99.5% (>4.644)
97-99.5% (3.053-4.644)
95-97% (2.684-3.053)
75-95% (1.663-2.684)
50-75% (1.189-1.663)
25-50% (0.869-1.189)
0-25% (≤ 0.869)
m/z 63.03: C2H6SH+ (ppb) SUMMER
>99.5% (>0.022)
97-99.5% (0.011-0.022)
95-97% (0.009-0.011)
75-95% (0.003-0.009)
50-75% (0.002-0.003)
25-50% (0.001-0.002)
0-25% (≤ 0.001)
m/z 63.03: C2H6SH+ (ppb) WINTER
>99.5% (>0.028)
97-99.5% (0.011-0.028)
95-97% (0.008-0.011)
75-95% (0.004-0.008)
50-75% (0.003-0.004)
25-50% (0.003-0.003)
0-25% (≤ 0.003)
m/z 63.04: C2H6O2H+ (ppb) SUMMER
>99.5% (>0.097)
97-99.5% (0.054-0.097)
95-97% (0.014-0.054)
75-95% (0.006-0.014)
50-75% (0.003-0.006)
25-50% (0.001-0.003)
0-25% (≤ 0.001)
m/z 63.04: C2H6O2H+ (ppb) WINTER
>99.5% (>0.120)
97-99.5% (0.071-0.120)
95-97% (0.063-0.071)
75-95% (0.025-0.063)
50-75% (0.005-0.025)
25-50% (0.002-0.005)
0-25% (≤ 0.002)
Latitude
Longitude
32°10'N
32°N
31°50'N
31°40'N
31°30'N
106°45'W
106°30'W
106°15'W
106°W
10 km
5 mi
W: Warehouse
R: Rail
T: TCEQ
C: City of El Paso
H: Hotspot

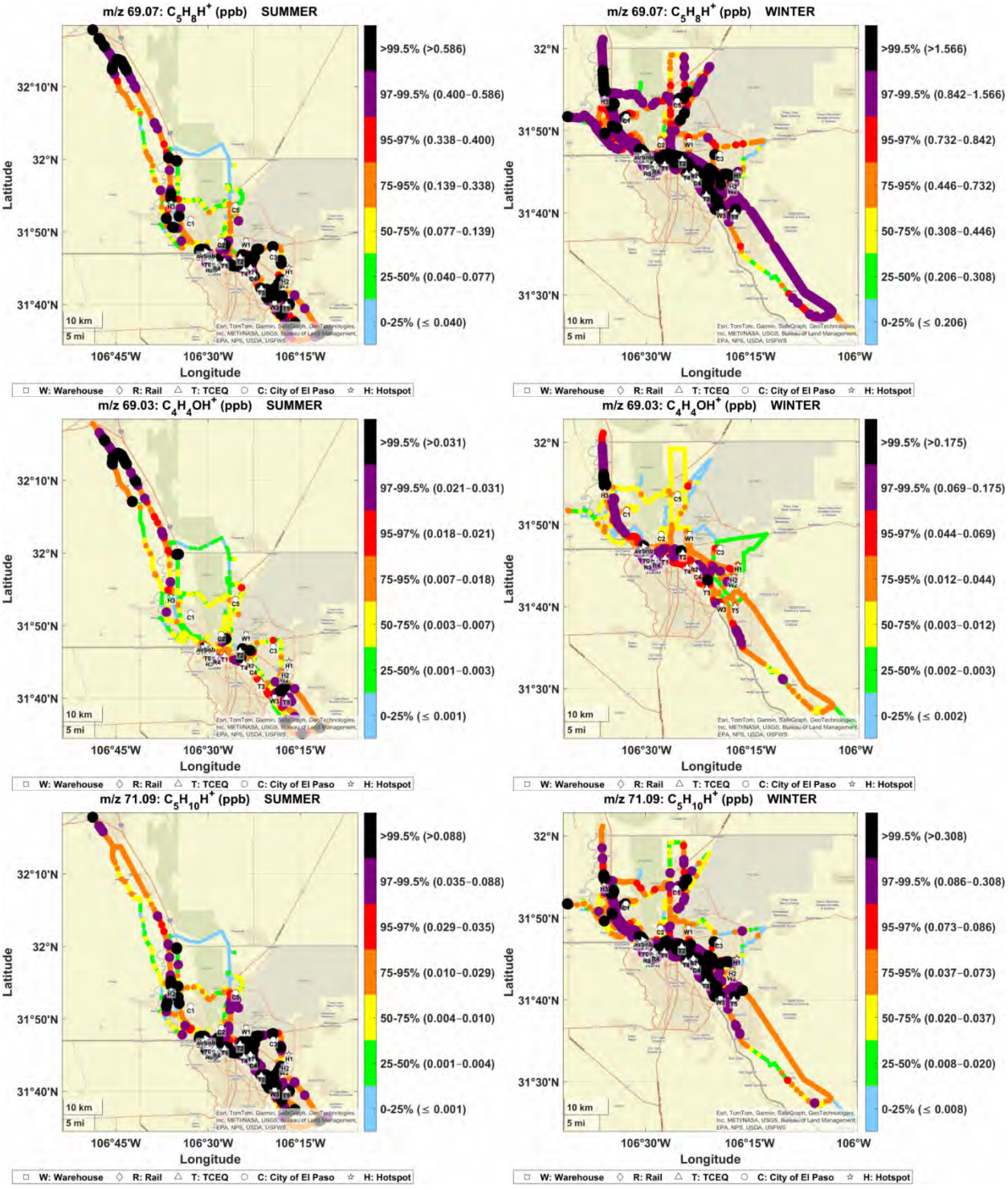
m/z 69.07: C5H8H+ (ppb) SUMMER
>99.5% (>0.586)
97-99.5% (0.400–0.586)
95-97% (0.338–0.400)
75-95% (0.139–0.338)
50-75% (0.077–0.139)
25-50% (0.040–0.077)
0-25% (≤ 0.040)
m/z 69.07: C5H8H+ (ppb) WINTER
>99.5% (>1.566)
97-99.5% (0.842–1.566)
95-97% (0.732–0.842)
75-95% (0.446–0.732)
50-75% (0.308–0.446)
25-50% (0.206–0.308)
0-25% (≤ 0.206)
m/z 69.03: C4H4OH+ (ppb) SUMMER
>99.5% (>0.031)
97-99.5% (0.021–0.031)
95-97% (0.018–0.021)
75-95% (0.007–0.018)
50-75% (0.003–0.007)
25-50% (0.001–0.003)
0-25% (≤ 0.001)
m/z 69.03: C4H4OH+ (ppb) WINTER
>99.5% (>0.175)
97-99.5% (0.069–0.175)
95-97% (0.044–0.069)
75-95% (0.012–0.044)
50-75% (0.003–0.012)
25-50% (0.002–0.003)
0-25% (≤ 0.002)
m/z 71.09: C5H10H+ (ppb) SUMMER
>99.5% (>0.088)
97-99.5% (0.035–0.088)
95-97% (0.029–0.035)
75-95% (0.010–0.029)
50-75% (0.004–0.010)
25-50% (0.001–0.004)
0-25% (≤ 0.001)
m/z 71.09: C5H10H+ (ppb) WINTER
>99.5% (>0.308)
97-99.5% (0.086–0.308)
95-97% (0.073–0.086)
75-95% (0.037–0.073)
50-75% (0.020–0.037)
25-50% (0.008–0.020)
0-25% (≤ 0.008)
Latitude
Longitude
32°10'N
32°N
31°50'N
31°40'N
31°30'N
106°45'W
106°30'W
106°15'W
106°W
10 km
5 mi
W: Warehouse
R: Rail
T: TCEQ
C: City of El Paso
H: Hotspot

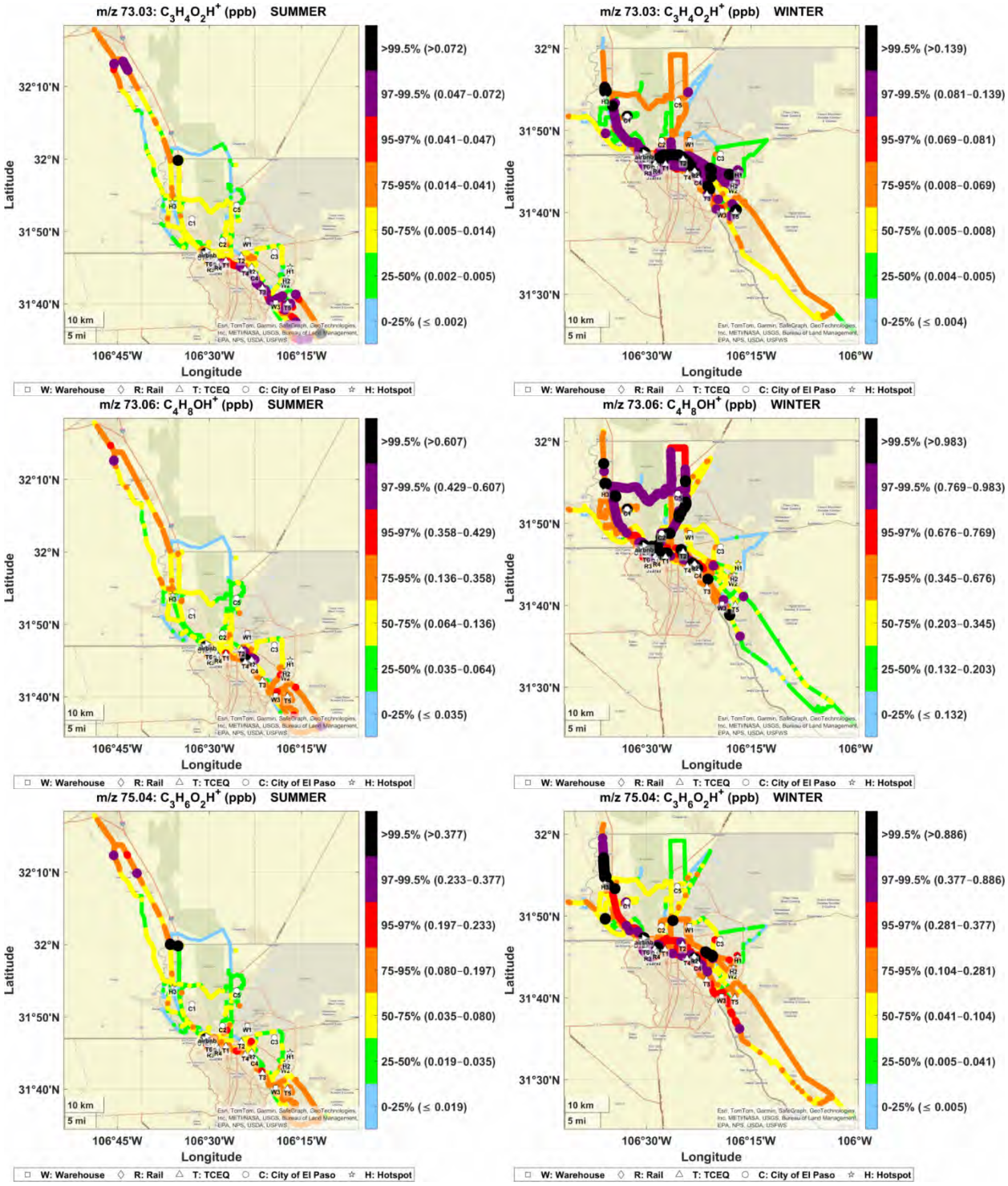
m/z 73.03: C3H4O2H+ (ppb) SUMMER
>99.5% (>0.072)
97-99.5% (0.047-0.072)
95-97% (0.041-0.047)
75-95% (0.014-0.041)
50-75% (0.005-0.014)
25-50% (0.002-0.005)
0-25% (≤ 0.002)
m/z 73.03: C3H4O2H+ (ppb) WINTER
>99.5% (>0.139)
97-99.5% (0.081-0.139)
95-97% (0.069-0.081)
75-95% (0.008-0.069)
50-75% (0.005-0.008)
25-50% (0.004-0.005)
0-25% (≤ 0.004)
m/z 73.06: C4H8OH+ (ppb) SUMMER
>99.5% (>0.607)
97-99.5% (0.429-0.607)
95-97% (0.358-0.429)
75-95% (0.136-0.358)
50-75% (0.064-0.136)
25-50% (0.035-0.064)
0-25% (≤ 0.035)
m/z 73.06: C4H8OH+ (ppb) WINTER
>99.5% (>0.983)
97-99.5% (0.769-0.983)
95-97% (0.676-0.769)
75-95% (0.345-0.676)
50-75% (0.203-0.345)
25-50% (0.132-0.203)
0-25% (≤ 0.132)
m/z 75.04: C3H6O2H+ (ppb) SUMMER
>99.5% (>0.377)
97-99.5% (0.233-0.377)
95-97% (0.197-0.233)
75-95% (0.080-0.197)
50-75% (0.035-0.080)
25-50% (0.019-0.035)
0-25% (≤ 0.019)
m/z 75.04: C3H6O2H+ (ppb) WINTER
>99.5% (>0.886)
97-99.5% (0.377-0.886)
95-97% (0.281-0.377)
75-95% (0.104-0.281)
50-75% (0.041-0.104)
25-50% (0.005-0.041)
0-25% (≤ 0.005)
Latitude
Longitude
32°10'N
32°N
31°50'N
31°40'N
31°30'N
106°45'W
106°30'W
106°15'W
106°W
10 km
5 mi
W: Warehouse
R: Rail
T: TCEQ
C: City of El Paso
H: Hotspot

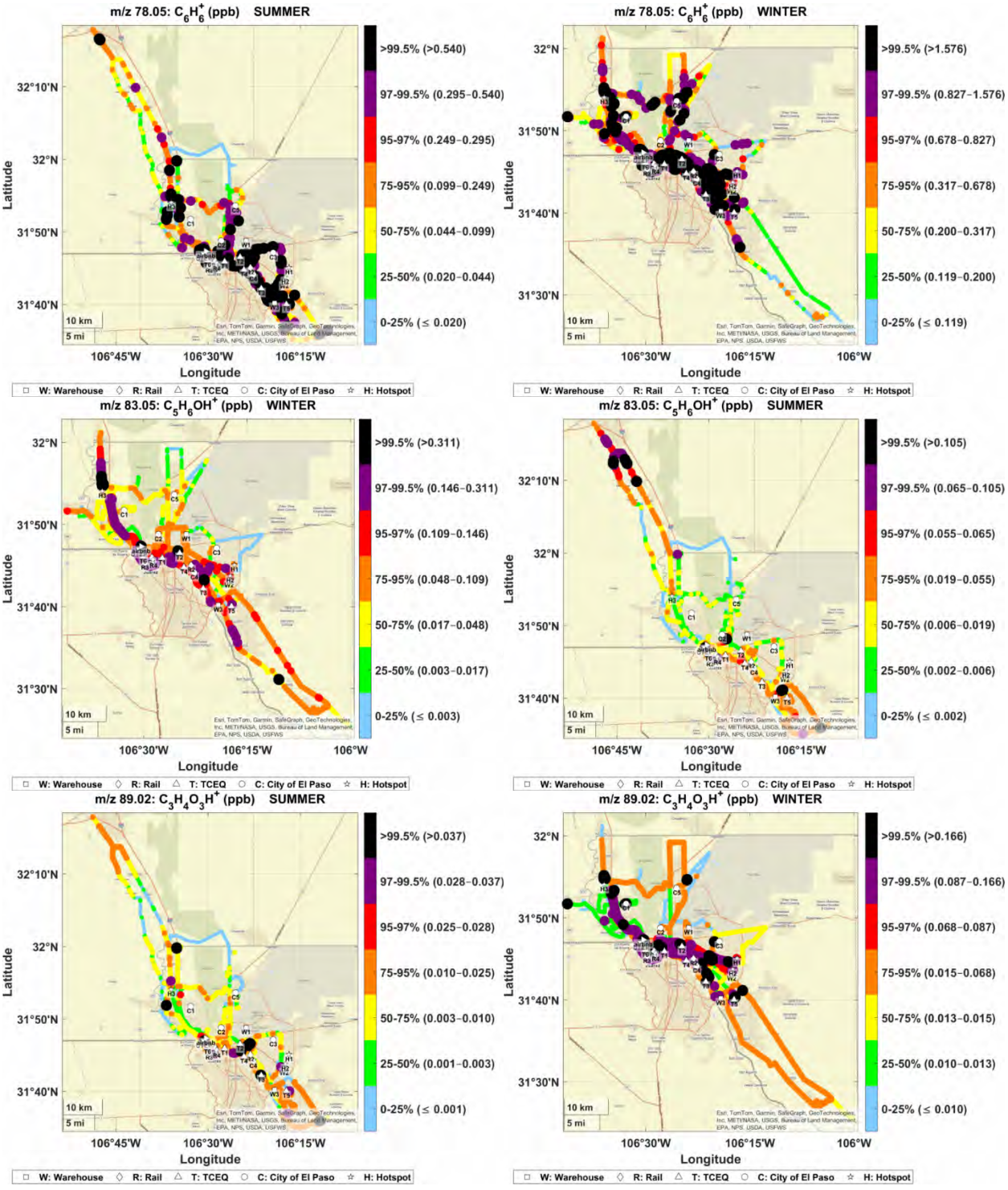
m/z 78.05: C6H6+ (ppb) SUMMER
>99.5% (>0.540)
97-99.5% (0.295-0.540)
95-97% (0.249-0.295)
75-95% (0.099-0.249)
50-75% (0.044-0.099)
25-50% (0.020-0.044)
0-25% (≤ 0.020)
m/z 78.05: C6H6+ (ppb) WINTER
>99.5% (>1.576)
97-99.5% (0.827-1.576)
95-97% (0.678-0.827)
75-95% (0.317-0.678)
50-75% (0.200-0.317)
25-50% (0.119-0.200)
0-25% (≤ 0.119)
m/z 83.05: C5H6OH+ (ppb) WINTER
>99.5% (>0.311)
97-99.5% (0.146-0.311)
95-97% (0.109-0.146)
75-95% (0.048-0.109)
50-75% (0.017-0.048)
25-50% (0.003-0.017)
0-25% (≤ 0.003)
m/z 83.05: C5H6OH+ (ppb) SUMMER
>99.5% (>0.105)
97-99.5% (0.065-0.105)
95-97% (0.055-0.065)
75-95% (0.019-0.055)
50-75% (0.006-0.019)
25-50% (0.002-0.006)
0-25% (≤ 0.002)
m/z 89.02: C3H4O3H+ (ppb) SUMMER
>99.5% (>0.037)
97-99.5% (0.028-0.037)
95-97% (0.025-0.028)
75-95% (0.010-0.025)
50-75% (0.003-0.010)
25-50% (0.001-0.003)
0-25% (≤ 0.001)
m/z 89.02: C3H4O3H+ (ppb) WINTER
>99.5% (>0.166)
97-99.5% (0.087-0.166)
95-97% (0.068-0.087)
75-95% (0.015-0.068)
50-75% (0.013-0.015)
25-50% (0.010-0.013)
0-25% (≤ 0.010)
Latitude
Longitude
W: Warehouse R: Rail T: TCEQ C: City of El Paso H: Hotspot

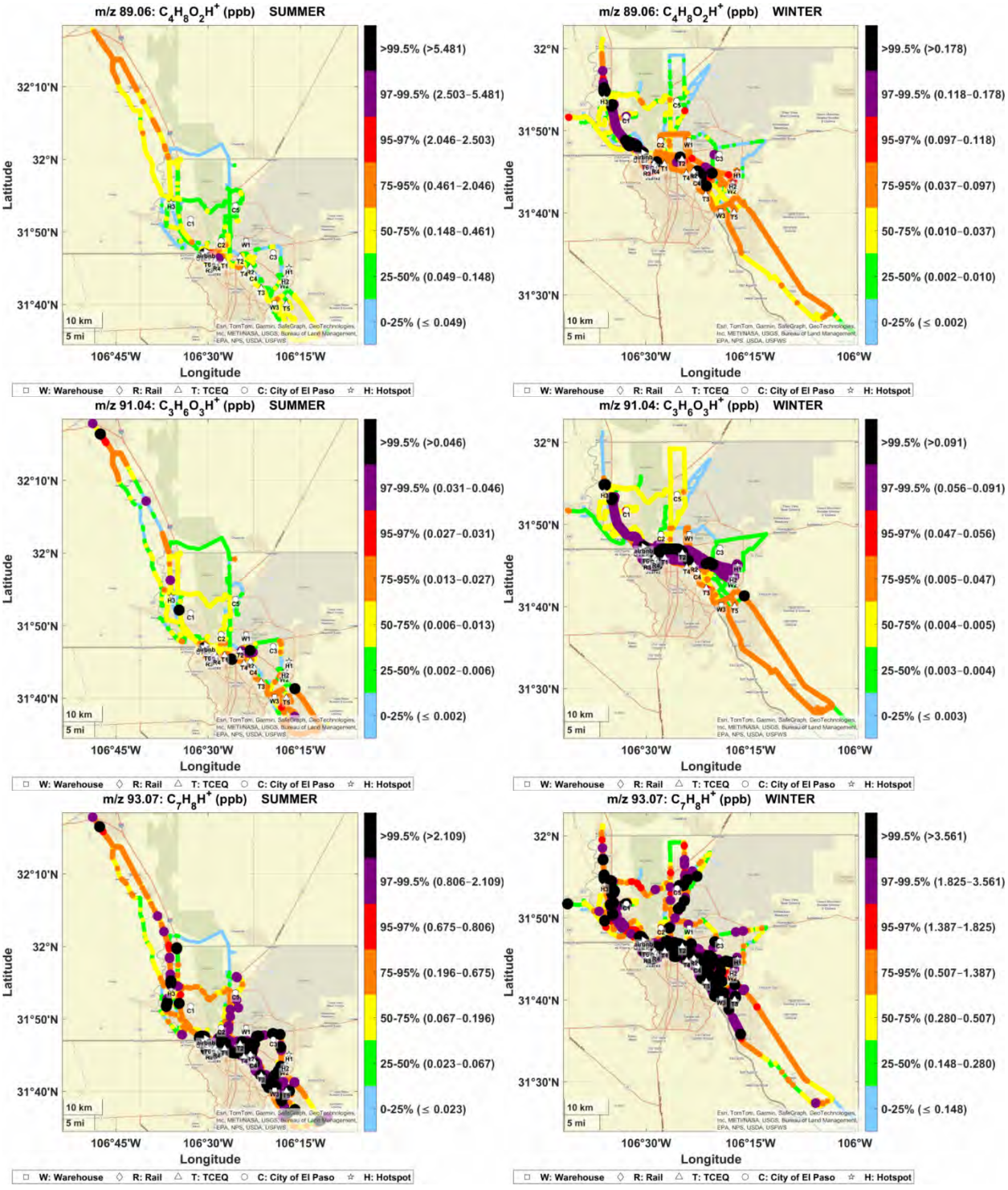
m/z 89.06: C4H8O2H+ (ppb) SUMMER
>99.5% (>5.481)
97-99.5% (2.503-5.481)
95-97% (2.046-2.503)
75-95% (0.461-2.046)
50-75% (0.148-0.461)
25-50% (0.049-0.148)
0-25% (≤ 0.049)
m/z 89.06: C4H8O2H+ (ppb) WINTER
>99.5% (>0.178)
97-99.5% (0.118-0.178)
95-97% (0.097-0.118)
75-95% (0.037-0.097)
50-75% (0.010-0.037)
25-50% (0.002-0.010)
0-25% (≤ 0.002)
m/z 91.04: C3H6O3H+ (ppb) SUMMER
>99.5% (>0.046)
97-99.5% (0.031-0.046)
95-97% (0.027-0.031)
75-95% (0.013-0.027)
50-75% (0.006-0.013)
25-50% (0.002-0.006)
0-25% (≤ 0.002)
m/z 91.04: C3H6O3H+ (ppb) WINTER
>99.5% (>0.091)
97-99.5% (0.056-0.091)
95-97% (0.047-0.056)
75-95% (0.005-0.047)
50-75% (0.004-0.005)
25-50% (0.003-0.004)
0-25% (≤ 0.003)
m/z 93.07: C7H8H+ (ppb) SUMMER
>99.5% (>2.109)
97-99.5% (0.806-2.109)
95-97% (0.675-0.806)
75-95% (0.196-0.675)
50-75% (0.067-0.196)
25-50% (0.023-0.067)
0-25% (≤ 0.023)
m/z 93.07: C7H8H+ (ppb) WINTER
>99.5% (>3.561)
97-99.5% (1.825-3.561)
95-97% (1.387-1.825)
75-95% (0.507-1.387)
50-75% (0.280-0.507)
25-50% (0.148-0.280)
0-25% (≤ 0.148)
Latitude
Longitude
32°10'N
32°N
31°50'N
31°40'N
31°30'N
106°45'W
106°30'W
106°15'W
106°W
10 km
5 mi
W: Warehouse
R: Rail
T: TCEQ
C: City of El Paso
H: Hotspot

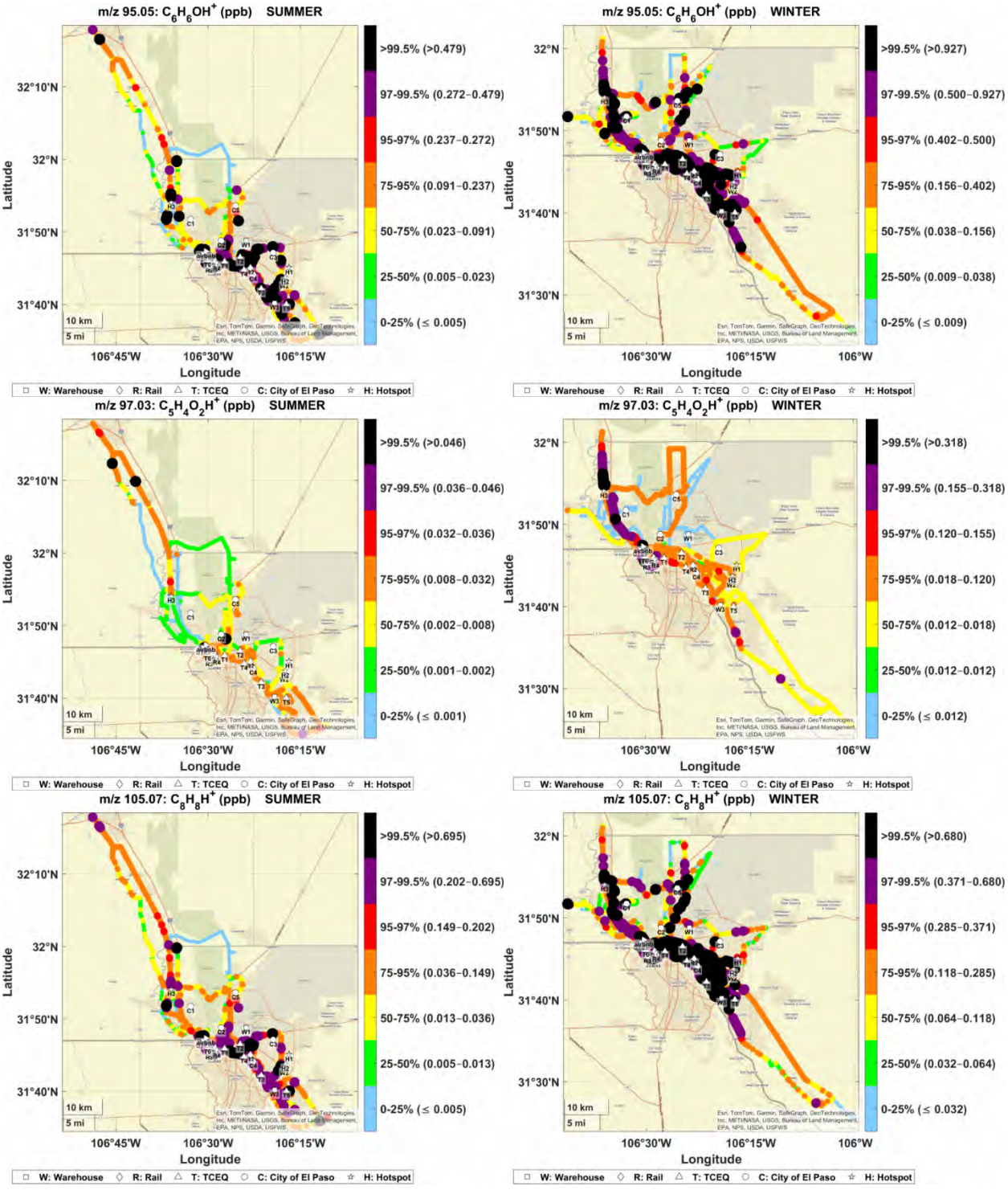
m/z 95.05: C6H6OH+ (ppb) SUMMER
>99.5% (>0.479)
97-99.5% (0.272-0.479)
95-97% (0.237-0.272)
75-95% (0.091-0.237)
50-75% (0.023-0.091)
25-50% (0.005-0.023)
0-25% (≤ 0.005)
m/z 95.05: C6H6OH+ (ppb) WINTER
>99.5% (>0.927)
97-99.5% (0.500-0.927)
95-97% (0.402-0.500)
75-95% (0.156-0.402)
50-75% (0.038-0.156)
25-50% (0.009-0.038)
0-25% (≤ 0.009)
m/z 97.03: C5H4O2H+ (ppb) SUMMER
>99.5% (>0.046)
97-99.5% (0.036-0.046)
95-97% (0.032-0.036)
75-95% (0.008-0.032)
50-75% (0.002-0.008)
25-50% (0.001-0.002)
0-25% (≤ 0.001)
m/z 97.03: C5H4O2H+ (ppb) WINTER
>99.5% (>0.318)
97-99.5% (0.155-0.318)
95-97% (0.120-0.155)
75-95% (0.018-0.120)
50-75% (0.012-0.018)
25-50% (0.012-0.012)
0-25% (≤ 0.012)
m/z 105.07: C8H8H+ (ppb) SUMMER
>99.5% (>0.695)
97-99.5% (0.202-0.695)
95-97% (0.149-0.202)
75-95% (0.036-0.149)
50-75% (0.013-0.036)
25-50% (0.005-0.013)
0-25% (≤ 0.005)
m/z 105.07: C8H8H+ (ppb) WINTER
>99.5% (>0.680)
97-99.5% (0.371-0.680)
95-97% (0.285-0.371)
75-95% (0.118-0.285)
50-75% (0.064-0.118)
25-50% (0.032-0.064)
0-25% (≤ 0.032)
Latitude
Longitude
32°10'N
32°N
31°50'N
31°40'N
31°30'N
106°45'W
106°30'W
106°15'W
106°W
10 km
5 mi
W: Warehouse
R: Rail
T: TCEQ
C: City of El Paso
H: Hotspot

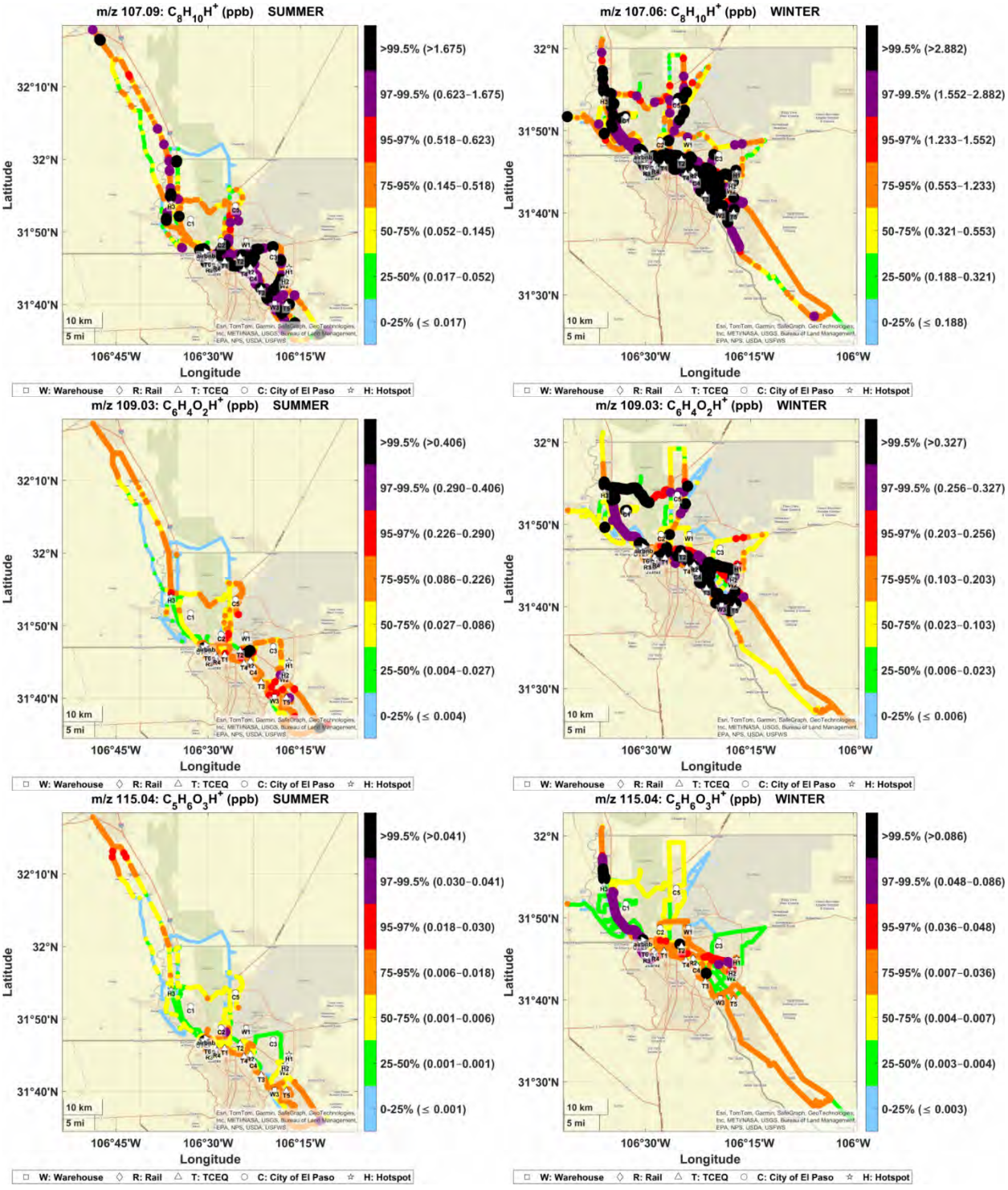
m/z 107.09: C8H10H+ (ppb) SUMMER
m/z 107.06: C8H10H+ (ppb) WINTER
m/z 109.03: C6H4O2H+ (ppb) SUMMER
m/z 109.03: C6H4O2H+ (ppb) WINTER
m/z 115.04: C5H6O3H+ (ppb) SUMMER
m/z 115.04: C5H6O3H+ (ppb) WINTER
Latitude
Longitude
32°10'N
32°N
31°50'N
31°40'N
31°30'N
106°45'W
106°30'W
106°15'W
106°W
10 km
5 mi
>99.5% (>1.675)
97-99.5% (0.623–1.675)
95-97% (0.518–0.623)
75-95% (0.145–0.518)
50-75% (0.052–0.145)
25-50% (0.017–0.052)
0-25% (≤ 0.017)
>99.5% (>2.882)
97-99.5% (1.552–2.882)
95-97% (1.233–1.552)
75-95% (0.553–1.233)
50-75% (0.321–0.553)
25-50% (0.188–0.321)
0-25% (≤ 0.188)
>99.5% (>0.406)
97-99.5% (0.290–0.406)
95-97% (0.226–0.290)
75-95% (0.086–0.226)
50-75% (0.027–0.086)
25-50% (0.004–0.027)
0-25% (≤ 0.004)
>99.5% (>0.327)
97-99.5% (0.256–0.327)
95-97% (0.203–0.256)
75-95% (0.103–0.203)
50-75% (0.023–0.103)
25-50% (0.006–0.023)
0-25% (≤ 0.006)
>99.5% (>0.041)
97-99.5% (0.030–0.041)
95-97% (0.018–0.030)
75-95% (0.006–0.018)
50-75% (0.001–0.006)
25-50% (0.001–0.001)
0-25% (≤ 0.001)
>99.5% (>0.086)
97-99.5% (0.048–0.086)
95-97% (0.036–0.048)
75-95% (0.007–0.036)
50-75% (0.004–0.007)
25-50% (0.003–0.004)
0-25% (≤ 0.003)
W: Warehouse
R: Rail
T: TCEQ
C: City of El Paso
H: Hotspot

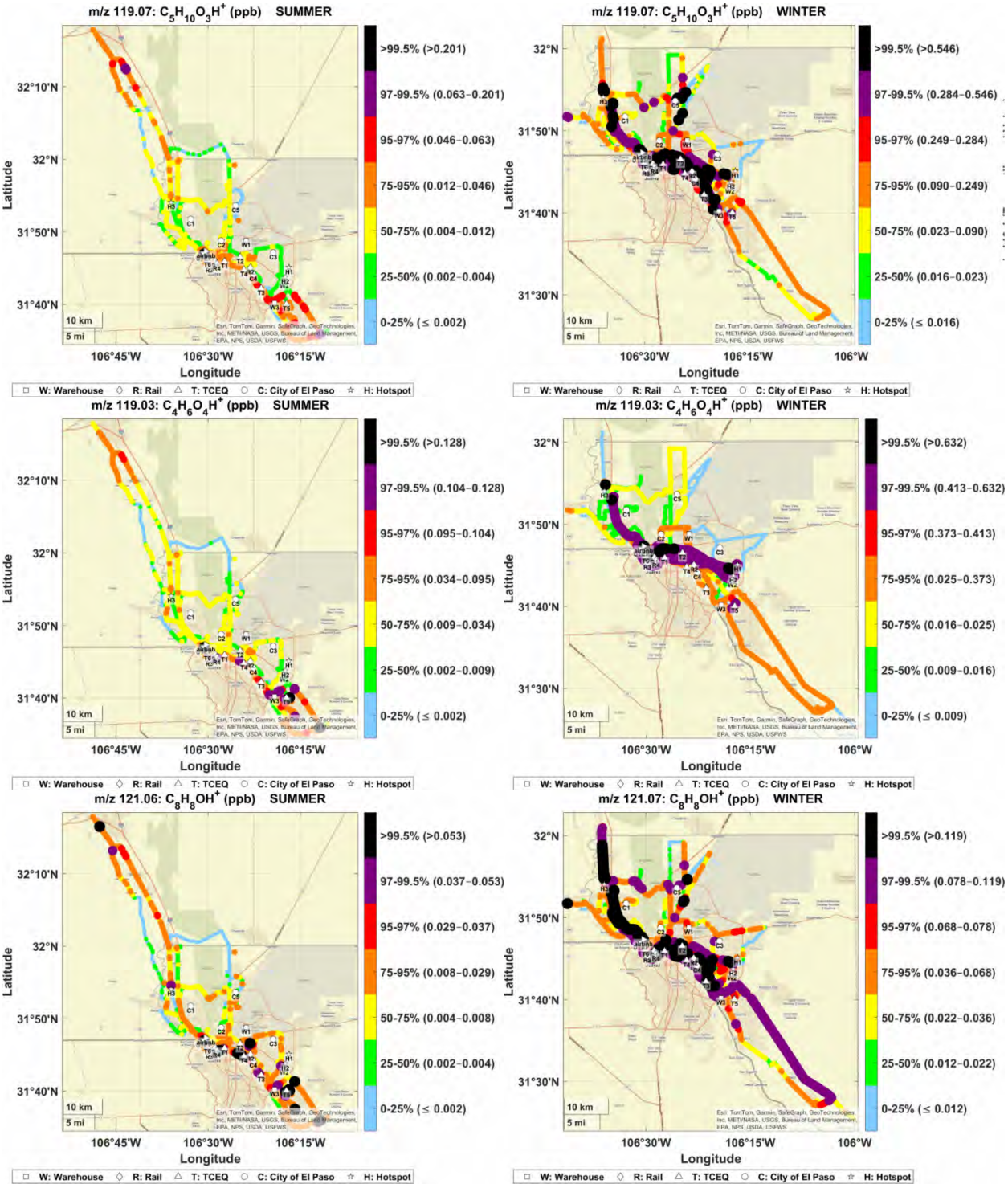
m/z 119.07: C5H10O3H+ (ppb) SUMMER
>99.5% (>0.201)
97-99.5% (0.063–0.201)
95-97% (0.046–0.063)
75-95% (0.012–0.046)
50-75% (0.004–0.012)
25-50% (0.002–0.004)
0-25% (≤ 0.002)
m/z 119.07: C5H10O3H+ (ppb) WINTER
>99.5% (>0.546)
97-99.5% (0.284–0.546)
95-97% (0.249–0.284)
75-95% (0.090–0.249)
50-75% (0.023–0.090)
25-50% (0.016–0.023)
0-25% (≤ 0.016)
m/z 119.03: C4H6O4H+ (ppb) SUMMER
>99.5% (>0.128)
97-99.5% (0.104–0.128)
95-97% (0.095–0.104)
75-95% (0.034–0.095)
50-75% (0.009–0.034)
25-50% (0.002–0.009)
0-25% (≤ 0.002)
m/z 119.03: C4H6O4H+ (ppb) WINTER
>99.5% (>0.632)
97-99.5% (0.413–0.632)
95-97% (0.373–0.413)
75-95% (0.025–0.373)
50-75% (0.016–0.025)
25-50% (0.009–0.016)
0-25% (≤ 0.009)
m/z 121.06: C8H8OH+ (ppb) SUMMER
>99.5% (>0.053)
97-99.5% (0.037–0.053)
95-97% (0.029–0.037)
75-95% (0.008–0.029)
50-75% (0.004–0.008)
25-50% (0.002–0.004)
0-25% (≤ 0.002)
m/z 121.07: C8H8OH+ (ppb) WINTER
>99.5% (>0.119)
97-99.5% (0.078–0.119)
95-97% (0.068–0.078)
75-95% (0.036–0.068)
50-75% (0.022–0.036)
25-50% (0.012–0.022)
0-25% (≤ 0.012)
Latitude
Longitude
32°10'N
32°N
31°50'N
31°40'N
31°30'N
106°45'W
106°30'W
106°15'W
106°W
10 km
5 mi
W: Warehouse
R: Rail
T: TCEQ
C: City of El Paso
H: Hotspot

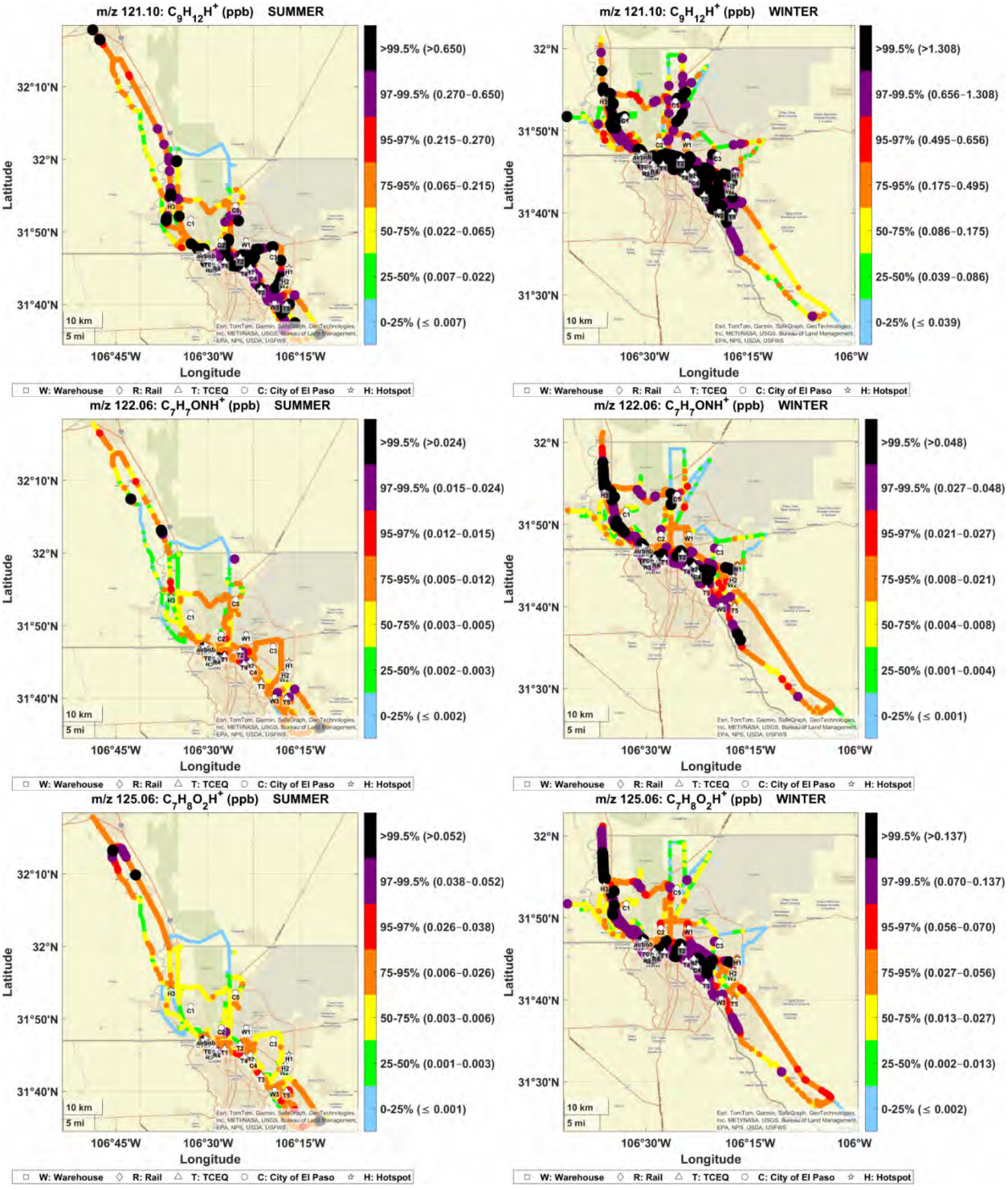
m/z 121.10: C9H12H+ (ppb) SUMMER
>99.5% (>0.650)
97-99.5% (0.270–0.650)
95-97% (0.215–0.270)
75-95% (0.065–0.215)
50-75% (0.022–0.065)
25-50% (0.007–0.022)
0-25% (≤ 0.007)
m/z 121.10: C9H12H+ (ppb) WINTER
>99.5% (>1.308)
97-99.5% (0.656–1.308)
95-97% (0.495–0.656)
75-95% (0.175–0.495)
50-75% (0.086–0.175)
25-50% (0.039–0.086)
0-25% (≤ 0.039)
m/z 122.06: C7H7ONH+ (ppb) SUMMER
>99.5% (>0.024)
97-99.5% (0.015–0.024)
95-97% (0.012–0.015)
75-95% (0.005–0.012)
50-75% (0.003–0.005)
25-50% (0.002–0.003)
0-25% (≤ 0.002)
m/z 122.06: C7H7ONH+ (ppb) WINTER
>99.5% (>0.048)
97-99.5% (0.027–0.048)
95-97% (0.021–0.027)
75-95% (0.008–0.021)
50-75% (0.004–0.008)
25-50% (0.001–0.004)
0-25% (≤ 0.001)
m/z 125.06: C7H8O2H+ (ppb) SUMMER
>99.5% (>0.052)
97-99.5% (0.038–0.052)
95-97% (0.026–0.038)
75-95% (0.006–0.026)
50-75% (0.003–0.006)
25-50% (0.001–0.003)
0-25% (≤ 0.001)
m/z 125.06: C7H8O2H+ (ppb) WINTER
>99.5% (>0.137)
97-99.5% (0.070–0.137)
95-97% (0.056–0.070)
75-95% (0.027–0.056)
50-75% (0.013–0.027)
25-50% (0.002–0.013)
0-25% (≤ 0.002)
Latitude
Longitude
32°10'N
32°N
31°50'N
31°40'N
31°30'N
106°45'W
106°30'W
106°15'W
106°W
10 km
5 mi
W: Warehouse
R: Rail
T: TCEQ
C: City of El Paso
H: Hotspot

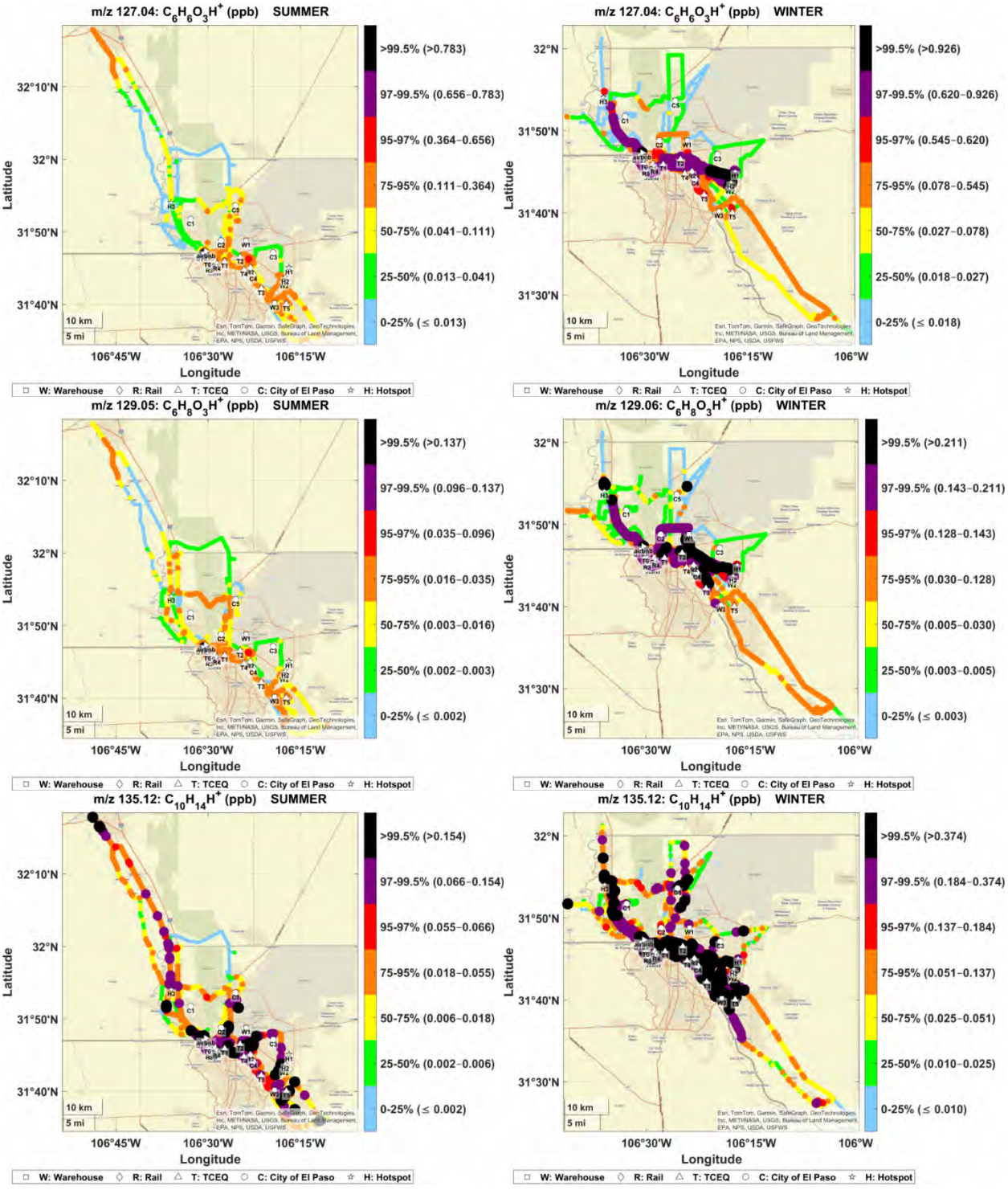
m/z 127.04: C6H6O3H+ (ppb) SUMMER
>99.5% (>0.783)
97-99.5% (0.656-0.783)
95-97% (0.364-0.656)
75-95% (0.111-0.364)
50-75% (0.041-0.111)
25-50% (0.013-0.041)
0-25% (≤ 0.013)
m/z 127.04: C6H6O3H+ (ppb) WINTER
>99.5% (>0.926)
97-99.5% (0.620-0.926)
95-97% (0.545-0.620)
75-95% (0.078-0.545)
50-75% (0.027-0.078)
25-50% (0.018-0.027)
0-25% (≤ 0.018)
m/z 129.05: C6H8O3H+ (ppb) SUMMER
>99.5% (>0.137)
97-99.5% (0.096-0.137)
95-97% (0.035-0.096)
75-95% (0.016-0.035)
50-75% (0.003-0.016)
25-50% (0.002-0.003)
0-25% (≤ 0.002)
m/z 129.06: C6H8O3H+ (ppb) WINTER
>99.5% (>0.211)
97-99.5% (0.143-0.211)
95-97% (0.128-0.143)
75-95% (0.030-0.128)
50-75% (0.005-0.030)
25-50% (0.003-0.005)
0-25% (≤ 0.003)
m/z 135.12: C10H14H+ (ppb) SUMMER
>99.5% (>0.154)
97-99.5% (0.066-0.154)
95-97% (0.055-0.066)
75-95% (0.018-0.055)
50-75% (0.006-0.018)
25-50% (0.002-0.006)
0-25% (≤ 0.002)
m/z 135.12: C10H14H+ (ppb) WINTER
>99.5% (>0.374)
97-99.5% (0.184-0.374)
95-97% (0.137-0.184)
75-95% (0.051-0.137)
50-75% (0.025-0.051)
25-50% (0.010-0.025)
0-25% (≤ 0.010)
Latitude
Longitude
32°10'N
32°N
31°50'N
31°40'N
31°30'N
106°45'W
106°30'W
106°15'W
106°W
10 km
5 mi
W: Warehouse
R: Rail
T: TCEQ
C: City of El Paso
H: Hotspot

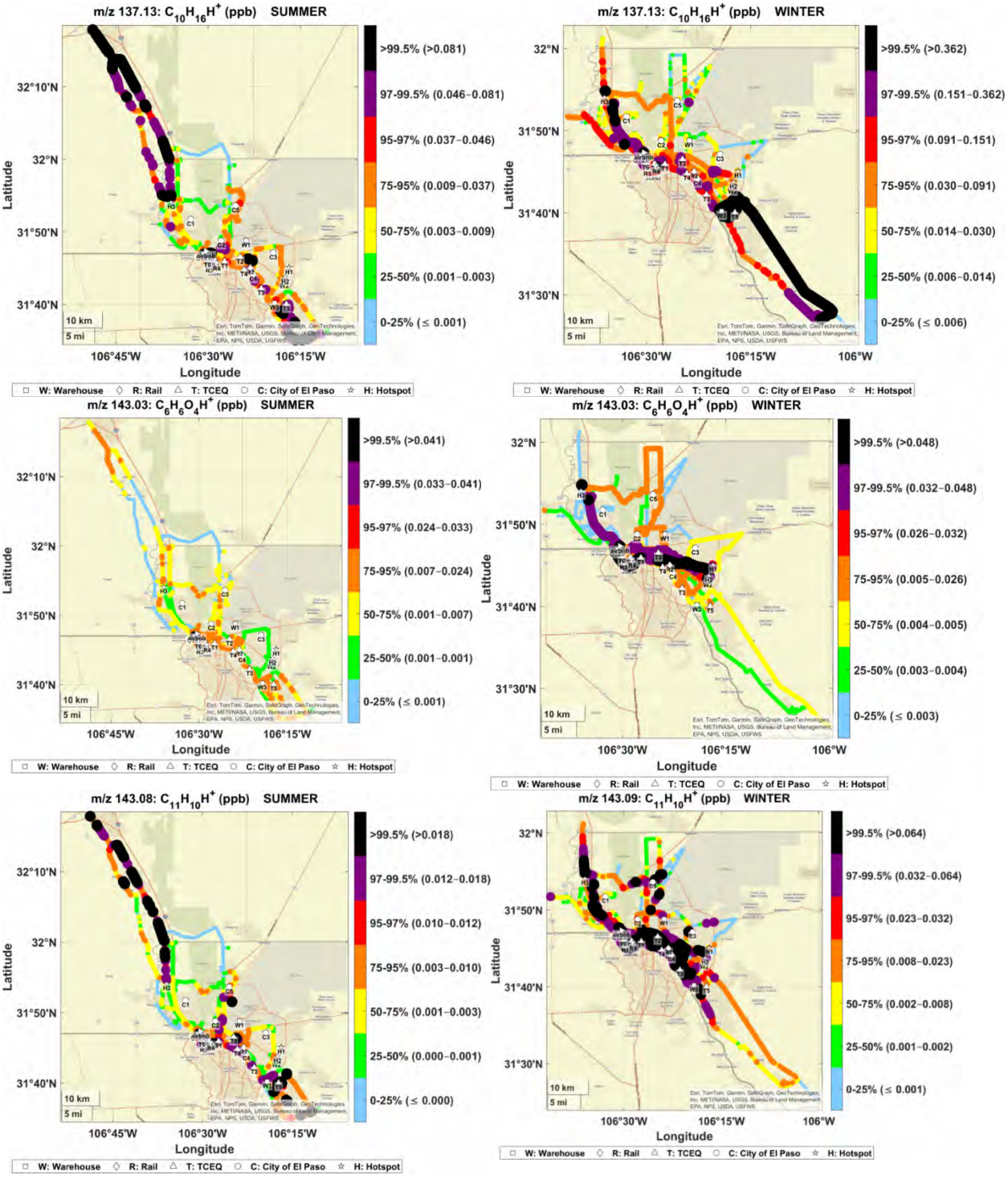
m/z 137.13: C10H16H+ (ppb) SUMMER
>99.5% (>0.081)
97-99.5% (0.046-0.081)
95-97% (0.037-0.046)
75-95% (0.009-0.037)
50-75% (0.003-0.009)
25-50% (0.001-0.003)
0-25% (≤ 0.001)
m/z 137.13: C10H16H+ (ppb) WINTER
>99.5% (>0.362)
97-99.5% (0.151-0.362)
95-97% (0.091-0.151)
75-95% (0.030-0.091)
50-75% (0.014-0.030)
25-50% (0.006-0.014)
0-25% (≤ 0.006)
m/z 143.03: C6H6O4H+ (ppb) SUMMER
>99.5% (>0.041)
97-99.5% (0.033-0.041)
95-97% (0.024-0.033)
75-95% (0.007-0.024)
50-75% (0.001-0.007)
25-50% (0.001-0.001)
0-25% (≤ 0.001)
m/z 143.03: C6H6O4H+ (ppb) WINTER
>99.5% (>0.048)
97-99.5% (0.032-0.048)
95-97% (0.026-0.032)
75-95% (0.005-0.026)
50-75% (0.004-0.005)
25-50% (0.003-0.004)
0-25% (≤ 0.003)
m/z 143.08: C11H10H+ (ppb) SUMMER
>99.5% (>0.018)
97-99.5% (0.012-0.018)
95-97% (0.010-0.012)
75-95% (0.003-0.010)
50-75% (0.001-0.003)
25-50% (0.000-0.001)
0-25% (≤ 0.000)
m/z 143.09: C11H10H+ (ppb) WINTER
>99.5% (>0.064)
97-99.5% (0.032-0.064)
95-97% (0.023-0.032)
75-95% (0.008-0.023)
50-75% (0.002-0.008)
25-50% (0.001-0.002)
0-25% (≤ 0.001)
Latitude
Longitude
W: Warehouse R: Rail T: TCEQ C: City of El Paso H: Hotspot

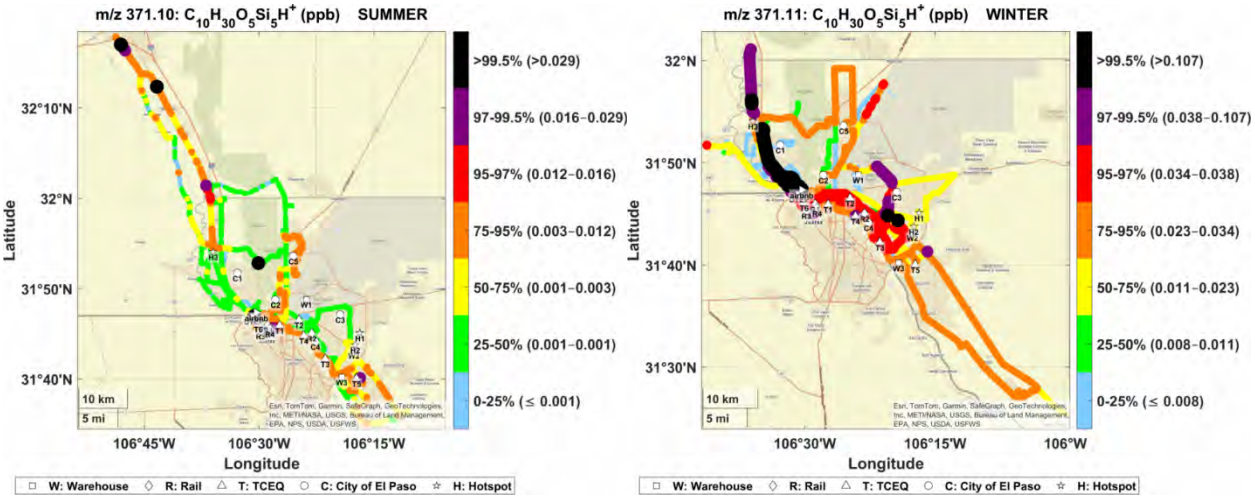

Appendix Figure E1. Maps for 40 prominent VOC ions observed using mobile measurements in the summer and winter campaigns. TCEQ and City of El Paso monitoring stations, as well as hotspots are depicted on the maps for the spatial reference.

Appendix Table E2. Look-up table with formula assignment and consistent compounds.

Detected *m/z*	**Chemical Formula**	**Consistent compounds**
42.033	$C_2H_3NH^+$	Acetonitrile
44.013	$CHONH^+$	Isocyanic acid
45.033	$C_2H_4OH^+$	Acetaldehyde+Ethylene Oxide+Ethylene glycol frag.
47.050	$C_2H_6OH^+$	Ethanol
57.033	$C_3H_4OH^+$	Acrolein + Propionic Acid frag.
57.070	$C_4H_8H^+$	Butene + Cyclobutane+**
59.049	$C_3H_6OH^+$	Acetone + Propanal
63.026	$C_2H_6SH^+$	Dimethyl sulfide + Ethanethiol
63.044	$C_2H_6O_2H^+$	Ethylene glycol
69.034	C_4H_4OH+	Furan
69.070	$C_5H_8H^+$	Isoprene + Cyclopentene (+ C5 alcohol and aldehyde frag.)

71.086	$C_5H_{10}H+$	Pentene + cyclopentane +**
73.029	$C_3H_4O_2H^+$	Acrylic acid
73.065	$C_4H_8OH^+$	Methyl ethyl ketone + Butanal
75.044	$C_3H_6O_2H^+$	Propionic acid + Methyl acetate
78.047	$C_6H_6^+$	Benzene[1]
83.049	$C_5H_6OH^+$	Methyl furan
89.024	$C_3H_4O_3H^+$	Ethylene carbonate
89.060	$C_4H_8O_2H^+$	Butyric acid + Ethyl acetate
91.039	$C_3H_6O_3H^+$	Dimethyl carbonate + Lactic acid
93.070	$C_7H_8H^+$	Toluene
95.049	$C_6H_6OH^+$	Phenol
97.029	$C_5H_4O_2H^+$	Furfural
105.069	$C_8H_8H^+$	Styrene
107.086	$C_8H_{10}H^+$	C8-aromatics (Xylenes and Ethylbenzene)
109.028	$C_6H_4O_2H^+$	Benzoquinone
115.039	$C_5H_6O_3H^+$	Glutamic anhydrite
119.034	$C_4H_6O_4H^+$	Succinic aldehyde
119.070	$C_5H_{10}O_3H^+$	Diethyl carbonate + Ethyl lactate
121.064	$C_8H_8OH^+$	Acetophenone
121.101	$C_9H_{12}H^+$	C9-Aromatics (Trimethylbenzene, Methylethylbenzene, Propylbenzene)
122.061	$C_7H_7NOH^+$	Acetylpyridine
125.059	$C_7H_8O_2H^+$	Guaiacol
127.039	$C_6H_6O_3H^+$	Hydroxymethylfurfural + Benzenetriols
129.055	$C_6H_8O_3H^+$	Bis(hydroxymethyl)furan

135.116	$C_{10}H_{14}H^+$	C10-Aromatics
137.132	$C_{10}H_{16}H^+$	Monoterpenes
143.033	$C_6H_6O_4H^+$	Benzenetetrols + other isomers
143.085	$C_{11}H_{10}H^+$	Methylnaphthalene
371.104	$C_{10}H_{30}O_5Si_5H^+$	D5-siloxane (decamethylcyclopentasiloxane)

Appendix F.

Table F.1 Summary statistics table for observed volume mixing ratios (ppbv) for 233 VOC ions in winter and summer campaigns which have passed the quality criteria and exceeded the average abundance threshold of 1 pptv. The ^{13}C isotopes have been used in QC and subsequently removed. Major fragments of total monoterpenes have been accounted for and removed. Methanol and acetic acid ions have been excluded from this table (pending further QC). Ethanol has been explicitly calibrated on its parent ion with fragment and cluster ions removed. Explicitly calibrated ions are denoted in bold – the remaining VOCs were calibrated from the fit of sensitivity and proton transfer reaction coefficients (*k*) and accounted for the sigmoidal transmission in the low mass region.

		WINTER								SUMMER							
m/z	**Formula**	**Mean**	**Median**	**P5**	**P25**	**P75**	**P95**	**P99.5**	**Std**	**Mean**	**Median**	**P5**	**P25**	**P75**	**P95**	**P99.5**	**Std**
41.0382	C3H4H+	0.3567	0.2769	0.0502	0.1581	0.4333	0.7654	2.556	0.7046	0.1374	0.0950	0.0288	0.0512	0.1767	0.3643	0.7290	0.6496
42.0091	--	0.0351	0.0181	0.0008	0.0014	0.0474	0.1179	0.3255	0.0864	0.0196	0.0151	0.0003	0.0088	0.0260	0.0487	0.0951	0.0226
42.0334	**C2H3NH+**	**0.1745**	**0.1725**	**0.0115**	**0.0748**	**0.2273**	**0.3662**	**0.6840**	**0.1910**	**0.1925**	**0.1300**	**0.0656**	**0.0964**	**0.1687**	**0.6457**	**1.1318**	**0.1972**
44.0128	CHONH+	0.0183	0.0017	0.0008	0.0010	0.0070	0.1000	0.2799	0.0478	0.0072	0.0035	0.0002	0.0004	0.0091	0.0257	0.0718	0.0110
44.0493	C2H5NH+	0.0017	0.0010	0.0005	0.0007	0.0017	0.0018	0.0375	0.0091								
44.9793	--									0.0054	0.0031	0.0003	0.0005	0.0079	0.0183	0.0333	0.0074
45.0330	**C2H4OH+**	**1.1453**	**0.8043**	**0.0097**	**0.2393**	**1.3735**	**3.0076**	**12.01**	**3.234**	**0.6532**	**0.4489**	**0.0115**	**0.2080**	**0.9157**	**1.837**	**2.7953**	**0.6308**
47.0125	CH2O2H+	0.0085	0.0017	0.0006	0.0013	0.0049	0.0343	0.0945	0.0679	0.0057	0.0027	0.0002	0.0012	0.0062	0.0206	0.0450	0.0077
47.0498	C2H6OH+	3.2190	1.4519	0.0614	0.6441	3.2562	8.3301	40.52	17.62	2.5763	0.8057	0.0877	0.2550	2.7509	11.61	23.5197	4.5746
49.0115	CH4SH+	0.0043	0.0017	0.0001	0.0006	0.0050	0.0165	0.0287	0.0168								
50.0149	--	0.0084	0.0043	0.0006	0.0011	0.0098	0.0265	0.0764	0.0310	0.0030	0.0013	0.0002	0.0005	0.0036	0.0116	0.0259	0.0065
51.0227	C4H2H+	0.0052	0.0025	0.0004	0.0009	0.0059	0.0169	0.0477	0.0189	0.0021	0.0011	0.0001	0.0003	0.0027	0.0074	0.0153	0.0042
51.0443	--	0.0101	0.0026	0.0002	0.0010	0.0066	0.0453	0.2037	0.0279	0.0247	0.0038	0.0002	0.0008	0.0177	0.1090	0.4677	0.0671
51.9947	--	0.0046	0.0018	0.0004	0.0005	0.0050	0.0174	0.0536	0.0095	0.0081	0.0051	0.0003	0.0027	0.0076	0.0283	0.0922	0.0138
53.0021	--	0.1281	0.0853	0.0072	0.0426	0.1452	0.3180	1.3568	0.2939	0.0505	0.0295	0.0018	0.0144	0.0643	0.1660	0.2927	0.1662
53.0385	C4H4H+	0.0226	0.0137	0.0013	0.0043	0.0281	0.0642	0.1876	0.0611	0.0101	0.0052	0.0005	0.0014	0.0135	0.0365	0.0621	0.0188
53.9920	--	0.0021	0.0011	0.0003	0.0005	0.0025	0.0069	0.0187	0.0035	0.0028	0.0018	0.0002	0.0010	0.0028	0.0093	0.0307	0.0046
54.0055	--	0.0050	0.0033	0.0004	0.0018	0.0056	0.0124	0.0492	0.0116	0.0020	0.0012	0.0002	0.0006	0.0024	0.0063	0.0109	0.0071
56.0494	C3H5NH+	0.0033	0.0012	0.0006	0.0009	0.0039	0.0098	0.0324	0.0142	0.0052	0.0043	0.0025	0.0035	0.0059	0.0106	0.0181	0.0033
57.0335	C3H4OH+	0.0680	0.0396	0.0023	0.0059	0.0856	0.2152	0.5580	0.1870	0.0387	0.0276	0.0022	0.0124	0.0554	0.1088	0.1730	0.0512
57.0697	C4H8H+	0.1409	0.1138	0.0163	0.0578	0.1751	0.3250	0.9324	0.2091	0.0454	0.0264	0.0042	0.0124	0.0573	0.1324	0.3688	0.1800
58.0287	C2H3ONH+	0.0025	0.0011	0.0006	0.0008	0.0021	0.0092	0.0262	0.0104	0.0017	0.0013	0.0003	0.0007	0.0023	0.0040	0.0074	0.0013
59.0491	**C3H6OH+**	**1.3629**	**1.1737**	**0.4152**	**0.8493**	**1.6381**	**2.7180**	**4.9039**	**1.278**	**1.2948**	**1.0465**	**0.5300**	**0.7346**	**1.6202**	**2.798**	**4.4060**	**0.7969**

59.9665	--									0.0053	0.0055	0.0003	0.0037	0.0065	0.0103	0.0161	0.0027
60.0445	C2H5ONH+	0.0288	0.0049	0.0027	0.0042	0.0169	0.1292	0.7691	0.1257	0.0226	0.0128	0.0009	0.0024	0.0321	0.0826	0.1415	0.0285
62.0232	CH3O2NH+	0.0036	0.0013	0.0007	0.0010	0.0038	0.0126	0.0327	0.0092	0.0027	0.0014	0.0003	0.0006	0.0035	0.0090	0.0162	0.0033
62.9632	--	0.0060	0.0056	0.0037	0.0048	0.0070	0.0095	0.0115	0.0018	0.0073	0.0049	0.0014	0.0040	0.0059	0.0210	0.0990	0.0124
63.0258	**C2H6SH+**	**0.0039**	**0.0035**	**0.0007**	**0.0028**	**0.0041**	**0.0081**	**0.0272**	**0.0056**	**0.0031**	**0.0018**	**0.0002**	**0.0008**	**0.0032**	**0.0089**	**0.0233**	**0.0129**
63.0440	C2H6O2H+	0.0169	0.0038	0.0007	0.0020	0.0242	0.0631	0.1186	0.0286	0.0068	0.0032	0.0006	0.0008	0.0061	0.0154	0.0979	0.0151
m/z	**Formula**	**Mean**	**Median**	**P5**	**P25**	**P75**	**P95**	**P99.5**	**Std**	**Mean**	**Median**	**P5**	**P25**	**P75**	**P95**	**P99.5**	**Std**
63.0539	CH6ON2H+	0.0043	0.0013	0.0004	0.0009	0.0051	0.0151	0.0469	0.0083								
64.9605	--									0.0024	0.0016	0.0004	0.0013	0.0019	0.0070	0.0312	0.0041
65.0386	C5H4H+	0.0088	0.0051	0.0007	0.0012	0.0107	0.0270	0.0714	0.0233	0.0030	0.0014	0.0002	0.0005	0.0034	0.0116	0.0252	0.0057
67.0545	C5H6H+	0.0297	0.0174	0.0019	0.0031	0.0384	0.0868	0.2480	0.0931	0.0095	0.0053	0.0006	0.0015	0.0124	0.0329	0.0646	0.0200
68.0131	C3HONH+	0.0010	0.0011	0.0002	0.0003	0.0015	0.0020	0.0034	0.0008								
68.0262	--	0.0028	0.0016	0.0006	0.0009	0.0038	0.0076	0.0169	0.0084	0.0012	0.0010	0.0002	0.0006	0.0016	0.0028	0.0045	0.0009
68.0501	**C4H5NH+**	**0.0182**	**0.0197**	**0.0018**	**0.0085**	**0.0239**	**0.0332**	**0.0616**	**0.0335**	**0.0017**	**0.0012**	**0.0002**	**0.0003**	**0.0023**	**0.0048**	**0.0099**	**0.0017**
68.9973	--	0.0030	0.0016	0.0007	0.0013	0.0044	0.0060	0.0117	0.0125	0.0045	0.0017	0.0005	0.0007	0.0042	0.0222	0.0281	0.0067
69.0336	C4H4OH+	0.0128	0.0027	0.0015	0.0018	0.0116	0.0454	0.1697	0.0793	0.0051	0.0027	0.0004	0.0007	0.0072	0.0179	0.0306	0.0064
69.0700	**C5H8H+**	**0.3547**	**0.3016**	**0.0331**	**0.1969**	**0.4414**	**0.7420**	**1.6974**	**0.5047**	**0.1123**	**0.0777**	**0.0151**	**0.0404**	**0.1401**	**0.3375**	**0.5893**	**0.1743**
69.9925	--	0.0036	0.0017	0.0009	0.0014	0.0028	0.0157	0.0302	0.0054								
71.0133	C3H2O2H+	0.0080	0.0040	0.0020	0.0025	0.0057	0.0210	0.0516	0.1026	0.0078	0.0032	0.0005	0.0010	0.0092	0.0328	0.0542	0.0121
71.0228	--									0.0022	0.0011	0.0003	0.0006	0.0027	0.0073	0.0171	0.0029
71.0493	**C4H6OH+**	**0.0911**	**0.0457**	**0.0047**	**0.0065**	**0.1300**	**0.3039**	**0.5713**	**0.2618**	**0.0698**	**0.0447**	**0.0019**	**0.0167**	**0.0987**	**0.2347**	**0.3718**	**0.0752**
71.0856	C5H10H+	0.0295	0.0187	0.0014	0.0067	0.0362	0.0735	0.2987	0.0787	0.0097	0.0041	0.0002	0.0014	0.0104	0.0291	0.0948	0.1418
72.0450	C3H5ONH+	0.0019	0.0013	0.0008	0.0010	0.0015	0.0044	0.0327	0.0088								
73.0285	C3H4O2H+	0.0152	0.0054	0.0033	0.0045	0.0077	0.0693	0.1379	0.0680	0.0110	0.0053	0.0006	0.0017	0.0142	0.0405	0.0721	0.0157
73.0650	C4H8OH+	0.2603	0.1972	0.0681	0.1276	0.3381	0.6670	0.9978	0.3071	0.1065	0.0639	0.0192	0.0349	0.1347	0.3607	0.6048	0.1133

74.0238	C2H3O2NH+	0.0076	0.0036	0.0017	0.0028	0.0044	0.0405	0.0725	0.0152	0.0057	0.0017	0.0005	0.0008	0.0073	0.0230	0.0356	0.0083
74.0605	C3H7ONH+	0.0106	0.0074	0.0008	0.0014	0.0146	0.0245	0.0850	0.0235								
75.0443	C3H6O2H+	0.0885	0.0381	0.0021	0.0043	0.1023	0.2863	0.9479	0.3574	0.0614	0.0350	0.0040	0.0185	0.0803	0.1959	0.3762	0.0724
76.0408	C2H5O2NH+									0.0028	0.0019	0.0005	0.0011	0.0035	0.0078	0.0186	0.0030
76.0756	C3H9ONH+	0.0054	0.0050	0.0005	0.0022	0.0076	0.0121	0.0198	0.0041								
77.0235	C2H4O3H+	0.0106	0.0085	0.0009	0.0041	0.0143	0.0278	0.0443	0.0115	0.0069	0.0043	0.0008	0.0021	0.0097	0.0203	0.0317	0.0072
77.0598	C3H8O2H+	0.1963	0.1620	0.0048	0.0655	0.2809	0.4904	0.9457	0.1877	0.1139	0.0795	0.0261	0.0509	0.1196	0.2773	1.0027	0.1451
78.0469	**C6H6+**	**0.2676**	**0.1962**	**0.0579**	**0.1166**	**0.3111**	**0.6670**	**1.6040**	**0.7169**	**0.0784**	**0.0442**	**0.0064**	**0.0201**	**0.0984**	**0.2491**	**0.5411**	**0.1695**
79.0391	C2H6O3H+	0.0583	0.0125	0.0051	0.0080	0.0516	0.2883	0.6602	0.1134	0.0577	0.0313	0.0034	0.0161	0.0552	0.1435	0.8035	0.1106
80.0365	CH5O3NH+	0.0018	0.0011	0.0004	0.0007	0.0013	0.0063	0.0210	0.0038	0.0019	0.0011	0.0002	0.0003	0.0021	0.0062	0.0206	0.0031
81.0337	C5H4OH+	0.0168	0.0061	0.0019	0.0023	0.0231	0.0581	0.1357	0.0429	0.0107	0.0029	0.0007	0.0012	0.0132	0.0480	0.0763	0.0156
81.0444	C4H4N2H+									0.0045	0.0018	0.0006	0.0014	0.0060	0.0156	0.0331	0.0058
m/z	**Formula**	**Mean**	**Median**	**P5**	**P25**	**P75**	**P95**	**P99.5**	**Std**	**Mean**	**Median**	**P5**	**P25**	**P75**	**P95**	**P99.5**	**Std**
81.9857	--	0.0017	0.0015	0.0005	0.0011	0.0021	0.0032	0.0069	0.0010								
82.0057	--	0.0020	0.0010	0.0005	0.0007	0.0017	0.0079	0.0134	0.0025								
82.9454	--									0.0036	0.0018	0.0007	0.0014	0.0028	0.0122	0.0481	0.0065
83.0493	C5H6OH+	0.0358	0.0151	0.0020	0.0031	0.0477	0.1118	0.4498	0.1248	0.0140	0.0064	0.0007	0.0015	0.0187	0.0551	0.1044	0.0194
83.0856	C6H10H+	0.0701	0.0630	0.0025	0.0395	0.0902	0.1447	0.4358	0.0777	0.0173	0.0105	0.0005	0.0046	0.0219	0.0584	0.1084	0.0401
84.0452	C4H5ONH+	0.0022	0.0014	0.0008	0.0011	0.0017	0.0073	0.0324	0.0072								
84.9422	--									0.0023	0.0012	0.0004	0.0009	0.0018	0.0078	0.0308	0.0042
84.9654	--	0.0142	0.0108	0.0031	0.0075	0.0213	0.0293	0.0498	0.0093	0.0052	0.0050	0.0002	0.0037	0.0065	0.0104	0.0167	0.0030
85.0285	C4H4O2H+	0.0116	0.0025	0.0012	0.0017	0.0084	0.0443	0.1068	0.0789	0.0069	0.0033	0.0006	0.0008	0.0090	0.0261	0.0463	0.0096
85.0648	C5H8OH+	0.0285	0.0199	0.0013	0.0067	0.0407	0.0805	0.1309	0.0614	0.0100	0.0054	0.0005	0.0024	0.0120	0.0359	0.0633	0.0122
85.1013	C6H12H+	0.0119	0.0067	0.0007	0.0015	0.0159	0.0331	0.1163	0.0303	0.0042	0.0017	0.0002	0.0006	0.0047	0.0139	0.0394	0.0480
86.0606	C4H7ONH+	0.0021	0.0010	0.0006	0.0009	0.0014	0.0058	0.0341	0.0102								

87.0442	C4H6O2H+	0.0398	0.0065	0.0025	0.0035	0.0452	0.1603	0.3321	0.1400	0.0284	0.0164	0.0009	0.0033	0.0385	0.1013	0.1702	0.0352
87.0805	C5H10OH+	3.8161	3.1783	2.2545	3.0176	3.6929	10.3841	10.3841	1.990	0.9431	0.9556	0.4500	0.7003	1.1746	1.429	1.4290	0.2749
88.0408	C3H5O2NH+	0.0037	0.0018	0.0013	0.0014	0.0020	0.0166	0.0339	0.0131	0.0028	0.0012	0.0003	0.0005	0.0039	0.0100	0.0208	0.0040
88.0761	C4H9ONH+	0.0034	0.0018	0.0004	0.0013	0.0031	0.0090	0.0370	0.0076								
89.0235	C3H4O3H+	0.0200	0.0124	0.0036	0.0077	0.0151	0.0676	0.1673	0.1684	0.0070	0.0027	0.0007	0.0008	0.0095	0.0253	0.0373	0.0089
89.0597	C4H8O2H+	0.0248	0.0092	0.0014	0.0017	0.0361	0.0982	0.1764	0.0405	0.4549	0.1471	0.0085	0.0486	0.4617	2.031	5.4496	0.8347
90.0914	C4H11ONH+	0.0050	0.0042	0.0005	0.0023	0.0071	0.0120	0.0162	0.0038								
90.9992	--									0.0029	0.0012	0.0002	0.0006	0.0046	0.0097	0.0115	0.0033
91.0390	C3H6O3H+	0.0097	0.0042	0.0023	0.0031	0.0050	0.0472	0.0912	0.0327	0.0089	0.0055	0.0006	0.0023	0.0126	0.0272	0.0458	0.0094
91.0541	C7H6H+	0.2675	0.1716	0.0442	0.0921	0.3126	0.7414	1.8802	0.6149	0.0906	0.0342	0.0025	0.0115	0.0984	0.3544	0.9905	0.1969
91.0752	C4H10O2H+	0.0720	0.0600	0.0063	0.0289	0.1047	0.1750	0.2395	0.0710	0.0221	0.0121	0.0017	0.0058	0.0237	0.0568	0.2714	0.0381
92.0345	C2H5O3NH+	0.0046	0.0025	0.0013	0.0020	0.0036	0.0183	0.0468	0.0076								
92.0607	--	0.0639	0.0389	0.0089	0.0203	0.0726	0.1862	0.5362	0.1588	0.0226	0.0087	0.0010	0.0032	0.0253	0.0874	0.2400	0.0579
93.0106	--									0.0027	0.0022	0.0008	0.0015	0.0032	0.0062	0.0115	0.0020
93.0354	--									0.0020	0.0014	0.0003	0.0007	0.0022	0.0062	0.0176	0.0030
93.0698	**C7H8H+**	**0.4476**	**0.2683**	**0.0364**	**0.1320**	**0.4893**	**1.3607**	**3.6613**	**1.251**	**0.1785**	**0.0676**	**0.0080**	**0.0233**	**0.1968**	**0.6750**	**2.1149**	**0.4608**
94.0415	--	0.0056	0.0021	0.0013	0.0015	0.0072	0.0194	0.0371	0.0134								

m/z	Formula	Mean	Median	P5	P25	P75	P95	P99.5	Std	Mean	Median	P5	P25	P75	P95	P99.5	Std
95.0492	C6H6OH+	0.1104	0.0330	0.0059	0.0085	0.1508	0.3968	0.9435	0.3335	0.0619	0.0237	0.0025	0.0047	0.0906	0.2364	0.4805	0.1095
97.0285	**C5H4O2H+**	**0.0262**	**0.0125**	**0.0019**	**0.0105**	**0.0184**	**0.1137**	**0.3082**	**0.2009**	**0.0068**	**0.0024**	**0.0004**	**0.0009**	**0.0076**	**0.0317**	**0.0460**	**0.0101**
97.0647	C6H8OH+	0.0239	0.0113	0.0018	0.0023	0.0355	0.0825	0.1570	0.0555	0.0094	0.0048	0.0005	0.0012	0.0121	0.0348	0.0698	0.0123
97.1012	C7H12H+	0.0320	0.0275	0.0012	0.0147	0.0430	0.0682	0.1982	0.0426	0.0092	0.0053	0.0008	0.0028	0.0111	0.0300	0.0576	0.0209
98.0606	C5H7ONH+	0.0021	0.0012	0.0004	0.0010	0.0014	0.0074	0.0190	0.0051								
99.0441	C5H6O2H+	0.0250	0.0086	0.0030	0.0056	0.0241	0.1056	0.1942	0.0601	0.0201	0.0056	0.0019	0.0026	0.0240	0.0885	0.1163	0.0284

99.0805	C6H10OH+	0.0290	0.0215	0.0014	0.0054	0.0429	0.0811	0.1202	0.0353	0.0092	0.0051	0.0005	0.0017	0.0118	0.0336	0.0576	0.0112
100.043	--	0.0031	0.0019	0.0011	0.0016	0.0022	0.0088	0.0298	0.0144								
100.077	C5H9ONH+	0.0038	0.0030	0.0006	0.0009	0.0051	0.0096	0.0448	0.0061								
100.936	--	0.0426	0.0372	0.0256	0.0319	0.0548	0.0663	0.0785	0.0141	0.0197	0.0203	0.0027	0.0171	0.0235	0.0291	0.0395	0.0078
101.023	C4H4O3H+	0.0093	0.0030	0.0014	0.0024	0.0052	0.0391	0.0922	0.0437	0.0029	0.0011	0.0002	0.0005	0.0036	0.0108	0.0167	0.0043
101.060	C5H8O2H+	0.0550	0.0333	0.0017	0.0035	0.0760	0.1533	0.6752	0.1317	0.0204	0.0073	0.0007	0.0016	0.0205	0.0890	0.1833	0.0334
101.096	C6H12OH+									0.0065	0.0041	0.0009	0.0022	0.0081	0.0202	0.0388	0.0068
102.057	C4H7O2NH+	0.0028	0.0012	0.0008	0.0010	0.0015	0.0094	0.0558	0.0108								
102.092	C5H11ONH+	0.0043	0.0034	0.0005	0.0012	0.0056	0.0091	0.0287	0.0083	0.0034	0.0025	0.0010	0.0017	0.0042	0.0088	0.0165	0.0027
102.933	--	0.0274	0.0239	0.0163	0.0204	0.0352	0.0428	0.0502	0.0091	0.0125	0.0128	0.0017	0.0107	0.0149	0.0187	0.0257	0.0050
103.039	C4H6O3H+	0.0097	0.0022	0.0015	0.0020	0.0053	0.0398	0.0920	0.0435	0.0053	0.0020	0.0006	0.0007	0.0066	0.0222	0.0442	0.0078
103.053	C8H6H+									0.0034	0.0019	0.0003	0.0007	0.0036	0.0114	0.0369	0.0055
103.075	C5H10O2H+	0.0132	0.0054	0.0007	0.0011	0.0163	0.0508	0.1081	0.0255	0.0154	0.0033	0.0003	0.0010	0.0125	0.0737	0.2046	0.0346
104.047	--									0.0016	0.0013	0.0004	0.0008	0.0019	0.0040	0.0078	0.0014
104.070	C4H9O2NH+	0.0048	0.0023	0.0005	0.0009	0.0055	0.0154	0.0372	0.0315								
104.107	C5H13ONH+	0.0016	0.0015	0.0002	0.0008	0.0023	0.0037	0.0054	0.0013								
104.930	--									0.0020	0.0021	0.0004	0.0017	0.0025	0.0031	0.0043	0.0008
105.019	C3H4O4H+	0.0020	0.0013	0.0008	0.0011	0.0022	0.0043	0.0141	0.0044	0.0032	0.0013	0.0004	0.0005	0.0037	0.0135	0.0207	0.0044
105.033	C7H4OH+	0.0060	0.0021	0.0011	0.0014	0.0073	0.0205	0.0528	0.0122	0.0037	0.0020	0.0004	0.0006	0.0040	0.0116	0.0414	0.0061
105.055	C4H8O3H+	0.0118	0.0033	0.0011	0.0018	0.0113	0.0485	0.1250	0.0241	0.0066	0.0030	0.0004	0.0008	0.0076	0.0238	0.0742	0.0113
105.070	C8H8H+	0.0988	0.0613	0.0091	0.0295	0.1152	0.2792	0.6922	0.3288	0.0397	0.0129	0.0015	0.0050	0.0364	0.1485	0.6943	0.0930
105.091	C5H12O2H+	0.0115	0.0093	0.0006	0.0046	0.0154	0.0289	0.0561	0.0121	0.0030	0.0014	0.0001	0.0006	0.0030	0.0098	0.0388	0.0057
106.051	C3H7O3NH+	0.0026	0.0020	0.0009	0.0011	0.0041	0.0046	0.0167	0.0027								
106.077	--	0.0499	0.0332	0.0093	0.0201	0.0595	0.1303	0.3300	0.1057	0.0152	0.0059	0.0006	0.0020	0.0165	0.0584	0.1718	0.0310
m/z	**Formula**	**Mean**	**Median**	**P5**	**P25**	**P75**	**P95**	**P99.5**	**Std**	**Mean**	**Median**	**P5**	**P25**	**P75**	**P95**	**P99.5**	**Std**

107.035	C3H6O4H+	0.0090	0.0105	0.0017	0.0055	0.0127	0.0145	0.0252	0.0112	0.0033	0.0016	0.0004	0.0006	0.0038	0.0113	0.0287	0.0050
107.048	C7H6OH+	0.0130	0.0034	0.0017	0.0021	0.0176	0.0453	0.1011	0.0345	0.0102	0.0052	0.0005	0.0020	0.0097	0.0418	0.1097	0.0166
107.086	C8H10H+	0.4626	0.3109	0.1052	0.1783	0.5420	1.2145	2.9394	1.008	0.1377	0.0530	0.0060	0.0176	0.1456	0.5192	1.6758	0.3059
108.065	C3H9O3NH+	0.0019	0.0012	0.0007	0.0009	0.0015	0.0056	0.0172	0.0044								
109.028	C6H4O2H+	0.0602	0.0199	0.0035	0.0058	0.0994	0.2065	0.3325	0.0775	0.0575	0.0272	0.0025	0.0036	0.0857	0.2240	0.4055	0.0779
109.101	C8H12H+	0.0312	0.0205	0.0026	0.0110	0.0366	0.0786	0.2667	0.0627	0.0066	0.0035	0.0003	0.0014	0.0084	0.0252	0.0435	0.0086
111.044	C6H6O2H+	0.0234	0.0041	0.0022	0.0030	0.0224	0.1036	0.2263	0.0598	0.0138	0.0062	0.0011	0.0015	0.0183	0.0554	0.0777	0.0176
111.117	C8H14H+	0.0127	0.0095	0.0014	0.0033	0.0178	0.0303	0.1053	0.0218	0.0038	0.0020	0.0002	0.0007	0.0044	0.0139	0.0265	0.0068
113.024	C5H4O3H+	0.0050	0.0023	0.0012	0.0020	0.0028	0.0208	0.0441	0.0123	0.0036	0.0013	0.0003	0.0006	0.0040	0.0155	0.0235	0.0051
113.060	C6H8O2H+	0.0163	0.0030	0.0013	0.0021	0.0228	0.0651	0.1290	0.0325	0.0085	0.0041	0.0005	0.0010	0.0119	0.0302	0.0500	0.0103
113.096	C7H12OH+	0.0133	0.0093	0.0006	0.0044	0.0189	0.0349	0.0625	0.0166	0.0030	0.0011	0.0001	0.0005	0.0027	0.0149	0.0300	0.0052
114.056	C5H7O2NH+	0.0018	0.0012	0.0005	0.0010	0.0016	0.0044	0.0171	0.0046								
114.092	C6H11ONH+	0.0021	0.0011	0.0005	0.0007	0.0030	0.0049	0.0128	0.0035								
115.039	C5H6O3H+	0.0086	0.0044	0.0017	0.0033	0.0058	0.0356	0.0841	0.0327	0.0048	0.0014	0.0006	0.0007	0.0057	0.0191	0.0407	0.0075
115.075	C6H10O2H+	0.0228	0.0107	0.0010	0.0018	0.0348	0.0759	0.1531	0.0433	0.0082	0.0024	0.0003	0.0008	0.0077	0.0405	0.0907	0.0148
115.111	C7H14OH+									0.0028	0.0016	0.0003	0.0008	0.0031	0.0093	0.0195	0.0033
116.037	--	0.0019	0.0011	0.0005	0.0010	0.0013	0.0074	0.0167	0.0042								
116.107	C6H13ONH+	0.0028	0.0012	0.0004	0.0008	0.0040	0.0087	0.0136	0.0035								
116.906	C35Cl3+	0.0724	0.0710	0.0569	0.0657	0.0804	0.0887	0.0972	0.0106	0.0380	0.0389	0.0092	0.0352	0.0433	0.0522	0.0625	0.0111
117.018	C4H4O4H+	0.0041	0.0021	0.0012	0.0014	0.0035	0.0165	0.0278	0.0061	0.0024	0.0010	0.0003	0.0004	0.0028	0.0098	0.0145	0.0031
117.054	C5H8O3H+	0.0067	0.0018	0.0008	0.0014	0.0059	0.0299	0.0600	0.0156								
117.069	C9H8H+	0.0087	0.0028	0.0006	0.0008	0.0091	0.0289	0.0990	0.0486								
117.091	C6H12O2H+	0.0120	0.0043	0.0008	0.0020	0.0169	0.0440	0.0654	0.0152	0.0077	0.0025	0.0004	0.0007	0.0087	0.0358	0.0658	0.0129
118.050	C4H7O3NH+	0.0015	0.0010	0.0008	0.0008	0.0013	0.0019	0.0172	0.0054								
118.087	C5H11O2NH+	0.0059	0.0043	0.0006	0.0014	0.0078	0.0148	0.0650	0.0114								

119.034	C4H6O4H+	0.0603	0.0160	0.0070	0.0093	0.0242	0.3739	0.6365	0.1668	0.0244	0.0088	0.0012	0.0018	0.0336	0.0947	0.1278	0.0346
119.070	C5H10O3H+	0.0715	0.0234	0.0051	0.0159	0.0885	0.2548	0.7502	0.1419	0.0133	0.0037	0.0012	0.0016	0.0125	0.0479	0.2008	0.0287
119.085	C9H10H+									0.0087	0.0031	0.0003	0.0007	0.0104	0.0345	0.0851	0.0159
120.093	--	0.0186	0.0106	0.0020	0.0051	0.0218	0.0562	0.1515	0.0523	0.0063	0.0027	0.0002	0.0008	0.0077	0.0230	0.0571	0.0116
121.029	C7H4O2H+	0.0028	0.0014	0.0006	0.0011	0.0020	0.0116	0.0247	0.0043								
m/z	**Formula**	**Mean**	**Median**	**P5**	**P25**	**P75**	**P95**	**P99.5**	**Std**	**Mean**	**Median**	**P5**	**P25**	**P75**	**P95**	**P99.5**	**Std**
121.065	**C8H8OH+**	**0.0274**	**0.0214**	**0.0014**	**0.0114**	**0.0353**	**0.0691**	**0.1768**	**0.0294**	**0.0071**	**0.0039**	**0.0005**	**0.0019**	**0.0075**	**0.0292**	**0.0524**	**0.0097**
121.101	C9H12H+	0.1516	0.0812	0.0091	0.0354	0.1684	0.4818	1.3638	0.5056	0.0576	0.0223	0.0019	0.0066	0.0658	0.2153	0.6529	0.1208
122.061	C7H7ONH+	0.0066	0.0037	0.0003	0.0006	0.0080	0.0212	0.0580	0.0300	0.0043	0.0032	0.0012	0.0020	0.0049	0.0122	0.0240	0.0039
122.897	--	0.0024	0.0024	0.0018	0.0021	0.0027	0.0031	0.0035	0.0005	0.0012	0.0013	0.0004	0.0011	0.0014	0.0018	0.0022	0.0004
123.028	C3H6O5H+	0.0017	0.0012	0.0009	0.0011	0.0015	0.0040	0.0114	0.0027								
123.044	C7H6O2H+	0.0053	0.0021	0.0008	0.0014	0.0061	0.0186	0.0359	0.0143	0.0028	0.0014	0.0002	0.0005	0.0032	0.0114	0.0186	0.0036
123.080	C8H10OH+	0.0056	0.0021	0.0004	0.0008	0.0061	0.0202	0.0701	0.0168	0.0022	0.0011	0.0001	0.0004	0.0025	0.0092	0.0186	0.0034
123.117	C9H14H+	0.0087	0.0063	0.0012	0.0019	0.0122	0.0218	0.0647	0.0149	0.0031	0.0014	0.0001	0.0004	0.0039	0.0129	0.0226	0.0044
124.076	C7H9ONH+	0.0029	0.0023	0.0003	0.0005	0.0038	0.0080	0.0227	0.0043								
125.023	C6H4O3H+	0.0085	0.0042	0.0013	0.0028	0.0072	0.0391	0.0692	0.0122	0.0137	0.0059	0.0011	0.0017	0.0165	0.0596	0.0866	0.0190
125.060	C7H8O2H+	0.0192	0.0121	0.0008	0.0020	0.0265	0.0574	0.1551	0.0446	0.0063	0.0032	0.0002	0.0012	0.0065	0.0261	0.0523	0.0095
125.132	C9H16H+	0.0052	0.0038	0.0007	0.0012	0.0072	0.0127	0.0425	0.0086								
127.039	C6H6O3H+	0.1060	0.0272	0.0079	0.0184	0.0685	0.5403	0.9342	0.1813	0.0967	0.0420	0.0073	0.0129	0.1113	0.3703	0.7826	0.1473
128.061	--									0.0024	0.0013	0.0004	0.0005	0.0033	0.0088	0.0158	0.0031
129.0545	C6H8O3H+	0.0274	0.0047	0.0031	0.0036	0.0287	0.1283	0.2125	0.0512	0.0130	0.0030	0.0013	0.0023	0.0163	0.0368	0.1364	0.0228
129.068	C10H8H+									0.0080	0.0038	0.0006	0.0014	0.0108	0.0281	0.0522	0.0099
129.090	C7H12O2H+	0.0168	0.0125	0.0006	0.0045	0.0223	0.0450	0.0949	0.0357	0.0029	0.0011	0.0002	0.0003	0.0027	0.0139	0.0283	0.0050
129.127	C8H16OH+									0.0018	0.0011	0.0002	0.0006	0.0021	0.0058	0.0117	0.0019
130.054	--	0.0018	0.0011	0.0008	0.0009	0.0013	0.0063	0.0178	0.0043								

130.086	C6H11O2NH+	0.0034	0.0019	0.0005	0.0007	0.0045	0.0100	0.0223	0.0111								
130.123	C7H15ONH+	0.0025	0.0021	0.0002	0.0012	0.0032	0.0059	0.0084	0.0026								
132.072	--	0.0026	0.0011	0.0007	0.0008	0.0013	0.0120	0.0245	0.0046								
132.101	C6H13O2NH+	0.0052	0.0043	0.0004	0.0023	0.0070	0.0120	0.0257	0.0057								
133.050	C5H8O4H+	0.0041	0.0014	0.0011	0.0013	0.0017	0.0176	0.0518	0.0154								
133.101	C10H12H+	0.0137	0.0077	0.0006	0.0029	0.0164	0.0433	0.1161	0.0351	0.0040	0.0016	0.0001	0.0005	0.0047	0.0153	0.0387	0.0069
134.108	--	0.0062	0.0037	0.0003	0.0017	0.0075	0.0189	0.0513	0.0165								
135.030	C4H6O5H+	0.0020	0.0013	0.0008	0.0010	0.0014	0.0069	0.0144	0.0030								
135.080	C9H10OH+	0.0066	0.0038	0.0005	0.0008	0.0088	0.0217	0.0497	0.0095	0.0025	0.0011	0.0002	0.0004	0.0030	0.0105	0.0167	0.0035
135.1165	C10H14H+	0.0433	0.0239	0.0021	0.0092	0.0494	0.1339	0.3863	0.1348	0.0147	0.0059	0.0004	0.0020	0.0178	0.0552	0.1543	0.0269
136.060	C4H9O4NH+	0.0115	0.0092	0.0029	0.0039	0.0126	0.0266	0.1128	0.0173	0.0055	0.0012	0.0007	0.0011	0.0021	0.0262	0.0520	0.0141
m/z	**Formula**	**Mean**	**Median**	**P5**	**P25**	**P75**	**P95**	**P99.5**	**Std**	**Mean**	**Median**	**P5**	**P25**	**P75**	**P95**	**P99.5**	**Std**
137.023	C7H4O3H+	0.0028	0.0018	0.0005	0.0007	0.0036	0.0075	0.0213	0.0051								
137.044	C4H8O5H+	0.0116	0.0043	0.0025	0.0031	0.0087	0.0632	0.1119	0.0231								
137.080	C5H12O4H+	0.0032	0.0019	0.0010	0.0015	0.0025	0.0091	0.0275	0.0108								
137.132	C10H16H+	0.1358	0.0659	0.0037	0.0274	0.1186	0.3140	1.0555	1.306	0.0313	0.0142	0.0008	0.0034	0.0396	0.1260	0.2509	0.0470
138.020	C6H3O3NH+	0.0016	0.0012	0.0002	0.0006	0.0022	0.0040	0.0093	0.0015								
138.091	C8H11ONH+	0.0040	0.0034	0.0004	0.0018	0.0052	0.0100	0.0255	0.0036								
139.0395	C7H6O3H+	0.0026	0.0011	0.0006	0.0009	0.0026	0.0102	0.0229	0.0039	0.0024	0.0010	0.0004	0.0005	0.0027	0.0097	0.0131	0.0030
139.075	C8H10O2H+	0.0077	0.0044	0.0005	0.0008	0.0102	0.0250	0.0777	0.0141								
139.112	C9H14OH+	0.0053	0.0042	0.0005	0.0020	0.0067	0.0144	0.0291	0.0083								
141.018	C6H4O4H+	0.0036	0.0018	0.0010	0.0012	0.0050	0.0137	0.0237	0.0041	0.0055	0.0026	0.0005	0.0008	0.0075	0.0226	0.0348	0.0073
141.054	C7H8O3H+	0.0027	0.0012	0.0008	0.0009	0.0019	0.0087	0.0486	0.0069								
141.090	C8H12O2H+	0.0031	0.0026	0.0004	0.0021	0.0038	0.0056	0.0156	0.0069								
141.127	C9H16OH+	0.0036	0.0030	0.0005	0.0018	0.0047	0.0076	0.0164	0.0061								

142.050	C6H7O3NH+	0.0011	0.0010	0.0007	0.0008	0.0012	0.0014	0.0069	0.0009								
143.0335	C6H6O4H+	0.0060	0.0043	0.0014	0.0030	0.0045	0.0259	0.0478	0.0079	0.0060	0.0014	0.0007	0.0009	0.0071	0.0249	0.0411	0.0087
143.0845	C11H10H+	0.0067	0.0019	0.0004	0.0007	0.0082	0.0238	0.0660	0.0237	0.0025	0.0013	0.0002	0.0004	0.0032	0.0095	0.0177	0.0035
143.106	C8H14O2H+	0.0071	0.0053	0.0004	0.0027	0.0085	0.0167	0.1054	0.0182								
143.1425	C9H18OH+	0.0102	0.0093	0.0006	0.0056	0.0133	0.0214	0.0470	0.0110	0.0016	0.0011	0.0001	0.0005	0.0019	0.0049	0.0114	0.0019
145.050	C6H8O4H+	0.0029	0.0014	0.0005	0.0010	0.0017	0.0130	0.0255	0.0065								
146.115	C7H15O2NH+	0.0020	0.0014	0.0002	0.0007	0.0026	0.0051	0.0119	0.0025								
146.976	--	0.0034	0.0014	0.0002	0.0006	0.0041	0.0122	0.0318	0.0052								
147.116	C11H14H+	0.0063	0.0036	0.0004	0.0008	0.0083	0.0208	0.0481	0.0133								
147.137	C8H18O2H+	0.0023	0.0017	0.0002	0.0007	0.0031	0.0058	0.0194	0.0030								
149.095	C10H12OH+	0.0022	0.0011	0.0003	0.0004	0.0031	0.0072	0.0174	0.0030								
149.132	C11H16H+	0.0069	0.0025	0.0009	0.0013	0.0084	0.0231	0.0608	0.0212	0.0025	0.0010	0.0001	0.0003	0.0031	0.0100	0.0263	0.0043
153.054	C8H8O3H+									0.0015	0.0011	0.0001	0.0005	0.0020	0.0044	0.0083	0.0015
153.127	C10H16OH+	0.0053	0.0044	0.0004	0.0021	0.0070	0.0141	0.0229	0.0059								
155.143	C10H18OH+	0.0016	0.0011	0.0002	0.0005	0.0021	0.0044	0.0105	0.0042								
157.121	C9H16O2H+	0.0025	0.0019	0.0003	0.0007	0.0033	0.0063	0.0134	0.0065								
157.159	C10H20OH+	0.0072	0.0058	0.0006	0.0029	0.0094	0.0160	0.0568	0.0118								
m/z	**Formula**	**Mean**	**Median**	**P5**	**P25**	**P75**	**P95**	**P99.5**	**Std**	**Mean**	**Median**	**P5**	**P25**	**P75**	**P95**	**P99.5**	**Std**
158.157	C9H19ONH+	0.0015	0.0011	0.0004	0.0006	0.0017	0.0035	0.0097	0.0022								
159.029	C6H6O5H+	0.0013	0.0010	0.0005	0.0009	0.0011	0.0037	0.0079	0.0011								
160.170	C9H21ONH+	0.0036	0.0036	0.0003	0.0022	0.0047	0.0072	0.0133	0.0023								
160.997	--	0.0016	0.0011	0.0004	0.0008	0.0016	0.0035	0.0084	0.0139								
161.132	C12H16H+	0.0035	0.0019	0.0002	0.0005	0.0045	0.0123	0.0249	0.0055								
161.153	C9H20O2H+	0.0045	0.0041	0.0003	0.0018	0.0061	0.0100	0.0237	0.0044								
171.06	--									0.0018	0.0014	0.0005	0.0009	0.0024	0.0041	0.0058	0.0012

171.137	C10H18O2H+	0.0016	0.0011	0.0002	0.0004	0.0021	0.0046	0.0085	0.0039								
171.174	C11H22OH+	0.0018	0.0015	0.0003	0.0005	0.0025	0.0041	0.0144	0.0040								
174.185	C10H23ONH+	0.0029	0.0027	0.0002	0.0016	0.0036	0.0060	0.0192	0.0029								
175.169	C10H22O2H+	0.0031	0.0024	0.0003	0.0008	0.0037	0.0069	0.0274	0.0056								
183.078	C8H10O3N2H+									0.0031	0.0025	0.0006	0.0017	0.0039	0.0074	0.0100	0.0020
205.195	C15H24H+	0.0053	0.0059	0.0005	0.0028	0.0068	0.0101	0.0110	0.0031								
207.031	C5H14O3Si3H+	0.2639	0.2580	0.1269	0.1782	0.2793	0.5112	0.5112	0.1190	0.1276	0.1034	0.0498	0.0982	0.1258	0.4707	0.4707	0.0840
223.065	**C6H18O3Si3H+**	**0.0040**	**0.0031**	**0.0005**	**0.0026**	**0.0039**	**0.0057**	**0.0440**	**0.0106**								
224.067	--	0.0013	0.0011	0.0003	0.0006	0.0012	0.0024	0.0102	0.0025								
225.046	--	0.0020	0.0016	0.0005	0.0010	0.0021	0.0032	0.0093	0.0049								
248.996	--	0.0012	0.0010	0.0002	0.0008	0.0015	0.0018	0.0061	0.0017								
274.275	C16H35O2NH+	0.0023	0.0013	0.0009	0.0010	0.0019	0.0079	0.0196	0.0038								
275.261	C16H34O3H+	0.0037	0.0016	0.0010	0.0013	0.0028	0.0144	0.0523	0.0081								
297.084	**C8H24O4Si4H+**	**0.0033**	**0.0032**	**0.0005**	**0.0021**	**0.0041**	**0.0056**	**0.0270**	**0.0034**								
316.091	--	0.0026	0.0024	0.0002	0.0016	0.0036	0.0049	0.0140	0.0021								
371.105	**C10H30O5Si5H+**	**0.0146**	**0.0107**	**0.0006**	**0.0053**	**0.0224**	**0.0339**	**0.1028**	**0.0250**	**0.0028**	**0.0012**	**0.0001**	**0.0006**	**0.0027**	**0.0121**	**0.0286**	**0.0048**
445.127	C12H36O6Si6H+	0.0078	0.0090	0.0006	0.0045	0.0103	0.0141	0.0141	0.0048								